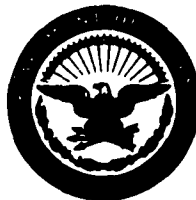


UNCLASSIFIED

AD 274 128

*Reproduced
by the*

**ARMED SERVICES TECHNICAL INFORMATION AGENCY
ARLINGTON HALL STATION
ARLINGTON 12, VIRGINIA**



UNCLASSIFIED

NOTICE: When government or other drawings, specifications or other data are used for any purpose other than in connection with a definitely related government procurement operation, the U. S. Government thereby incurs no responsibility, nor any obligation whatsoever; and the fact that the Government may have formulated, furnished, or in any way supplied the said drawings, specifications, or other data is not to be regarded by implication or otherwise as in any manner licensing the holder or any other person or corporation, or conveying any rights or permission to manufacture, use or sell any patented invention that may in any way be related thereto.

274128

ASTIA

274128

FINAL REPORT

DRI No. 2025

COPY #21

THE DYNAMICS OF TERMINAL BALLISTICS

Ballistic Evaluation Procedures for Armored Grille Designs

Rodney F. Recht

Thomas W. Ipson

DENVER RESEARCH INSTITUTE

University of Denver
(Colorado Seminary)

1 February 1962

Research to Develop Design Procedures
for Optimum Armor Air-Flow Grille Designs.
Contract No. DA-23-072-ORD-1302, Performed
under the Technical Supervision of the
Research and Engineering Directorate,
Ordnance Tank Automotive Command,
Detroit Arsenal.

NOX

N 62-3-1

FINAL REPORT

THE DYNAMICS OF TERMINAL BALLISTICS

Ballistic Evaluation Procedures for Armored Grille Designs

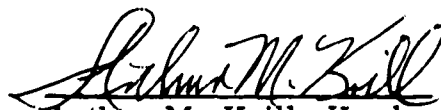
DENVER RESEARCH INSTITUTE

**University of Denver
(Colorado Seminary)**

1 February 1962

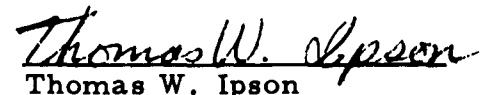
**Research to Develop Design Procedures
for Optimum Armor Air-Flow Grille Designs.
Contract No. DA-23-072-ORD-1302, Performed
under the Technical Supervision of the
Research and Engineering Directorate,
Ordnance Tank Automotive Command,
Detroit Arsenal.**

APPROVED BY:


**Arthur M. Krill, Head
Mechanics Division**

SUBMITTED BY:


**Rodney F. Recht
Project Supervisor**


**Thomas W. Ipson
Research Engineer**

FOREWORD

This report was prepared under Department of the Army Project No. 548-03-001, Army Ordnance Contract No. DA-23-072-ORD-1302, Denver Research Institute Project No. 198, "Research and Development to Determine Optimum Armor Intake and Exhaust Grilles." The work was administered under the technical direction of the Research and Engineering Directorate, Ordnance Tank Automotive Command, Detroit Arsenal, with Mr. H. Spiro as Project Engineer.

This report is UNCLASSIFIED when detached from the Appendices which are classified CONFIDENTIAL.

ABSTRACT

The terminal ballistic dynamics of small arms projectiles and fragment simulating projectiles are presented. These dynamics include the post-impact residual velocity and direction of projectiles, projectile break-up and dispersion of projectile fragments, and the mechanics of plate perforation. Ricochet dynamics concerning steel, aluminum, and titanium armor materials have been determined experimentally for impact obliquities up to 60 degrees. Analytical equations which accurately predict the dynamics of ballistic perforation were derived and confirmed by experimental data. These equations consider the effects of obliquity, plate thickness, edge impact and projectile shape.

A ballistic evaluation procedure, based upon the defined terminal ballistic dynamics, was developed. While the procedure was developed specifically for the evaluation of grilles, it can be used equally well for evaluating any armoring concept or the performance of projectiles.

Several prototype grilles were designed and evaluated. Some of these will be fabricated and ballistically proof-tested.

TABLE OF CONTENTS

	<u>Page</u>
I. OBJECT	1
II. SUMMARY	3
III. CONCLUSIONS AND RECOMMENDATIONS	9
IV. INTRODUCTION	11
V. DETAILS	13
A. Terminal Ballistic Dynamics of Projectiles and Fragments	13
1. Ballistic Ricochet Dynamics	14
Test Procedures	14
Test Results	19
2. Ballistic Perforation Dynamics; Full Impact	48
The Characteristics of Ballistic Plate Perforation.	48
Residual Velocity Equation for Normal Impact	53
Residual Velocity Equation for Oblique Impact	55
Determination of β , the Angular Change in Fragment Direction	56
Thin Plates Perforated by Cylinders	59
Thick Aluminum Plates Perforated by Steel Cylinders	65
Plates Perforated by Penetrating Projectiles	67
The Angular Change in Direction, Penetrating Projectiles	69
Projectile Break-up	71
3. Ballistic Perforation Dynamics; Partial or Edge Impact	74
Residual Velocity Equation for Edge Impacts	75

TABLE OF CONTENTS (Cont.)

	<u>Page</u>
The Angular Change in Direction.	
Partial Impact	85
Projectile Break-up; Edge Impact	85
4. Minimum Perforation Velocity and Ballis- tic Limit Velocity	85
Full Impact	86
Minimum Perforation Velocity for Edge Impacts	88
B. Procedure for the Ballistic Evaluation of Armored Grille Designs	91
1. Perforation - Full Impact	97
2. Perforation - Partial Impact	102
3. Ricochet	104
4. Grille Minimum Perforation Velocity	106
5. Form 198-5	106
6. Limitations of the Procedure	108
7. Form 198-3C	109
C. Grille Design	109
1. Prototype Design	111
2. Ballistic Analyses	112
Ballistic Evaluation. Grille Design No. 198-051	112
3. Prototype Evaluation	113
VI. BIBLIOGRAPHY	115
VII. APPENDICES (The Appendices are classified CON- FIDENTIAL and are bound under separate cover)	
Part A. Ballistic Data. Tables A-I through A-XII, and Figures A-1 through A-72 (see Lists of Tables and Figures)	
Part B. Bibliography of Pertinent Literature	

LIST OF FIGURES (Cont.)

<u>Number</u>	<u>Title</u>	<u>Page</u>
10.	Ricochet Dynamics. Ricochet Impacts. 0.50 Cal. Ball M2 Projectile. Aluminum Armor MIL 46027. 60 Degree Obliquity. Velocities in Feet per Second	26
11.	Ricochet Dynamics. Ricochet Impacts. 20 mm., 825-Grain WAL FSP. Aluminum Armor MIL 46027. 40 and 50 Degree Obliquity Velocities in Feet per Second	27
12.	Ricochet Dynamics. Ricochet Impacts. 20 mm., 825-Grain WAL FSP. Aluminum Armor MIL 46027. 60 Degree Obliquity. Velocity in Feet per Second	28
13.	Ricochet Dynamics. Ricochet Impacts. 0.50 Cal. APM 2 Projectile. Titanium Armor 4Al-4V. 40 and 60 Degree Obliquity. Velocities in Feet per Second	29
14.	Ricochet Dynamics. Ricochet Impacts. 0.50 Cal. Ball M2 Projectile. Titanium Armor 4Al-4V. 50 and 60 Degree Obliquity. Velocities in Feet per Second	30
15.	Ricochet Dynamics. Ricochet Impacts. 50 Cal., 207-Grain WAL FSP. Titanium Armor 4Al-4V. 30, 40, and 50 Degree Obliquity. Velocities in Feet per Second	31
16.	Ricochet Dynamics. Ricochet Impacts. 20 mm., 825-Grain WAL FSP. Titanium Armor 4Al-4V. 30 and 40 Degree Obliquity. Velocities in Feet per Second	32
17.	Ricochet Dynamics. Fragmentation. 0.30 Cal. Ball M2 Projectile. Reading Left to Right, Top and Bottom, 30, 40, 50 and 60 Degree Obliquities . .	35
18.	Ricochet Dynamics. Fragmentation. 0.50 Cal. Ball M2 Projectile, 30 and 40 Degree Obliquities, Top and Bottom	36

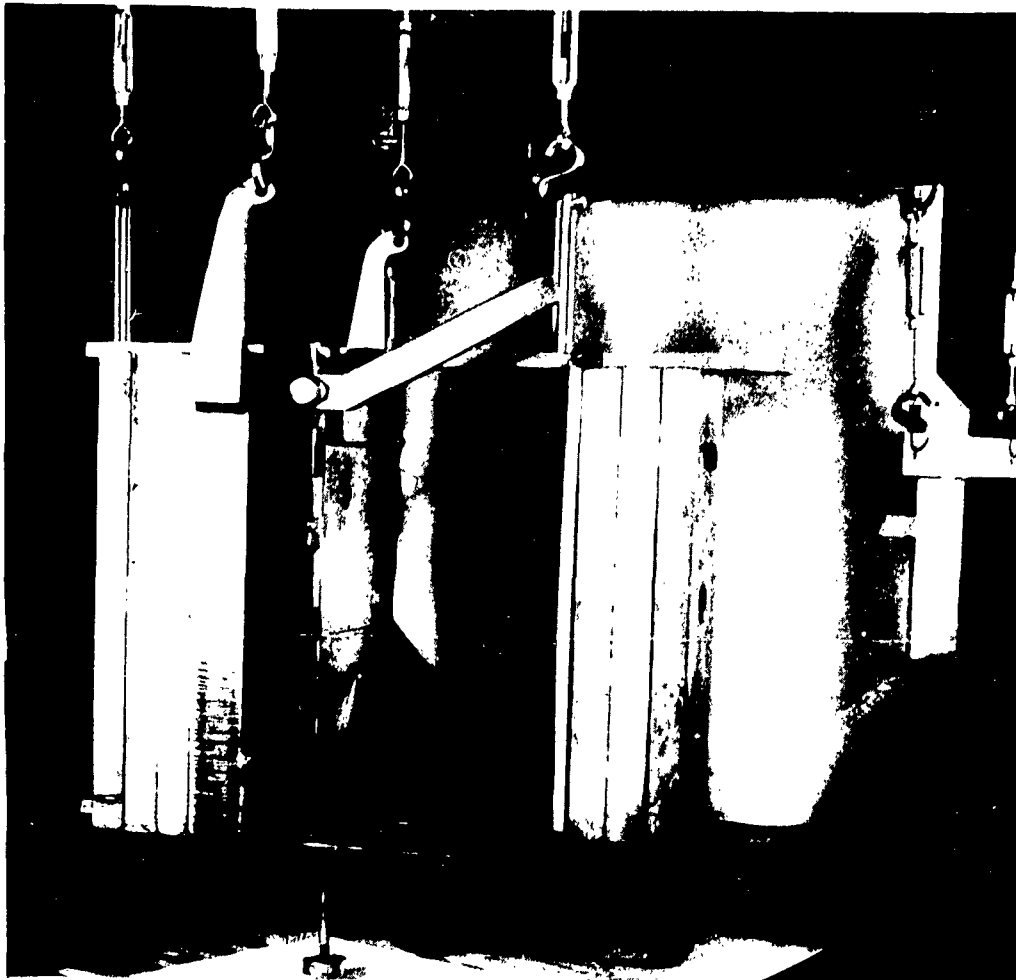


Figure 2. Ricochet Dynamics. Ballistic Test Apparatus. Target and Catch Pendulums



Figure 3. Ricochet Dynamics. Ballistic Test Apparatus. Pendulums and Velocity Coils

The target pendulum incorporates a counter-balance which places the center of gravity of the pendulum at the point of projectile impact. This prevents the creation of torsional moments which would complicate the pendulum trace. Four-wire support, arranged symmetrically about the center of gravity, was used so that the pendulum could swing with equal ease in any direction. Both the pendulum proper and the counter-weight were constructed of plates so that the pendulum weight could be changed. Weight was adjusted during testing so that the pendulum swing did not exceed 3 inches; length of the pendulum suspension was about 5 feet.

The catch pendulum is faced with Celotex and foam rubber through which the projectile or its fragments pass to be stopped in sand. Its suspension is similar to that of the target pendulum. During testing, the catch pendulum was placed so that the resultant rebound momentum would be absorbed near the center of gravity. No provision was made to adjust the weight of the catch pendulum, aside from varying the amount of sand. In some cases not all of the fragments were captured by the catch pendulum. For this reason, the measured remaining momentum was used only to check momentum triangles. In almost all cases the momentum measured by the catch pendulum agreed closely with the value obtained by vectorially subtracting the impulse transferred to the target plate from the initial momentum.

Where the projectile or fragment simulator removes a relatively small amount of mass from the target plate, and remains intact after impact, accurate calculations of remaining velocity, V_r , impact energy, and remaining kinetic energy can be performed using the momentum triangles.

Fortunately, it was found that the mass removed from the plate was negligible compared to projectile mass, except at high obliquity and high velocity. A test series to determine the extent of the calculation error due to the removal of plate mass showed that mass ejected from steel plates, subjected to ricochet impact by armor-piercing projectiles, did not exceed $3\frac{1}{2}$ percent of projectile mass at impact velocities up to 2500 ft/sec or 8 percent up to 3100 ft/sec. Impacts with aluminum and titanium involved

even less ejected plate mass. Fragment simulators did not remove measurable mass at any obliquity or velocity when impacting steel. The percent error in computation of residual velocity, V_r (computed by dividing remaining momentum by projectile mass), or impact and remaining kinetic energies cannot numerically exceed the above percentages of ejected mass. This error is in a direction to predict high residual velocities which is conservative from the point of view of grille design.

Only the armor-piercing and ball projectiles were subject to general break-up, which occurred at all test obliquities and at all but the lowest velocities. If all fragments of the projectile possess the same velocity, no error is introduced by break-up in the computation of residual velocity. Even when the projectile fragments do not possess identical velocities, the average residual velocity of the fragments is computed accurately by dividing the remaining momentum by the projectile mass. Only the computation of energies may be in error. It was shown that the error in the computation of remaining kinetic energy should not exceed 10 percent as the result of break-up. Since this error possesses the opposite sense, it is compensated, at least partially, by the error due to plate mass removal.

Test Results. Typical ricochet impacts are shown in Figures 4 through 16, pages 20 through 32. Only the AP penetrates the surface of steel to any great extent at the standard velocities. Ball projectiles slide off the surface of both steel and titanium. The FSP penetrates the surface of titanium and steel to some extent at high velocities and low obliquities. As would be expected, aluminum is penetrated readily by all projectiles. Because of this, aluminum is a very good ricochet energy absorber; the projectile enters the surface easily, loses kinetic energy, and has a difficult time emerging. Titanium behaves in a manner similar to steel being somewhat more easily penetrated than steel and thereby absorbing more energy during the ricochet.

Ricochet can be characterized in the following manner. At very low impact velocities the projectiles do not penetrate the plate surface to any extent. The component of velocity parallel to the plate is reduced very little during impact. On the



Figure 4. Ricochet Dynamics. Ricochet Impacts. 0.50 Cal. APM-2 Projectile. Homogeneous Steel Armor MIL 12560. Reading Left to Right, Top and Bottom, Obliquity and Velocity in FPS. 30°-2120, 30°-1635, 40°-1975, 40°-2720



Figure 5. Ricochet Dynamics. Ricochet Impacts. 0.50 Cal. APM-2 Projectile. Homogeneous Steel Armor MIL 12560. Reading Left to Right, Top to Bottom, Obliquity and Velocity in FPS. 50°-3060, 50°-3100, 50°-3060, 50°-3080

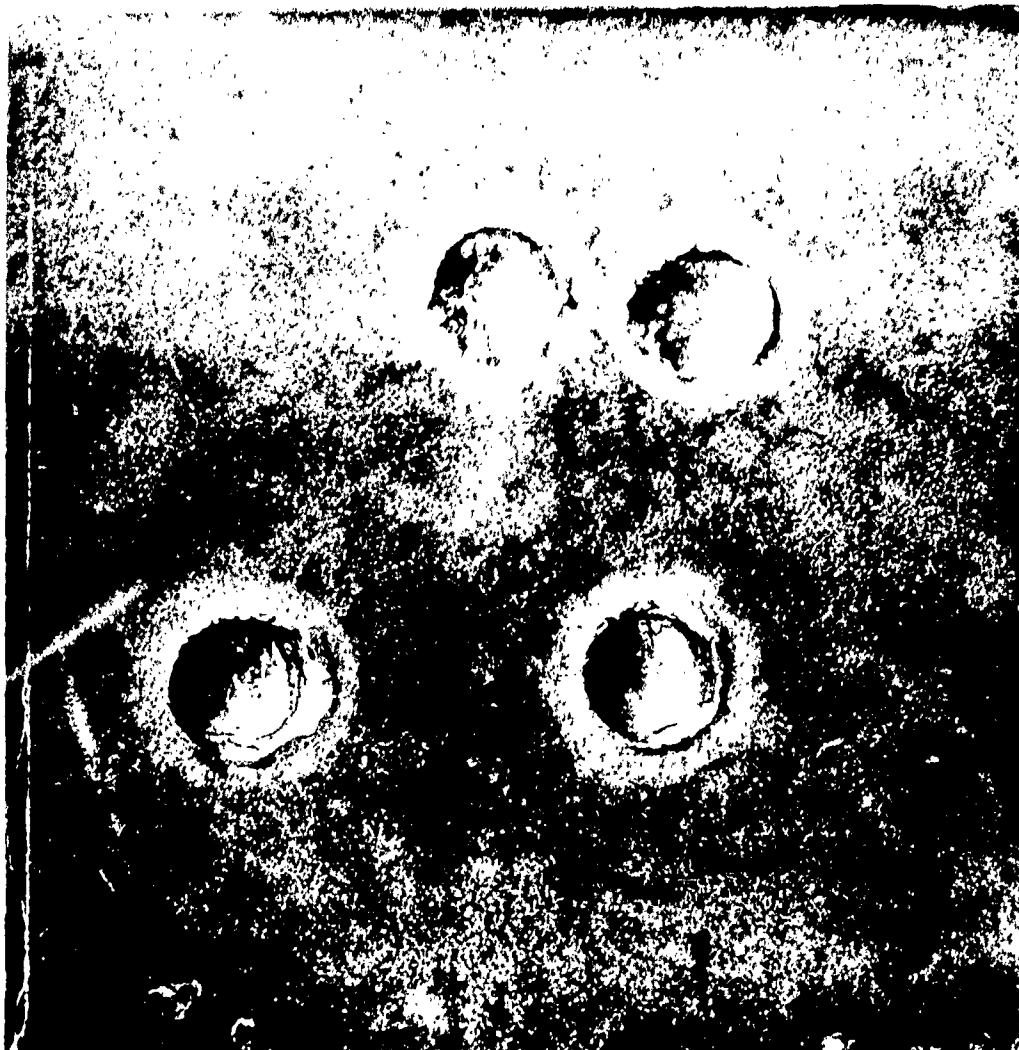


Figure 6. Ricochet Dynamics. Ricochet Impacts. 0.50 Cal. 207-Grain WAL FSP. Homogeneous Steel Armor MIL 12560. Reading Left to Right, Top and Bottom, Obliquity and Velocity in FPS. 30°-2950, 30°-3150, 30°-3440, 30°-3380



Figure 7. Ricochet Dynamics. Ricochet Impacts. 0.30 Cal. APM-2 Projectile. Aluminum Armor MIL 46027. 60 Degree Obliquity. Velocities in Feet per Second

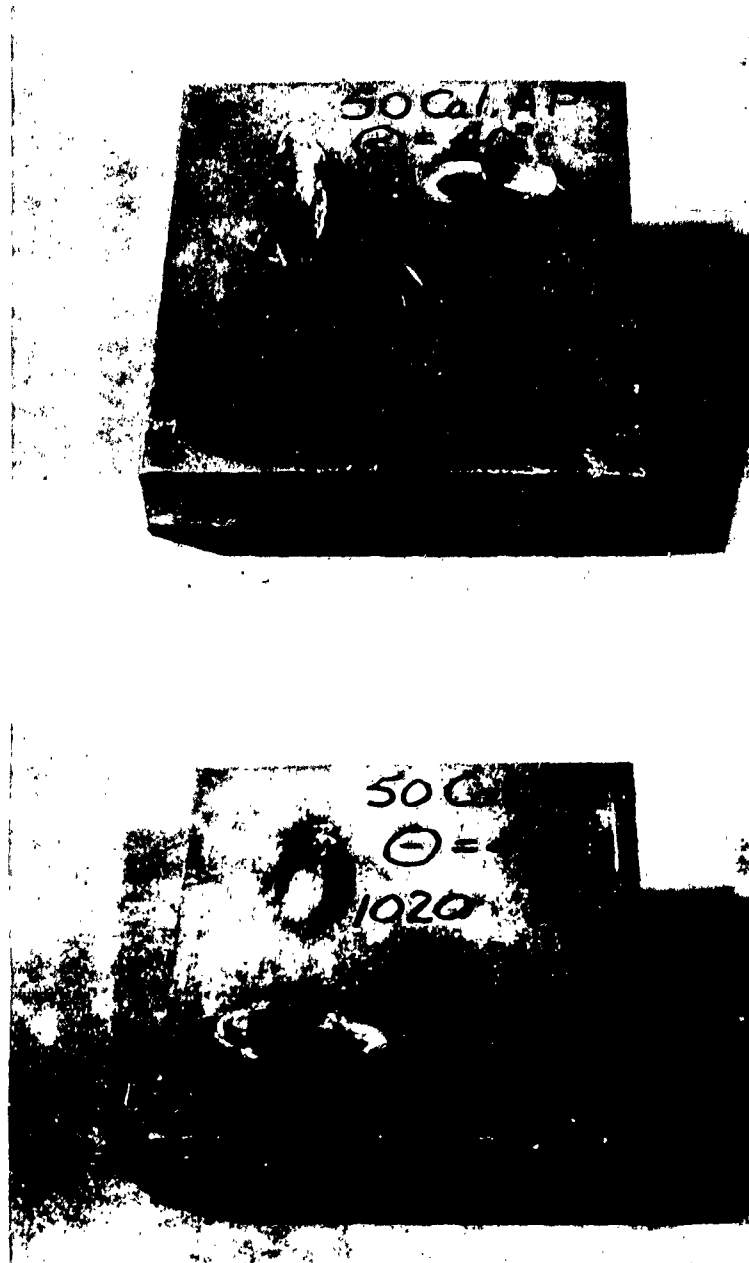


Figure 8. Ricochet Dynamics. Ricochet Impacts. 0.50 Cal. APM-2 Projectile. Aluminum Armor MIL 46027. 40 Degree Obliquity. Velocities in Feet per Second



Figure 9. Ricochet Dynamics. Ricochet Impacts. 0.50 Cal. Ball M2.
Aluminum Armor MIL 46027. 50 Degree Obliquity.
Velocity in Feet per Second

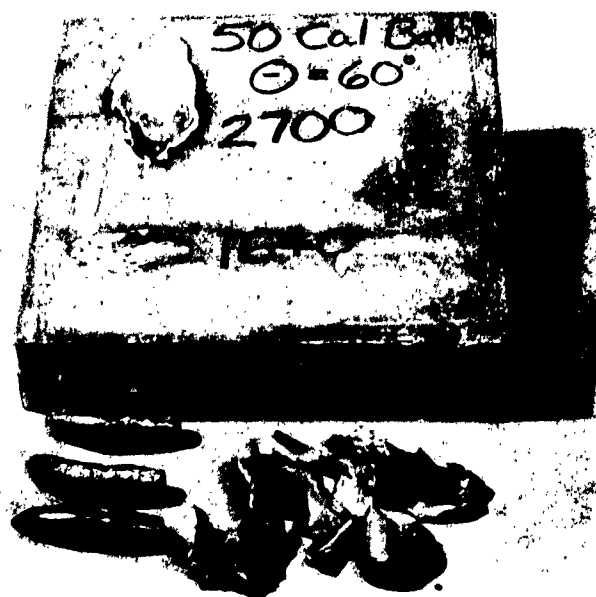


Figure 10. Ricochet Dynamics. Ricochet Impacts. 0.50 Cal. Ball M2 Projectile. Aluminum Armor MIL 46027. 60 Degree Obliquity. Velocities in Feet per Second

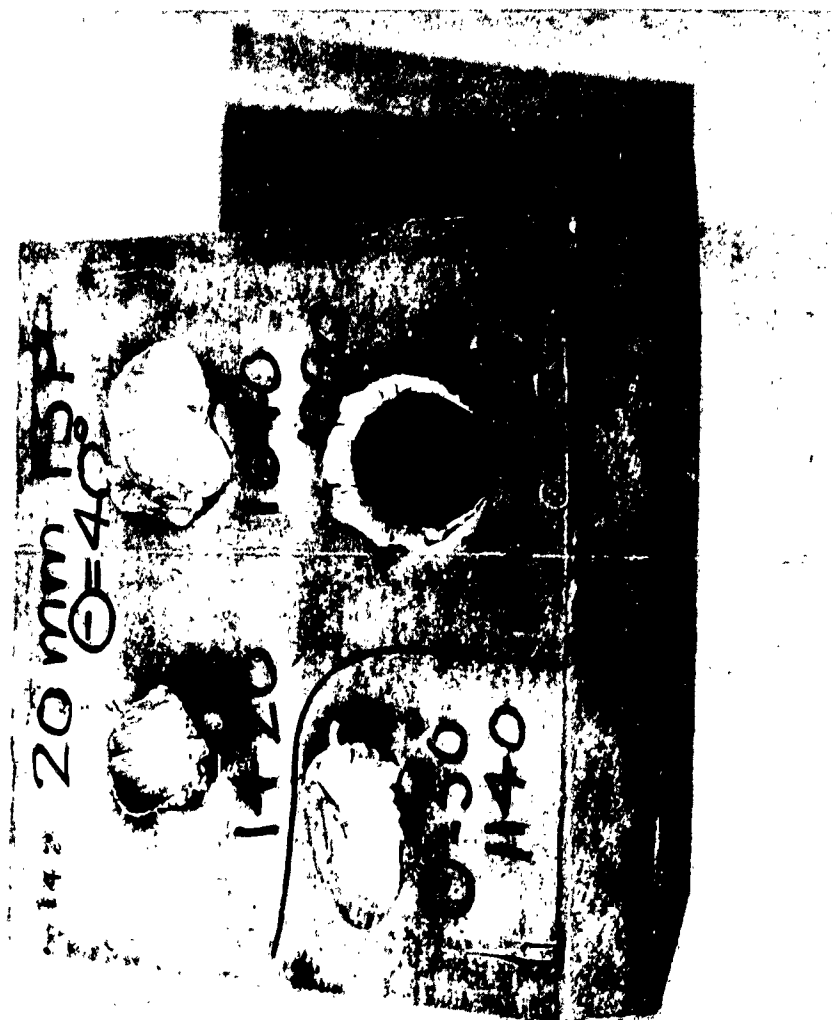


Figure 11. Ricochet Dynamics. Ricochet Impacts. 20 mm., 825-Grain WAL FSP. Aluminum Armor MIL 46027. 40 and 50 Degree Obliquity Velocities in Feet per Second



Figure 12. Ricochet Dynamics. Ricochet Impacts. 20 mm., 825-Grain WAL FSP. Aluminum Armor MIL 46027. 60 Degree Obliquity. Velocity in Feet per Second



Figure 13. Ricochet Dynamics. Ricochet Impacts. 0.50 Cal. APM 2 Projectile. Titanium Armor 4Al-4V. 40 and 60 Degree Obliquity. Velocities in Feet per Second



Figure 14. Ricochet Dynamics. Ricochet Impacts. 0.50 Cal. Ball M2 Projectile. Titanium Armor 4Al-4V. 50 and 60 Degree Obliquity. Velocities in Feet per Second



Figure 15. Ricochet Dynamics. Ricochet Impacts. 50 Cal., 207-Grain WAL FSP. Titanium Armor 4Al-4V. 30, 40, and 50 Degree Obliquity. Velocities in Feet per Second



Figure 16. Ricochet Dynamics. Ricochet Impacts. 20 mm., 825-Grain WAL FSP. Titanium Armor 4Al-4V. 30 and 40 Degree Obliquity. Velocities in Feet per Second

contrary, even at these low velocities, the rebound velocity in the normal direction is low compared to the normal component of impact velocity. This component of rebound in the direction normal to the plate decreases as impact velocity increases due to the more severe plastic deformation, which causes the impact to be more inelastic. Thus, projectiles tend to slide off the plate with a velocity nearly equal to the parallel component of the impact velocity.

The rebound obliquity angle, θ_r , is measured in the same way as the impact obliquity angle θ , that is, with respect to a normal to the plate. Hence, at low velocities, as velocities and inelasticity increase, the rebound obliquity angle also increases; the result of decreased rebound from the surface. At higher velocities penetration of the surface becomes significant. The result of this is to increase normal rebound, decrease the parallel velocity component, and decrease the rebound obliquity; the ricocheting projectile is forced to rise out of the scoop. Thus, in general, rebound obliquity curves display a maximum rebound obliquity (a velocity at which the normal rebound is a minimum).

Aluminum is easily penetrated and for this reason, scooping begins at very low velocities; rebound obliquity decreases rapidly with increasing impact velocity. At relatively low velocities all types of projectiles imbed readily in aluminum. Ricochet from aluminum surfaces does not occur at high velocities, except when the obliquity is high.

The ratio of ricochet velocity to impact velocity, V_r/V , diminishes as surface penetration becomes significant. Until this occurs, the ratio is approximately constant, resulting in straight lines on plots of residual and impact velocity. During ricochet tests utilizing relatively thin plates, the above ratio decreases rapidly as the minimum perforation velocity (ballistic limit) is approached.

Figures A-1 through A-21, pages 13 through 33, in Part A of the Appendix represent the experimentally determined relationships which exist between rebound velocity, V_r , rebound obliquity, θ_r , impact velocity, V , and impact obliquity, θ .

Figures 17 through 28, pages 35 through 46, illustrate fragmentation due to ricochet with steel plates. This fragmentation is typical of that observed for ricochet with titanium. This may be confirmed by a comparison with Figures 13 through 16, pages 29 through 32. Ball and AP projectiles almost always break up into fragments during oblique impact. Once a grille succeeds in breaking up a projectile, it must function to contain all fragments having lethal or damaging potential. Thus, a major function of a grille is to contain fragments whether they originate as projectile fragments or bursting shell fragments.

At even moderate velocities, the soft lead-antimony core of the 0.30 cal. Ball disintegrates upon impact. The mild steel core of the 0.50 cal. Ball yields to hard steel or titanium armor. At low obliquity the frontal distortion of this projectile occurs very rapidly, resulting in inertial circumferential tensile stresses which split the flattened portion into fingers which break off as the result of high impact velocities. Axial and bending stresses combine to break projectiles at the center. At high obliquities, the Ball projectile flattens against the steel or titanium plate, breaking up only at very high velocities.

The hard steel AP cores can be made to shatter during normal impact with steel or titanium only when the velocity is high (above normal service velocity). Shattering occurs when axial compressive stresses produce shearing and tensile hoop stresses which exceed the strength of the core material. The projectile breaks up near the nose since axial stress decreases from maximum to zero from nose to tail (this effect is intensified by reduced frontal cross-sections).

At zero obliquity, a matching AP projectile will commonly defeat armor without breaking up. However, at obliquities greater than 20-degrees, the projectile will break up at moderate velocities (1500 ft/sec at 20-degrees, 1000 ft/sec at 30-degrees). Bending stresses, which increase in severity with impact obliquity, add to the axial stresses, causing the projectile to break up.

At the usual impact velocities, the time involved in impact has been determined to be of the order of 100 micro-seconds; the time required for the elastic wave to travel the length of the 0.50

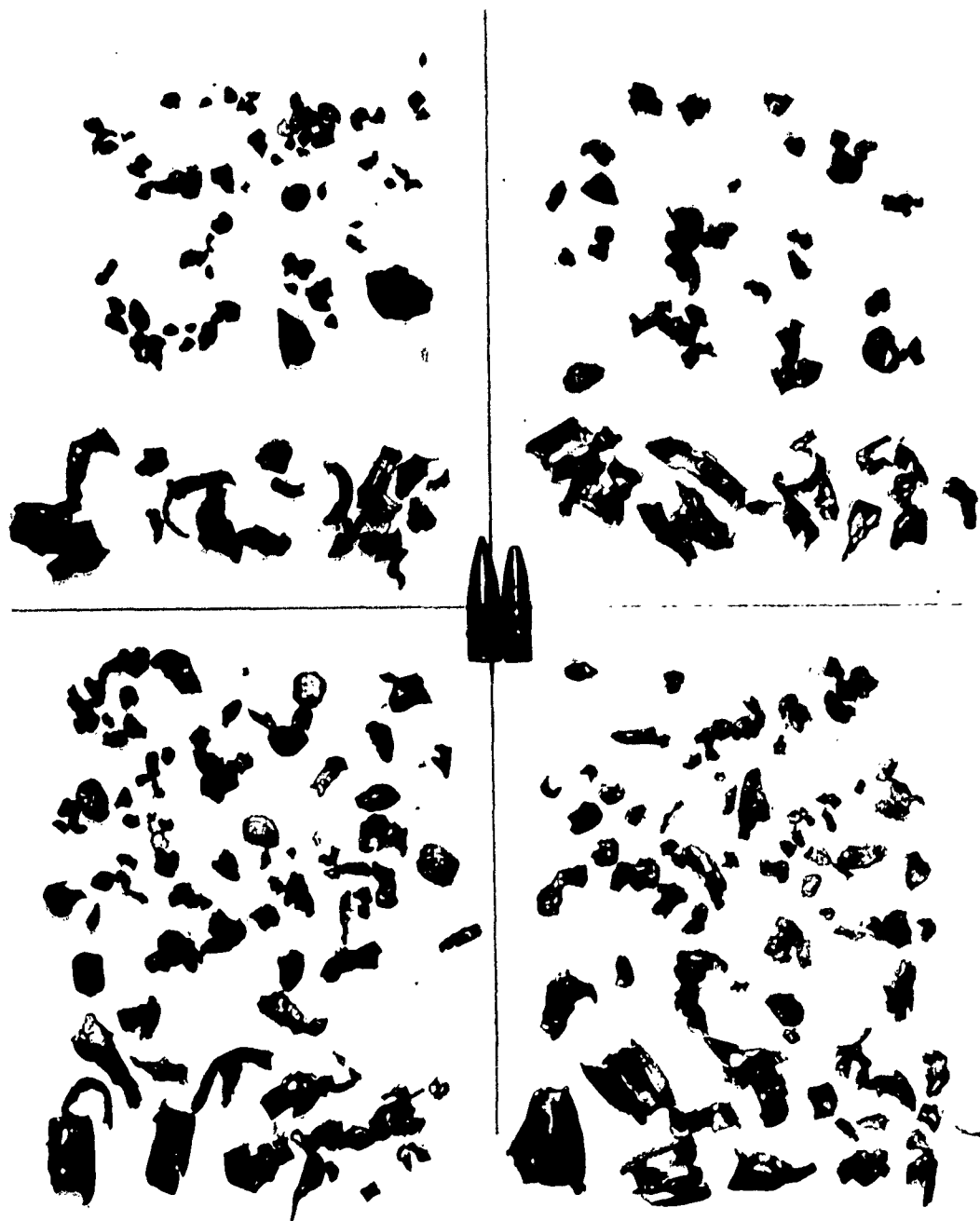


Figure 17. Ricochet Dynamics. Fragmentation. 0.30 Cal. Ball M2 Projectile. Reading Left to Right, Top and Bottom, 30, 40, 50 and 60 Degree Obliquities



Figure 18. Ricochet Dynamics. Fragmentation. 0.50 Cal. Ball M2 Projectile, 30 and 40 Degree Obliquities, Top and Bottom



Figure 19. Ricochet Dynamics. Fragmentation. 0.50 Cal. Ball M2 Projectile, 50 and 60 Degree Obliquities, Top and Bottom

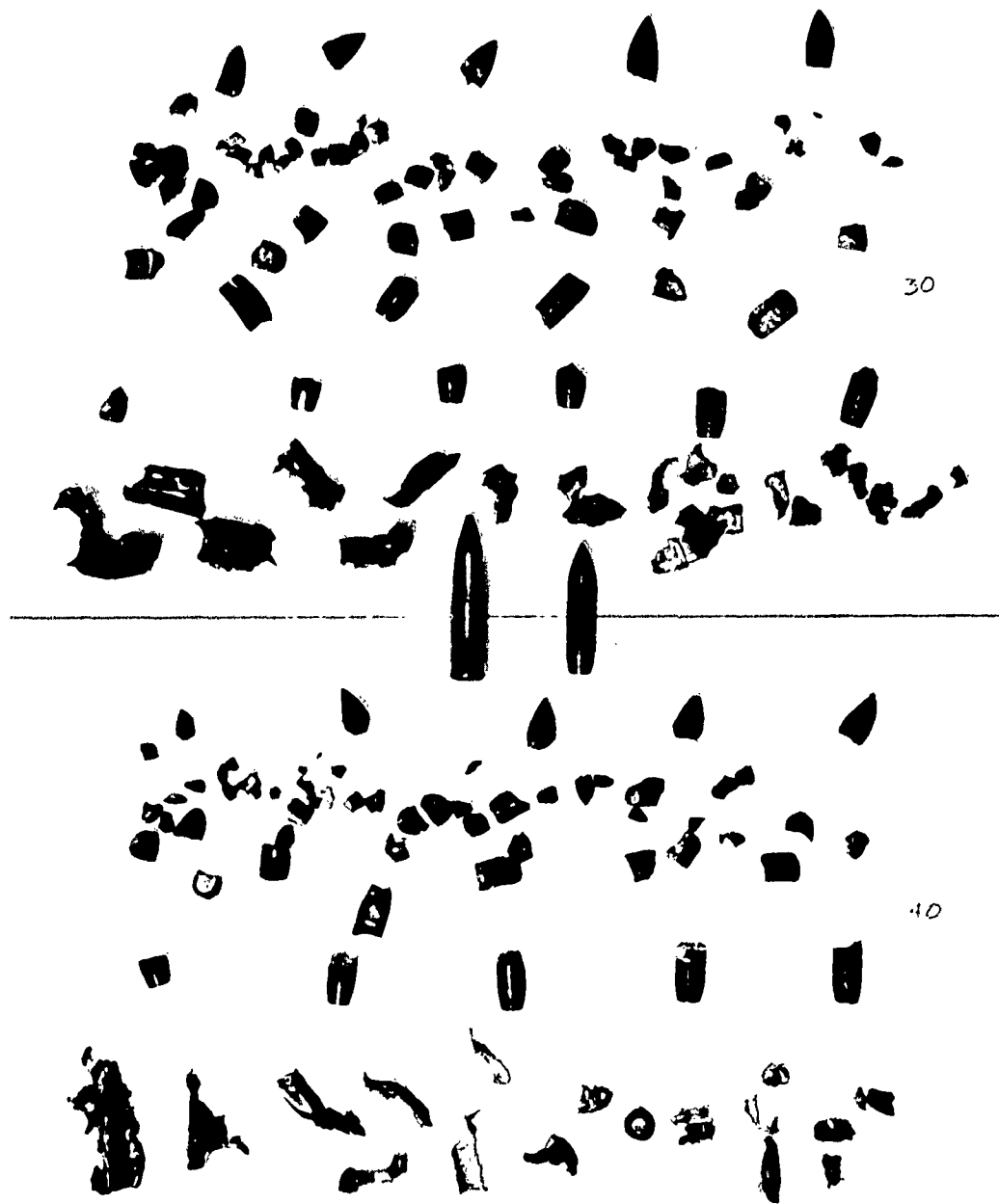


Figure 20. Ricochet Dynamics. Fragmentation. 0.30 Cal. APM 2 Projectile. 30 and 40 Degree Obliquities, Top and Bottom

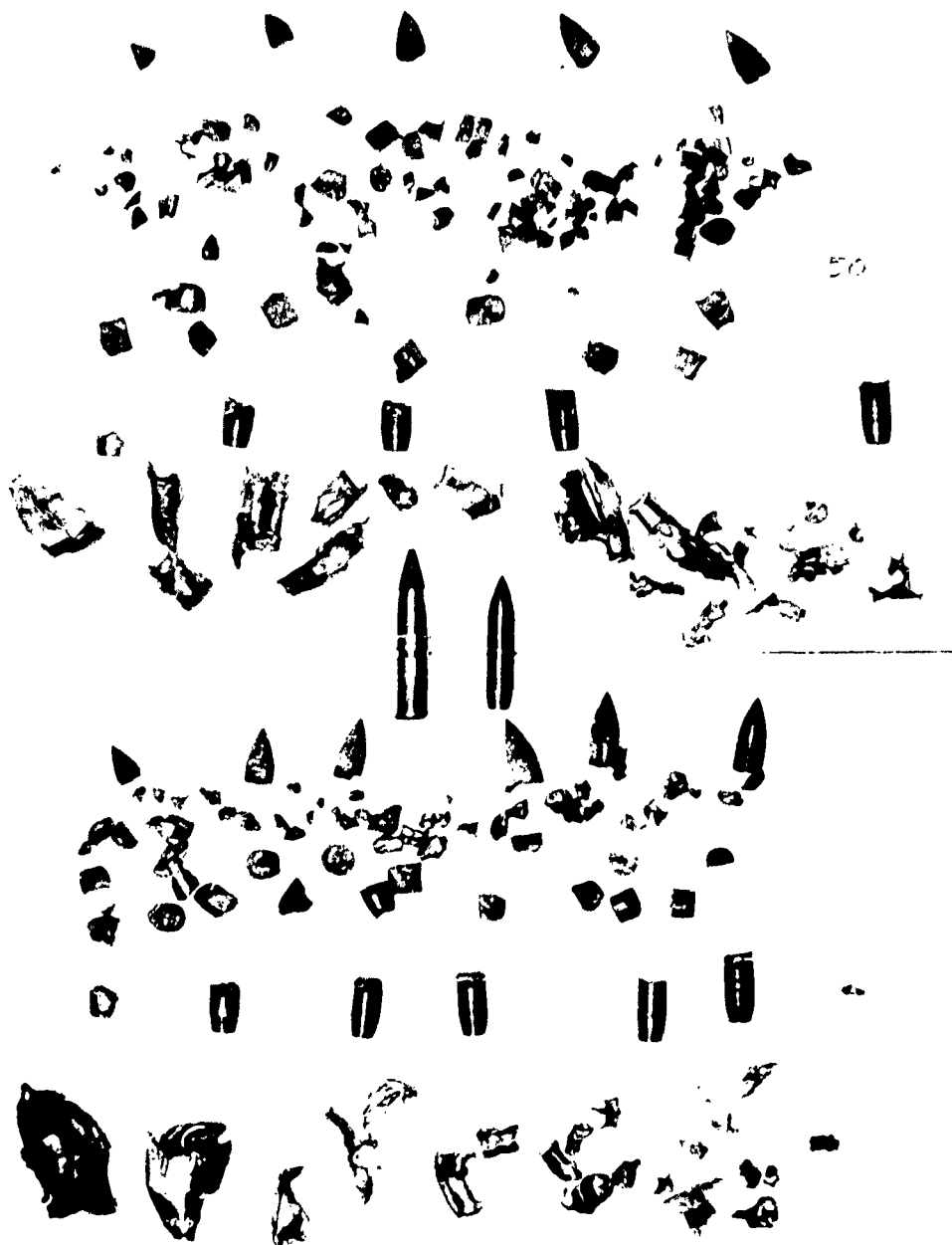


Figure 21. Ricochet Dynamics. Fragmentation. 0.30 Cal. APM 2 Projectile. 50 and 60 Degree Obliquities, Top and Bottom



Figure 22. Ricochet Dynamics. Fragmentation. 0.50 Cal. APM 2 Projectile. 30 and 40 Degree Obliquities, Top and Bottom

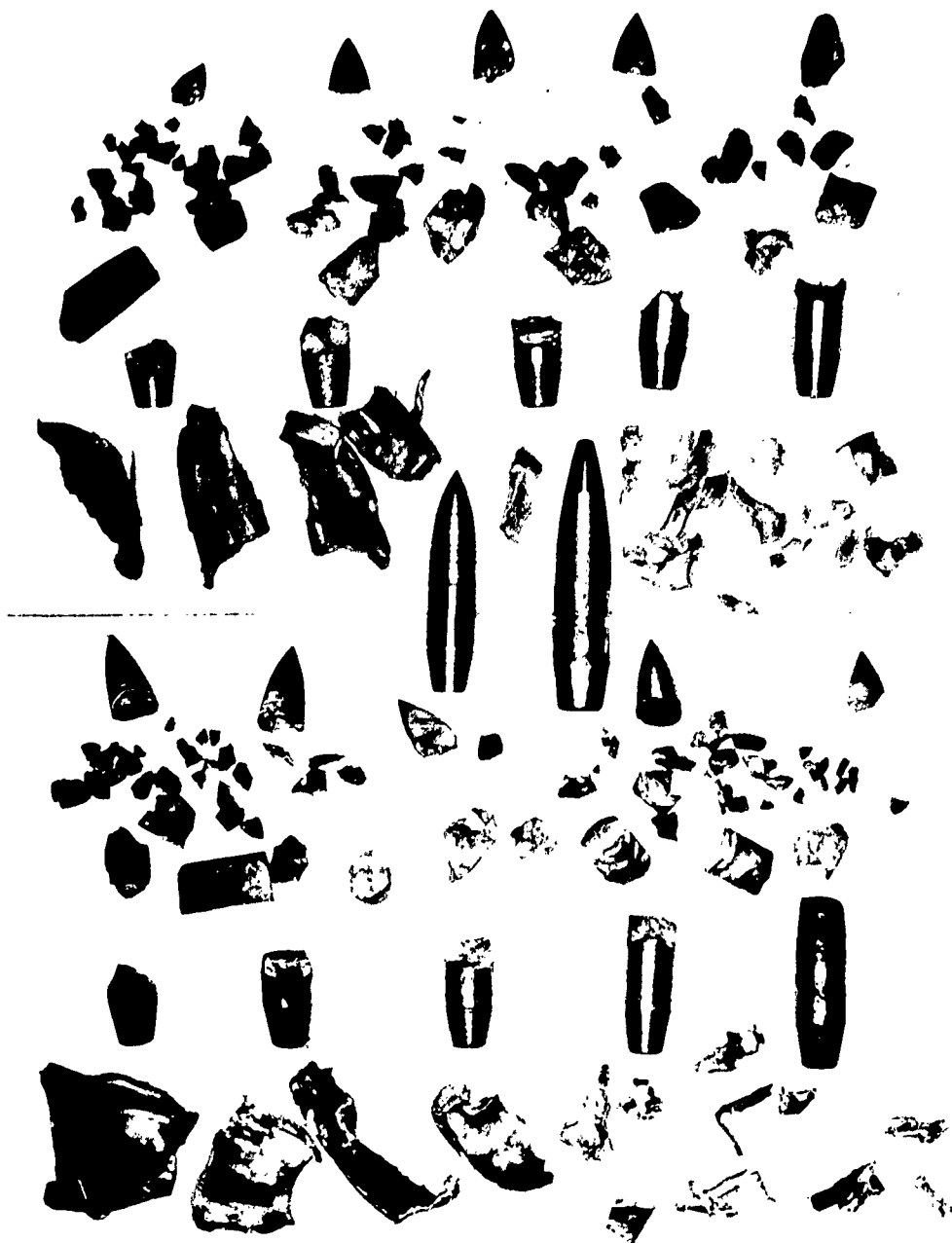


Figure 23. Ricochet Dynamics. Fragmentation. 0.50 Cal. APM 2 Projectile. 50 and 60 Degree Obliquities, Top and Bottom

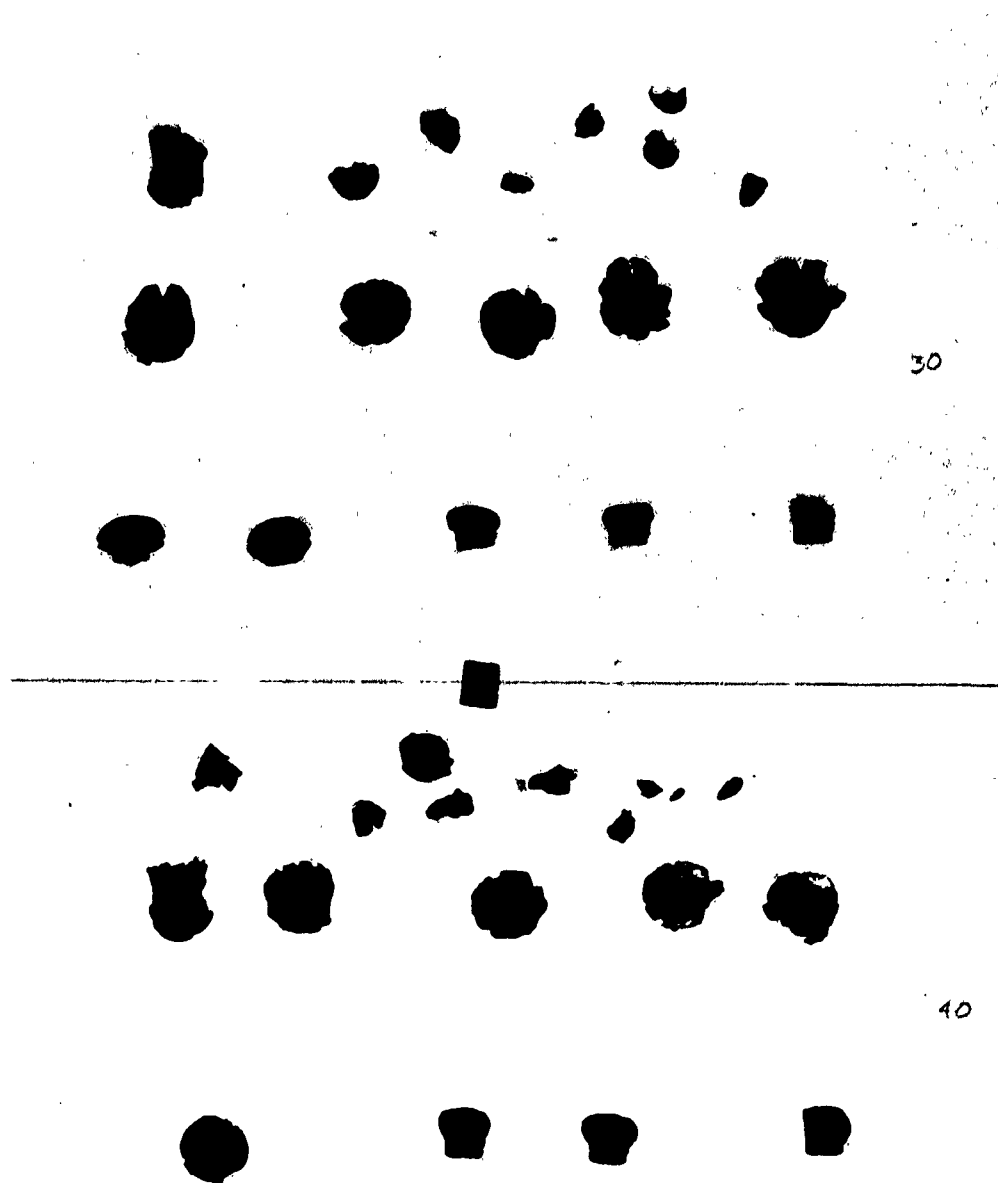


Figure 24. Ricochet Dynamics. Fragmentation. 0.30 Cal. 44-Grain WAL FSP. 30 and 40 Degree Obliquities, Top and Bottom

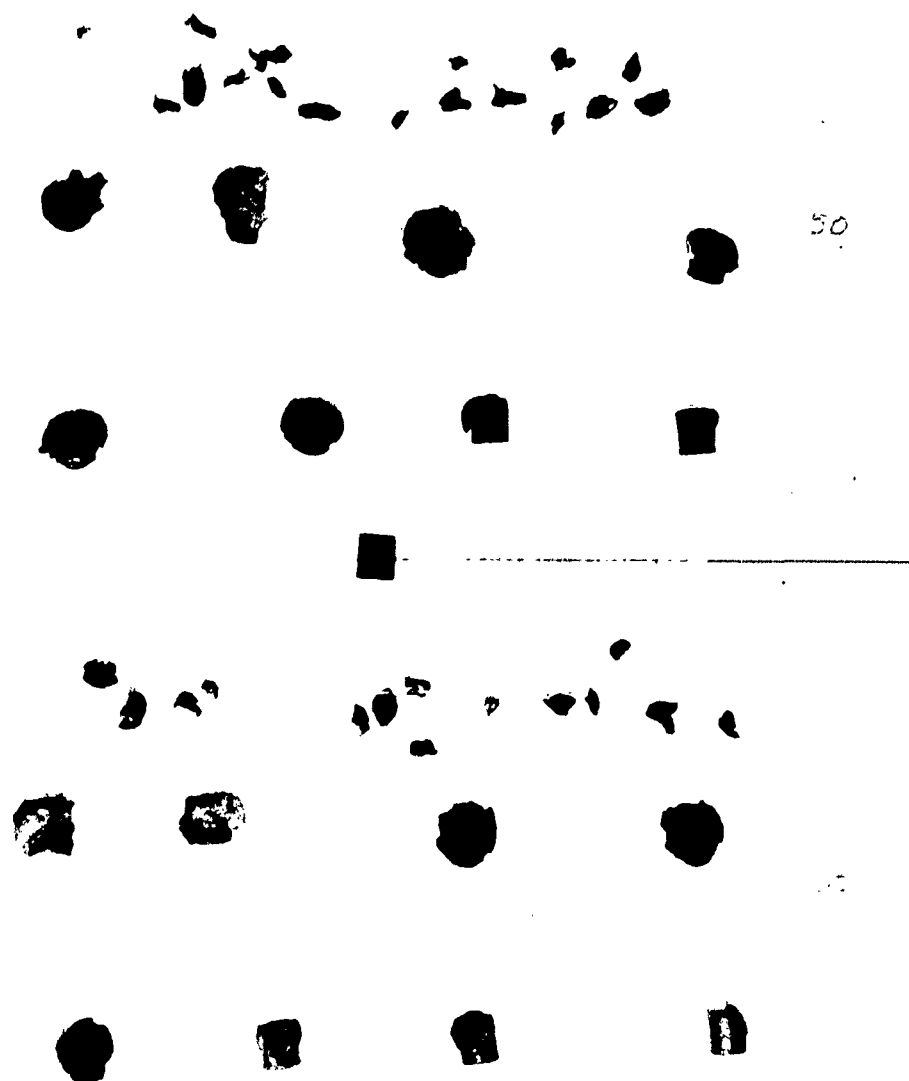


Figure 25. Ricochet Dynamics. Fragmentation. 0.30 Cal. 44-Grain WAL FSP. 50 and 60 Degree Obliquities, Top and Bottom

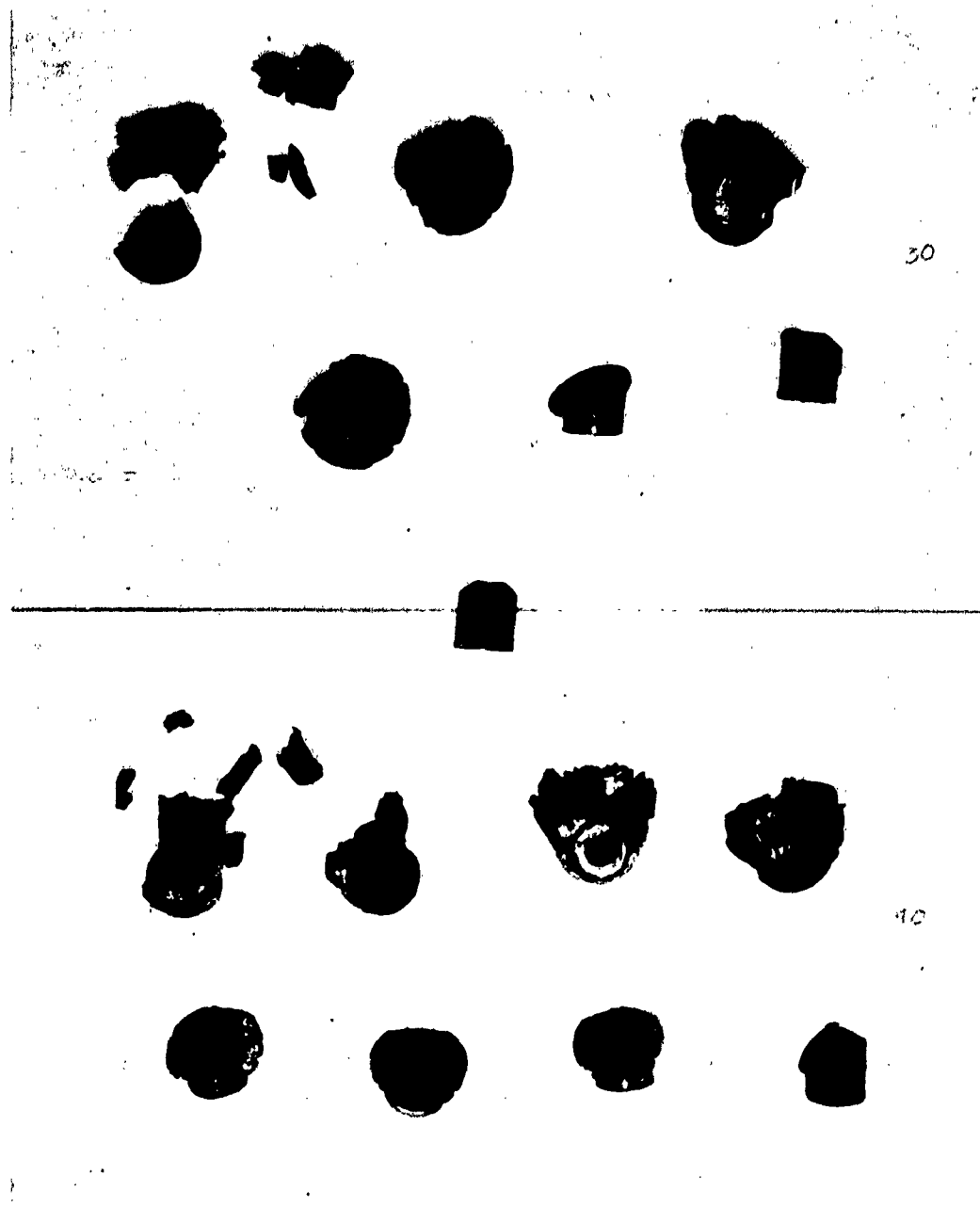


Figure 26. Ricochet Dynamics. Fragmentation. 0.50 Cal. 207-Grain WAL FSP. 30 and 40 Degree Obliquities, Top and Bottom

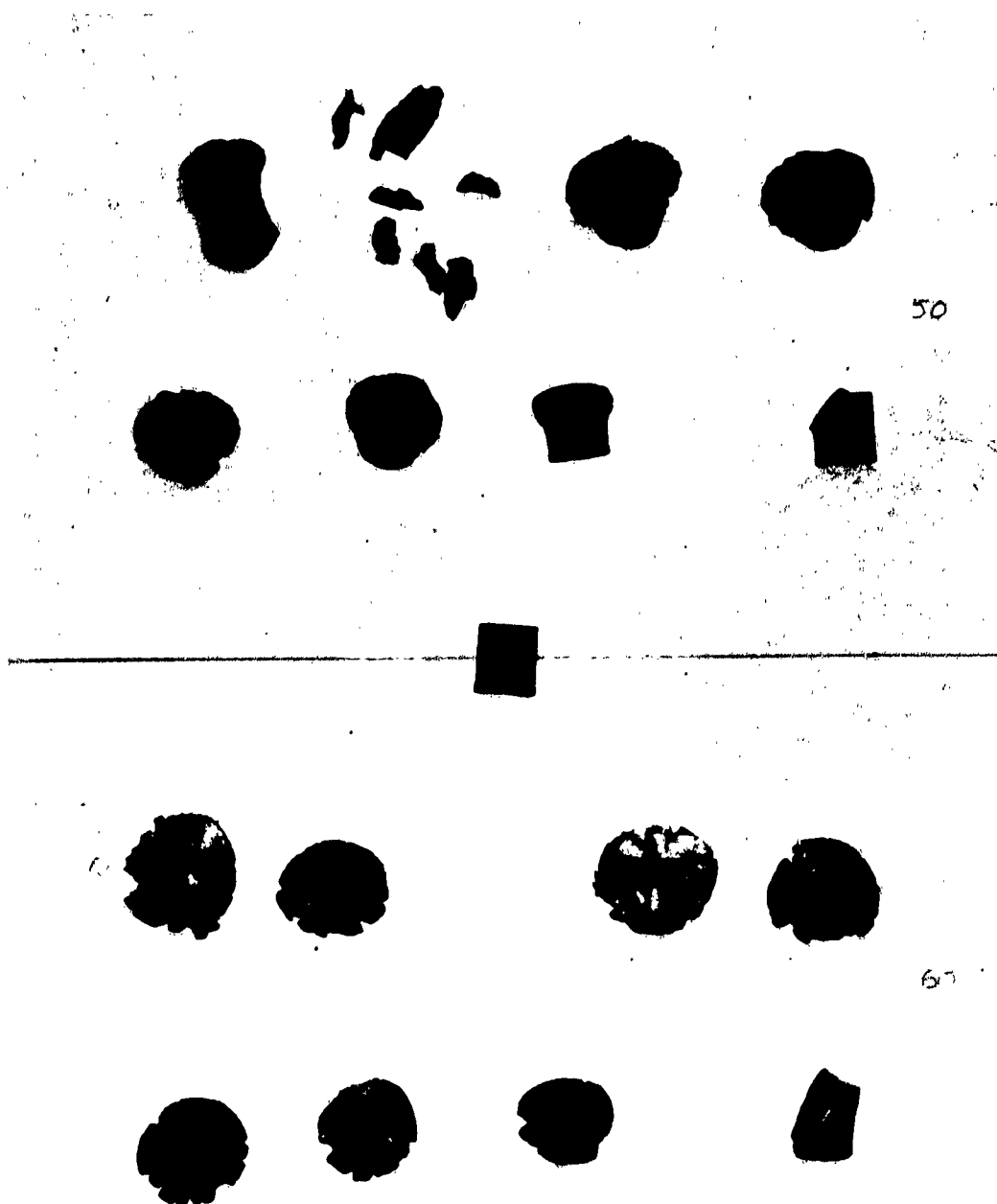


Figure 27. Ricochet Dynamics. Fragmentation. 0.50 Cal. 207-Grain WAL FSP. 50 and 60 Degree Obliquities, Top and Bottom

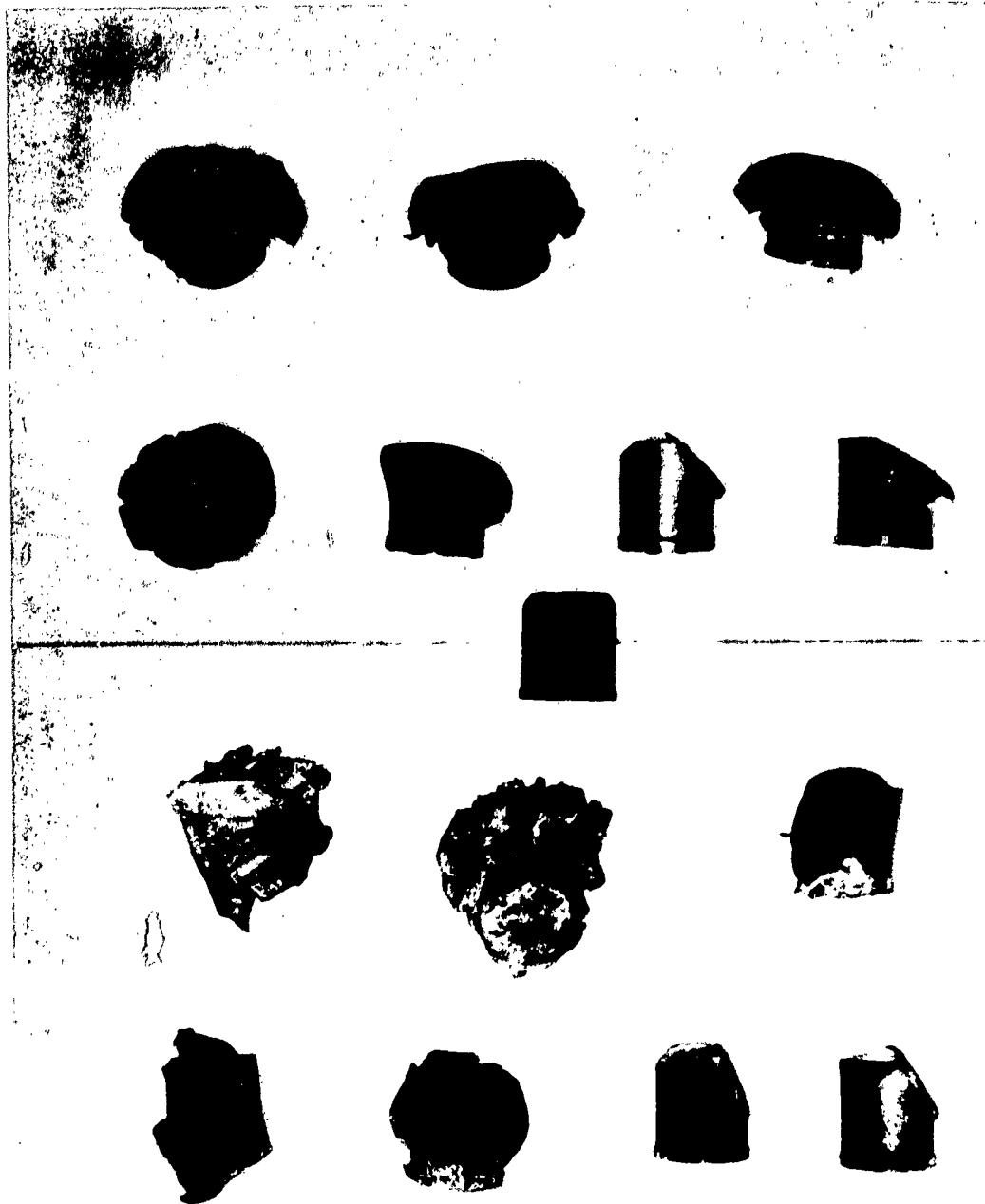


Figure 28. Ricochet Dynamics. Fragmentation. 20 mm., 825-Grain WAL FSP. 30 and 40 Degree and 50 and 60 Degree Obliquities, Top and Bottom

cal. AP is about 10 micro-seconds. Thus, it is reasonable to assume for stress analyses that stresses are set up without delay in the projectile. A preliminary stress analysis, at several impact obliquities, of the 0.50 cal. AP M2 was performed on a National Science Foundation grant. Compressive stresses due to combined axial and bending stresses near the center of the 0.50 cal. projectile were computed to be about 250,000 psi at a 30-degree obliquity, 600,000 psi at a 60-degree obliquity (impact velocity, 2100 ft/sec).

The fragmentation tables, Tables A-III through A-VII, pages 3 through 7, Part A of the Appendix, reveal the extent of fragmentation for various projectiles at several obliquities as the result of impact with steel. Considering the 0.50 cal. AP, it will be noted that the number of fragments decreases with increasing obliquity. At high obliquity the bending stresses are maximum; however, once the projectile breaks, these stresses are greatly reduced. The projectile tends to break in the region of high bending stress. At low obliquity the reduced bending stresses combine with the higher forward axial stresses to produce a large region of high stress throughout the forward two-thirds of the projectile (axial stresses decrease from nose to tail; bending stresses are maximum near the middle). The axial stresses within the 0.30 cal. AP projectile are much lower than those within the 0.50 cal. AP which accounts for the low number of fragments at low obliquity. The FSP has a low length-to-diameter ratio (unity); bending stresses depend approximately upon the square of the L/d ratio. Thus, in the simulator, bending stresses are small; it does not break up at any obliquity. The exception occurs at very high velocities, where the impact stresses cause severe mushrooming and petalling.

Dispersion of AP and Ball projectile fragments, resulting from projectile break-up during ricochet, was measured and plotted as a function of rebound obliquity. One dispersion limit is the surface of the plate since some fragments merely slide along the surface without rebounding. The other limit was found to approach 20 degrees measured from the rebound obliquity angle, θ_r . Thus the facts concerning dispersion are closely represented by assuming that rebounding projectile fragments are dispersed through an angle of $(90^\circ - \theta_r + 20^\circ)$ or $(110^\circ - \theta_r)$ measured from the surface of the plate.

2. Ballistic Perforation Dynamics, Full Impact

A punch-press operation is characterized by the virtual absence of acceleration in which the processes concerning penetration and perforation of plates are completely related to geometry and to the strength of the materials involved. This quasi-static condition is obviously a very special case within the general realm of penetration and perforation dynamics. Inertia exerts no influence upon this special case. Inertia is responsible for all forces created during penetration or perforation of a plate by a free fragment; thus, it is not surprising to find that, in general, the dynamics of ballistic plate perforation cannot be related directly to the quasi-static perforation process.

Analytical equations of the types required to define impact and perforation dynamics have been developed. These equations concern both blunt and sharp-nosed fragments perforating plates normally and at oblique impact angles. Derivations and confirming experimental data, which are presented here, specifically concern the high-velocity impact range up to about 4000 ft/sec.

The Characteristics of Ballistic Plate Perforation. Important general characteristics of the ballistic perforation process can be illustrated by considering the normal axial impact of a cylinder with a relatively thin plate as depicted in Figure 29, page 49. An extensive study of this type of impact perforation has been performed. This study reveals two distinct steps in the perforation process in the range of impact velocities considered here. The first of these steps primarily concerns the inertial effects of the colliding masses. The projectile mass decelerates and target plug mass accelerates; plastic deformation of the projectile and target material occurs as the result of the extreme compression forces arising from the inertial characteristics of the impact. In a plate, this compression force is increased by a non-inertial component due to the initial resistance to shear encountered at the plug periphery (this component becomes unimportant as impact velocities increase). The collision is highly inelastic and the projectile and plug masses attain approximately the same velocity. Even though accelerations are very high, the distance the plug moves during the first step is relatively slight

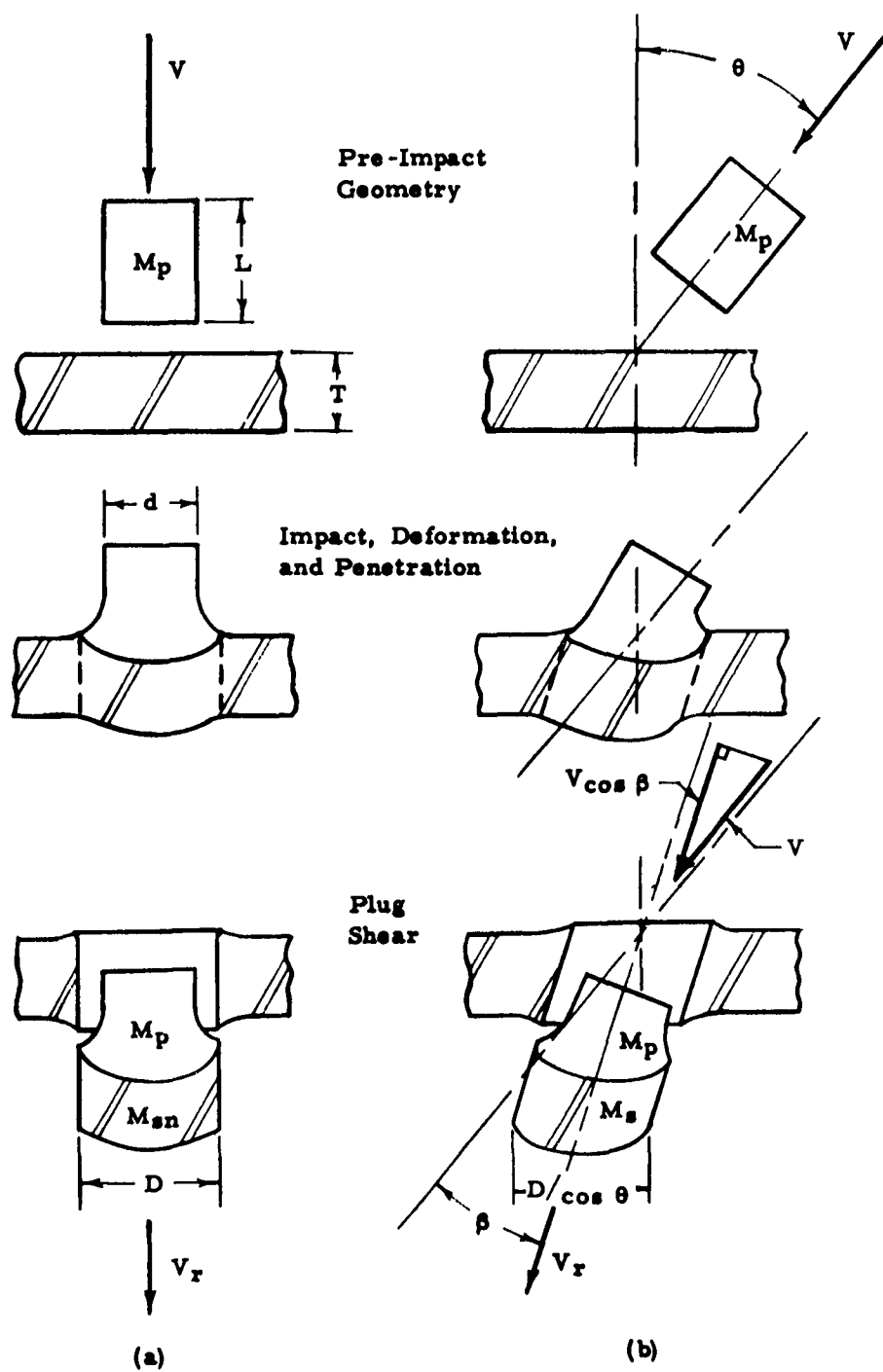


Figure 29. Characteristic Perforation of Thin Plates by Blunt Fragments

(less than $\frac{V}{C} T$, where V , C , and T are impact velocity, plate material sonic velocity, and plate thickness). The second step concerns the actual circumferential shearing of the plate material and is synonymous to a quasi-static "punch press" perforation process, except that the plug itself becomes part of the "inertia punch" after being accelerated by the projectile. Static shear strength is replaced by dynamic shear strength. Figure 29, page 49, illustrates typical high velocity impacts in both the normal and oblique directions, assuming completely inelastic impact.

The minimum pressure acting between two colliding elastic bodies of the same material can be found as follows. Consider two identical cylinders, having any length, L , impacting axially. The cylinders have opposing velocities of $\frac{V}{2}$, so that their impact velocity is V . Since the impact is symmetrical, the impact interface velocity must immediately equal zero, and the cylinders begin to compress. The free ends of the cylinders continue to travel at the velocity $\frac{V}{2}$ until a sonic wave has time to travel the length of a cylinder, L (assuming $\frac{V}{2}$ is less than the sonic velocity in the material). Thus, at a time, $\frac{L}{C}$, where C is the sonic velocity in the material, the free surface has moved a distance $\frac{V}{2} \frac{L}{C}$. The average unit strain in the material is therefore, $\frac{V}{2C}$; thus, the average stress is $\frac{EV}{2C}$. But in a material constrained to deform uniaxially $C \approx \sqrt{\frac{E}{\rho}}$ and the average compressive stress or pressure is given by,

$$p = \frac{EV}{2C} \approx \rho \frac{CV}{2} \quad (1)$$

Where,

p is pressure (psi)

ρ is mass density ($\frac{\text{lb-sec}^2}{\text{in}^4}$)

V is impact velocity (in/sec)

C is plate material sonic velocity (in/sec)

E is the elastic modulus (psi)

The compressive pressure computed by equation (1) will apply with good accuracy to the impact being considered because of the short times involved; the material will sustain extremely high compressive stresses (as will a fluid) as the result of inertia. For example, the value of free-impact pressure computed from this equation is about 2,000,000 psi for an impact velocity of 2600 ft/sec ($C = 19,500$ ft/sec for steel). Compare this extremely high value of pressure with the 200,000 psi maximum static compressive pressure acting on a 3/4-inch diameter punch during a punch press operation concerning a 1/2-inch thick steel plate. Dynamic shear strength has been shown to be commonly from two to three times the static value; thus, the contribution, due to the dynamic circumferential shear strength, to the impact pressure might be about 500,000 psi during the perforation of a 1/2-inch plate by a 3/4-inch diameter projectile impacting at a velocity of 2600 ft/sec.

The energy which will be required to perforate a plate will be equal to the sum of the energies consumed in both perforation steps. The energy remaining after a completely inelastic free-collision of the projectile with a plate plug of the same diameter as the projectile, may be obtained by applying the conservation of momentum, as follows.

If V is the projectile velocity prior to an inelastic impact with a free mass equal to the mass of the plug, and V_f is the post-impact velocity of the projectile-plug mass, the following relation can be written:

$$M_p V = (M_p + M_{sn}) V_f \quad (2)$$

$$\text{or, } V_f = \frac{M_p}{M_p + M_{sn}} V \quad (3)$$

Where, M_p and M_{sn} are the projectile and plug masses. The energy consumed during this inelastic free impact is the initial kinetic energy less the remaining kinetic energy,

$$E_f = \frac{1}{2} M_p V^2 - \frac{1}{2} (M_p + M_{sn}) V_f^2 = \left[1 - \frac{M_p}{M_p + M_{sn}} \right] \frac{1}{2} M_p V^2 \quad (4)$$

which can be modified using equation (1) to,

$$E_f = 2 \left[1 - \frac{M_p}{M_p + M_{sn}} \right] M_p \frac{p^2}{\rho^2 C^2} \quad (5)$$

Thus, the free impact energy is a function of the free impact pressure as shown by equation (5). During impact with a plate, a component of pressure is added to the free-impact pressure due to the presence of the circumferential shear area. As noted previously, when the ratio V/C is small, displacement of the plug during the time involved in the first step of the perforation process is also very small. Thus, the circumferential shear area which is active during this first step, is very nearly equal to the initial (maximum) shear area, πDT . The component of pressure due to this shear area is,

$$p_s \approx \frac{\pi DT \tau}{\pi D^2/4} = \frac{4T\tau}{D} \quad (6)$$

Where τ is the dynamic shear stress - psi.

Adding this component of pressure to equation (5) produces a relationship for the total impact energy,

$$E_i = 2 \left[1 - \frac{M_p}{M_p + M_{sn}} \right] M_p \frac{(p + p_s)^2}{\rho^2 C^2} \quad (7)$$

If the impact velocity is just sufficient to perforate the plate, this impact energy (Step 1) plus the shear work ($1/2 \pi D \tau T^2$) to remove the plug (Step 2) must equal the initial kinetic energy. Substituting equation (1) for p , equation (6) for p_s , V_{xn} for V , where V_{xn} is the minimum perforation velocity, and writing the indicated energy balance, $KE = E_i + W_s$,

$$\frac{1}{2} M_p V_{xn}^2 = \frac{2M_p}{\rho^2 C^2} \left[1 - \frac{M_p}{M_p + M_{sn}} \right] \left[\frac{\rho C V_{xn}}{2} + \frac{4T\tau}{D} \right]^2 + \frac{1}{2} \pi D \tau T^2 \quad (8)$$

Solving for the minimum perforation velocity, substituting $\frac{\pi d^2 L \rho}{4}$ for M_p and $\frac{\pi D^2 T \rho}{4}$ for M_{sn} , and letting $D = d$, results in the following expression:

$$V_{xn} = \frac{8\tau T^2}{\rho C d L} \left[1 + \sqrt{1 + \frac{L}{T} + \frac{\rho C^2 d (L + T)}{16 \tau T^2}} \right] \quad (9)$$

Where,

τ is dynamic shear strength (psi)

ρ is mass density ($\frac{\text{lb} - \text{sec}^2}{\text{in}^4}$)

C is sonic velocity (in/sec)

V_{xn} is minimum perforation velocity (normal incidence)
(in/sec)

d is projectile and plug diameter (inches)

T is plate thickness (inches)

L is projectile length (inches)

Substitution of known values of V_{xn} for thin plates ($\frac{T}{L} < \frac{1}{2}$, $\frac{T}{d} < \frac{1}{2}$), in equation (9) results in computed values for dynamic shear strength about two to three times greater than static shear strength values. High speed machining experiments support these values for dynamic shear strength.^{1, 2, 3*} Surprisingly, shearing strain rates during high speed machining are often equivalent to those observed in high speed impact perforation of plates. These machining experiments show that after an exponential transition from one value of dynamic shearing strength to a lower value, dynamic shearing strength becomes essentially constant and independent of strain rate.

Residual Velocity Equation for Normal Impact. The general equation for the residual velocity of blunt fragments will be developed upon the basis of a relatively thin plate and a cylindrical fragment so that the perforation process depicted in Figure 29, page 49, will be pertinent; a plug retaining a length equal to the plate thickness, T , will be considered. Projectile and plug will emerge with almost the same velocity due to the inelastic character of the impact.⁴ As noted previously, the perforation will proceed in two steps. The first step will primarily concern deceleration of the projectile and

* Superscripts refer to references in Bibliography, Section VI, page 115.

acceleration of the plug mass. The second step will concern the actual circumferential shearing of the plug. The presence of the shear area will increase the deformation energy expended during the first step by contributing a force component to the deceleration force. For simplicity, it is convenient to lump this portion of the deformation energy with the shear energy expended in the second step; the term, W_s , then represents all of the energy or work expended due to the presence of the shear area. An energy balance can now be written which includes the free impact energy, E_f (deformation energy consumed during inelastic impact between the projectile and a free plug), the total shear and deformation work due to the presence of the shear area, W_s , and the remaining kinetic energies of projectile and plug, thus,

$$1/2 M_p V^2 = E_f + W_s + 1/2 M_p V_r^2 + 1/2 M_{sn} V_r^2 \quad (10)$$

Substituting equation (4) into equation (10) and solving for the work due to the presence of the shear area, W_s ,

$$W_s = \left[\frac{M_p}{M_p + M_{sn}} \right] 1/2 M_p V^2 - 1/2 (M_p + M_{sn}) V_r^2 \quad (11)$$

Let V_{xn} (minimum perforation velocity) be the unique value of the impact velocity, V , which will cause the plate to be perforated so that the residual fragment velocity, V_r , is zero. When $V = V_{xn}$ equation (11) becomes,

$$W_s = \left[\frac{M_p}{M_p + M_{sn}} \right] 1/2 M_p V_{xn}^2 \quad (V_r = 0) \quad (12)$$

Equation (12) yields an accurate value for the shear and deformation work due to the presence of the circumferential shear area, when $V = V_{xn}$. This work is primarily a function of the dynamic shear strength, τ , of the plate material. If it is assumed that τ is constant, W_s will not change rapidly with impact velocity. Thus, at impact velocities near the minimum perforation velocity, V_{xn} , equation (12) can be substituted for W_s in equation (10). Making this substitution, and solving for the residual velocity, results in the following equation:

$$V_r = \frac{M_p}{M_p + M_{sn}} \sqrt{V^2 - V_{xn}^2} = \frac{\sqrt{V^2 - V_{xn}^2}}{1 + M_{sn}/M_p} \quad (13)$$

While the assumption of almost constant dynamic shear strength over rather wide ranges of strain rate can be defended,^{1, 2, 3} the form of the equation shows such defense to be relatively unimportant. This value for W_s given by equation (12) is correct when impact velocities are close to V_{xn} . At higher velocities, the effect of the dynamic shear strength, whose influence is represented in the equation by V_{xn} , see equation (9), becomes inconsequential. For instance, if the dynamic strength were to increase by 30 percent as V was increased to $2V_{xn}$, W_s would also increase by about 30 percent, as would V_{xn}^2 . Even for this completely unrealistic large change in dynamic shear strength, the residual velocity computed by equation (13) would be only 5 percent higher than the value obtained by taking into account this change in shear strength.

Equation (13) assumes that the masses involved in the impact are the same as those ejected. The projectile commonly spreads out, as shown in Figure 29, page 49, to the extent that some of the laterally displaced projectile mass is sheared off and remains as a ring on the impact surface.

At very high impact velocities this laterally extruded material together with similarly extruded plate material may react as a fluid and be ejected at high velocities, as in the formation of a crater. If M_{pr} and M_{snr} are used to represent ejected masses in the energy balance, equation (10), the residual velocity equation becomes,

$$V_r = M_p \sqrt{\frac{V^2 - V_{xn}^2}{(M_p + M_{sn})(M_{pr} + M_{snr})}} \quad (14)$$

Residual Velocity Equation for Oblique Impact. If the fragment strikes the plate obliquely as shown in Figure 29 (b), page 49, difficulties arise due to the conditions of non-symmetry which exist. The fragment is likely to change direction during the perforation; the fragment and plug may emerge in different directions, and have corresponding different velocities. For the present, assume that the plug possesses the same velocity and moves in the same direction as the fragment after perforation. Prior to impact the fragment path was defined by the angle of

obliquity, θ . The total angular change in direction of the fragment as it passes through the plate will be denoted by β ; thus, the post-perforation obliquity would be defined by $(\theta - \beta)$. The turning point is very near the surface, since during the first perforation step the projectile moves through a distance not exceeding $\frac{V}{C} T$. Note

that the entire component of the initial total momentum, $M_p V$, which is perpendicular to the emergent path, will be transferred to the plate; only the momentum in the direction defined by β will be involved in the perforation. Therefore, the perforation can be thought of as one in which the fragment has a pre-impact direction parallel to the emergent direction and an initial velocity of $V \cos \beta$ (consult Figure 30(a) page 57.) The plug mass, M_s , will be different than M_{sn} , since the oblique strike will alter the fragment presented area in the direction of perforation and the manner of fragment deformation.

V_x is the minimum impact velocity which will result in plate perforation; a different value of V_x is associated with each impact obliquity. When $V = V_x$, the fragment will change its direction by a characteristic angle, β_x . As V increases, β decreases; thus, only at $V = V_x$ does the change in direction equal β_x . The value corresponding to V_{xn} (equation (13)) for the case of oblique impact would be only the component of the ballistic limit velocity in the direction defined by β (not β_x); thence, this corresponding value would be $V_x \cos \beta$.

It is now possible to define the oblique perforation as approximately equivalent to a normal perforation where in equation (13): V is replaced by $V \cos \beta$, V_{xn} is replaced by $V_x \cos \beta$, and M_{sn} is replaced by M_s . Making these substitutions results in the following equation for oblique perforation:

$$V_r = \frac{M_p \cos \beta}{M_p + M_s} \sqrt{V^2 - V_x^2} = \frac{\cos \beta \sqrt{V^2 - V_x^2}}{1 + M_s/M_p} \quad (15)$$

Determination of β , the Angular Change in Fragment Direction.

The momentum triangle which depicts the perforation dynamics of Figure 29 (b), page 49, is shown in Figure 30 (a), page 57. I, the impulse transferred to the plate (not to the plate plug), and $(M_p + M_s) V_r$, the total remaining momentum of the fragment and plate plug,

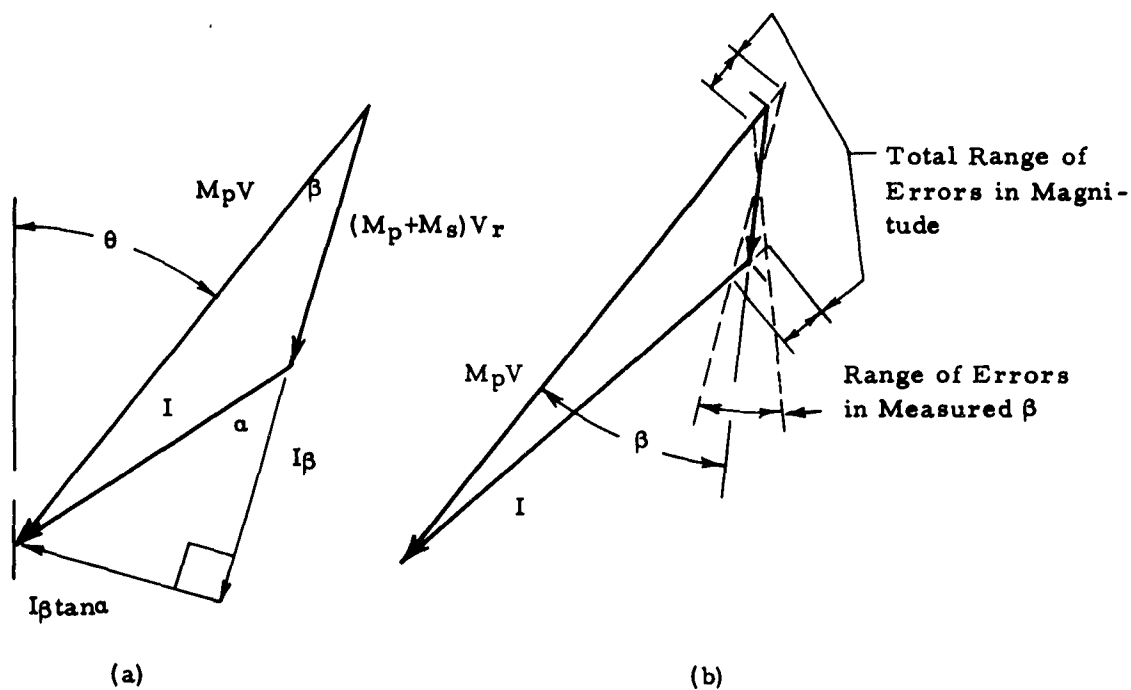


Figure 30. Typical Momentum Triangles for Oblique Perforation of Thin Plates. Illustration of the Manner by which Small Errors in Measured Vector Magnitude can Produce High-Percentage Errors in Measured Values of β

must vectorially add to equal the initial fragment momentum, $M_p V$. Impulse can be transferred to the plate only through the circumferential shear area. The force exerted by this area in the direction of V_r , depends on the dynamic circumferential strength of the plate. If this force has a value associated only with the position of the plug, the impulse, I , must decrease directly with the time associated with plug shearing. Hence, β will decrease rapidly as velocity increases, since (1) the momentum vectors will increase with the velocity, and (2) the impulse vector will decrease approximately as the inverse of velocity.

An approximate relationship for β can be developed in the following manner. The component of impulse transferred to the plate in the direction of V_r is shown on Figure 30 (a) as I_β . Since the total value of I is proportional to the time, t , during which the circumferential shearing force is acting, I_β will also be directly related to this time. The time involved is approximately proportional to the inverse of the average shear velocity. Recalling that the perforation takes place in two steps, ((1) fragment deceleration and (2) plug shear) the average shear velocity will be

$$\frac{\left(\frac{M_p}{M_p + M_s} \right) V \cos \beta + V_r}{2}, \text{ and not } \frac{V \cos \beta + V_r}{2}, \text{ since the frag-}$$

ment-plug combination cannot have a momentum greater than the total impact momentum. Thus, an approximation of I_β can be written in terms of the velocities,

$$I_\beta \approx K_1 t \approx \frac{2 K_2}{\left(\frac{M_p}{M_p + M_s} \right) V \cos \beta + V_r} \quad (16)$$

Where K_1 and K_2 are constants.

When $V_r = 0$; $V = V_x$, $\beta = \beta_x$, and $I_\beta = M_p V_x \cos \beta_x$ (see Figure 30 (a)),

$$\text{Then, } I_\beta = M_p V_x \cos \beta_x \approx \frac{2 K_2}{\left(\frac{M_p}{M_p + M_s} \right) V_x \cos \beta_x} \quad (17)$$

Rearranging,

$$K_2 \approx \frac{M_p^2 V_x^2 \cos^2 \beta_x}{2 (M_p + M_s)} \quad (18)$$

Substituting equation (15) for V_r , equation (18) for K_2 , and $\frac{M_p V \sin \beta}{\tan \alpha}$ for I_β , into equation (16) and simplifying yields,

$$\sin \beta \cos \beta = \frac{\cos^2 \beta_x \tan \alpha}{\frac{V^2}{V_x^2} + \frac{V}{V_x} \sqrt{\frac{V^2}{V_x^2} - 1}} \quad (19)$$

Inspection of Figure 30, page 57, will show that as V_r becomes smaller and approaches zero, α will approach β , which in turn becomes β_x at $V_r = 0$. Experimental momentum triangles show that β decreases much more rapidly than α . While α does tend to decrease as V_r increases, the assumption that it remains constant will not cause high percentage errors in the calculated value for β , except when values of β are very small; thus, angular error in the prediction of the emergent angle will not be increased significantly by this assumption. Modification of equation (19), letting $\alpha = \beta_x$, results in the following expression for the prediction of the angular change in the fragment direction, β :

$$\sin \beta \cos \beta = \frac{\sin \beta_x \cos \beta_x}{\frac{V^2}{V_x^2} + \frac{V}{V_x} \sqrt{\frac{V^2}{V_x^2} - 1}} \quad (20)$$

V_x and β_x must be determined experimentally.

Thin Plates Perforated by Cylinders. Perforation conditions as depicted in Figure 29, page 49, closely represent the case concerning thin plates and cylindrical projectiles. The fragment deforms laterally and shears out a plug which has a thickness approximately that of the plate, T , and a diameter, D . If the impact is oblique, the plug is approximately elliptical in shape having a major axis, $D/\cos \theta$, and a minor axis, D ; the plug mass will be closely approximated as $\frac{M_s n}{\cos \theta}$. Providing

that the projectile and plate have the same density, the term, $1 + \frac{M_s}{M_p}$ in equation (15) can be replaced by $1 + \frac{D^2}{d^2} \frac{T}{L \cos \theta}$ (assuming that the fragment loses no mass during the perforation). Making these substitutions, equation (15) can be written for thin plates (i. e., those for which $\frac{T}{L} \leq \frac{1}{2}$) and cylindrical fragments as,

$$V_r = \frac{\cos \beta \sqrt{V^2 - V_x^2}}{1 + \frac{D^2}{d^2} \left(\frac{T}{L \cos \theta} \right)} \quad (21)$$

It has been determined experimentally that V_x can be closely approximated by $\frac{V_{xn}}{\cos \theta}$, thereby reducing the empirical inputs required for solution of the equation.

β is determined using equation (20). β is always small, except near the minimum perforation velocity, V_x , and at high obliquity. Small errors in β will have negligible effect on $\cos \beta$ and the prediction of residual velocity, V_r . β_x must be determined empirically; however, for thin plates perforated by cylinders the use of $\beta_x = \theta$ should suffice for most cases. β_x cannot exceed θ .

Figure 31, page 61, displays the curve defined by equation (20) for the case where $\beta_x = \theta = 45^\circ$. Experimental data is also plotted. Mild steel plates (190 BHN) were perforated by cylindrical steel fragments ($R_c = 30$; 285 BHN) at an impact obliquity of 45° . The scatter of the experimental data is due to the measurement technique. Post-perforation dynamics were measured using pendulums to measure impulse transfer, I , and residual fragment momentum $(M_p + M_s) V_r$; velocity was measured to determine pre-impact fragment momentum $M_p V$. While individual impulse and momentum measurements are accurate within about 5 percent, angular errors in measurement of β within the momentum triangle are magnified by even these small errors in the magnitude of the measurements, especially when V_r is relatively small. Figure 30 (b), page 57, shows how this measurement of β can be affected drastically by small errors in the measured values of $M_p V$ and I .

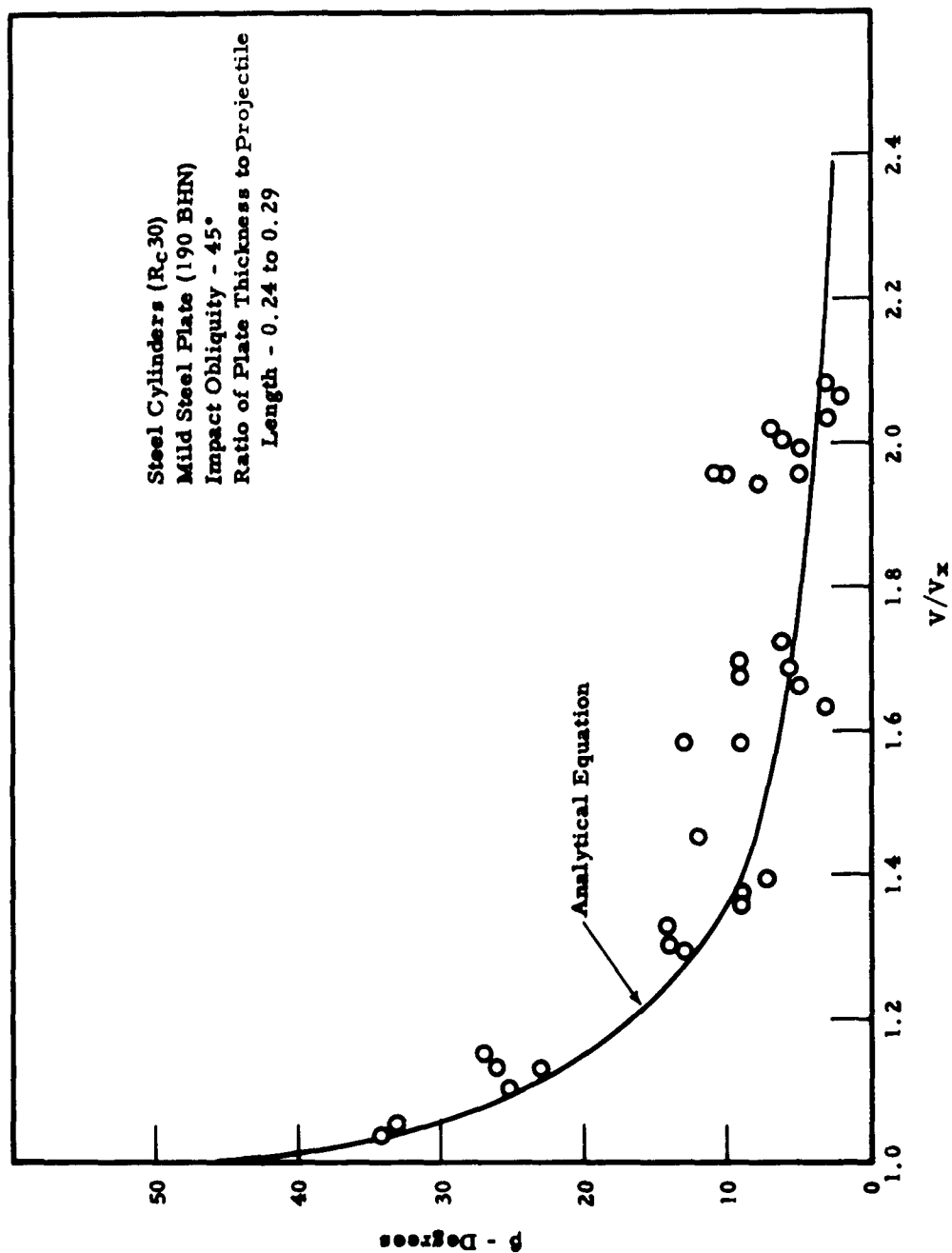


Figure 31. Angular Change in Direction of Cylindrical Fragments. Oblique Perforation of Thin Plates

The ratio, D^2/d^2 , depends on the absolute and relative strengths of the fragment and plate materials, the V/V_x , T/L and T/d ratios, and possibly to a small degree upon the impact obliquity. Measurements of D were made and an accurate (but unwieldy) empirical formula was derived for D^2/d^2 ; the general application of this formula has not been verified adequately, and presentation here would serve no useful purpose. The use of unity for this ratio results in a computation for residual velocity which is somewhat higher than actual; thus, such an assumption would be conservative when analyzing a grille.

The solid curves shown on Figure 32, page 63, represent the theoretical relationships for three normal-impact test geometries as computed by equation (21), using experimentally determined values for $V_x(V_{xn})$, and D^2/d^2 . As can be seen, the experimentally measured values for V_r are predicted very well by the equation. This test series utilized the same types of cylinders and plates used in obtaining the data plotted on Figure 31.

Equation (21) was applied to normal-impact residual velocity data as reported by the Ballistics Research Laboratory.⁴ The plates (Rockwell B50 to B68) and cylinders (Rockwell B96) used in the reported experiments were considerably softer than those used at the Denver Research Institute. $\frac{T}{L}$ values ranged from 0.08 to 0.59. Hole area was measured; however, since considerable plate deformation was observed, values of D^2/d^2 obtained using hole area would probably define a larger plug than actually was ejected. In addition, when firing against heavier plates these softer projectiles lost up to 30 percent of their mass, which was left as a ring within the hole. Loss of projectile mass has an effect on the computation of residual velocity which is opposite to that of increased plug mass. Values for D^2/d^2 are small for thin plates and the error imposed by using a value of unity is not great. For the above reasons, a value of unity was assigned to D^2/d^2 for calculating theoretical values for V_r . The correlation between calculated and observed values is shown in Figure 33, page 64.

Other correlations of published data have been made with equally as good or better results.⁵ These correlations involve a number of materials.

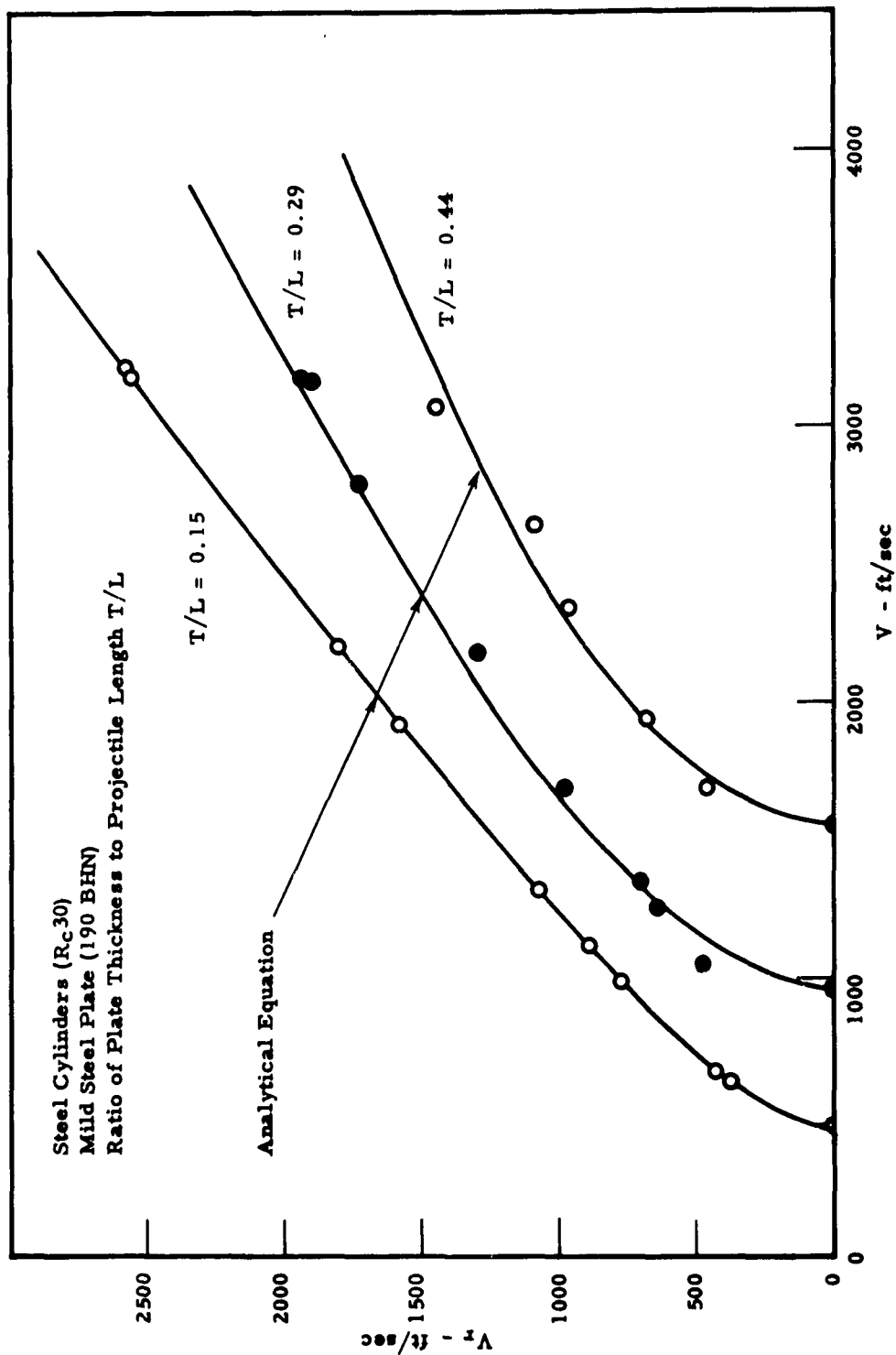


Figure 32. Post-Perforation Velocity of Cylindrical Fragments. Normal Impact with Relatively Thin Plates

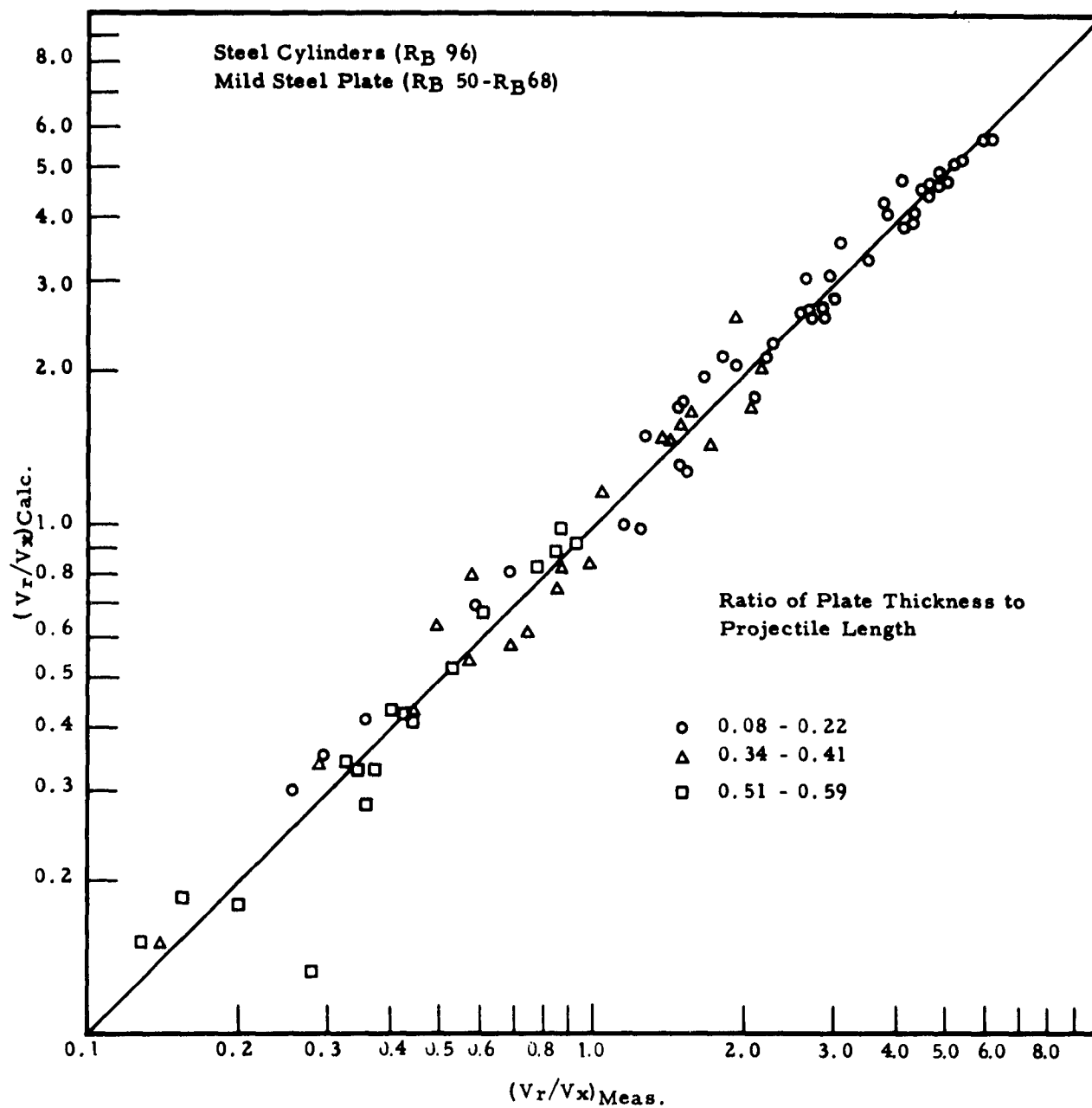


Figure 33. Post-Perforation Velocity of Cylindrical Fragments. Normal Impact with Relatively Thin Plates. Correlation of Data Published by the Ballistics Research Laboratory Using Denver Research Institute Analytical Equation

A series of tests was performed at an impact obliquity of 45° . This is the same test series from which the experimental data points shown on Figure 31, page 61, were obtained. Experimentally determined values of D^2/d^2 , V_x , and β , were used in equation (21) to determine the theoretical curves shown on Figure 34, page 66. Equation (21) assumes that the fragment and plug emerge in the same direction with the same velocity. For normal perforation this assumption is quite valid; however, for oblique perforation the plug is likely to take a direction closer to the normal and emerge at a somewhat lower velocity than the fragment. Residual velocity was measured by dividing the total measured momentum of fragment and plug by the sum of their masses; hence, at the higher T/L ratios, data points may be plotted somewhat below the actual fragment post-perforation velocities. The agreement between prediction and experiment is judged to be very good considering the degree of obliquity involved.

Thick Aluminum Plates Perforated by Steel Cylinders.

Consider a thick aluminum plate being perforated normally ($\theta = 0^\circ$) by a steel cylinder. The circumferential shear area of the plug is large and the stress level imposed by the impulse transfer during initial impact falls below the circumferential dynamic shear strength of the aluminum plate. This forces the fragment to penetrate the plate, pushing material outward and toward the impact surface. As in the case of the thin plate, the fragment deforms at the same time, increasing its frontal area; however, during this type of impact, the steel projectile does not lose any mass. As the penetration proceeds, the circumferential shear area decreases, shearing stresses increase and a plug is finally ejected which has a length considerably less than the plate thickness. In the case of thin plates, the impact plug mass and the ejected plug mass are properly considered to be equal. When considering thick plates this assumption is inappropriate. The more general form of equation (13) is required. If, for normal perforation by cylinders, the value for $\frac{M_{sn}}{M_p}$ is taken to be

$\Omega \frac{D^2 T}{d^2 L}$, equation (14) can be written,

$$V_r = \sqrt{\frac{V^2 - V_{xn}^2}{\left[1 + \frac{M_{snr}}{M_p}\right] \left[1 + \Omega \frac{D^2 T}{d^2 L}\right]}} \quad (22)$$

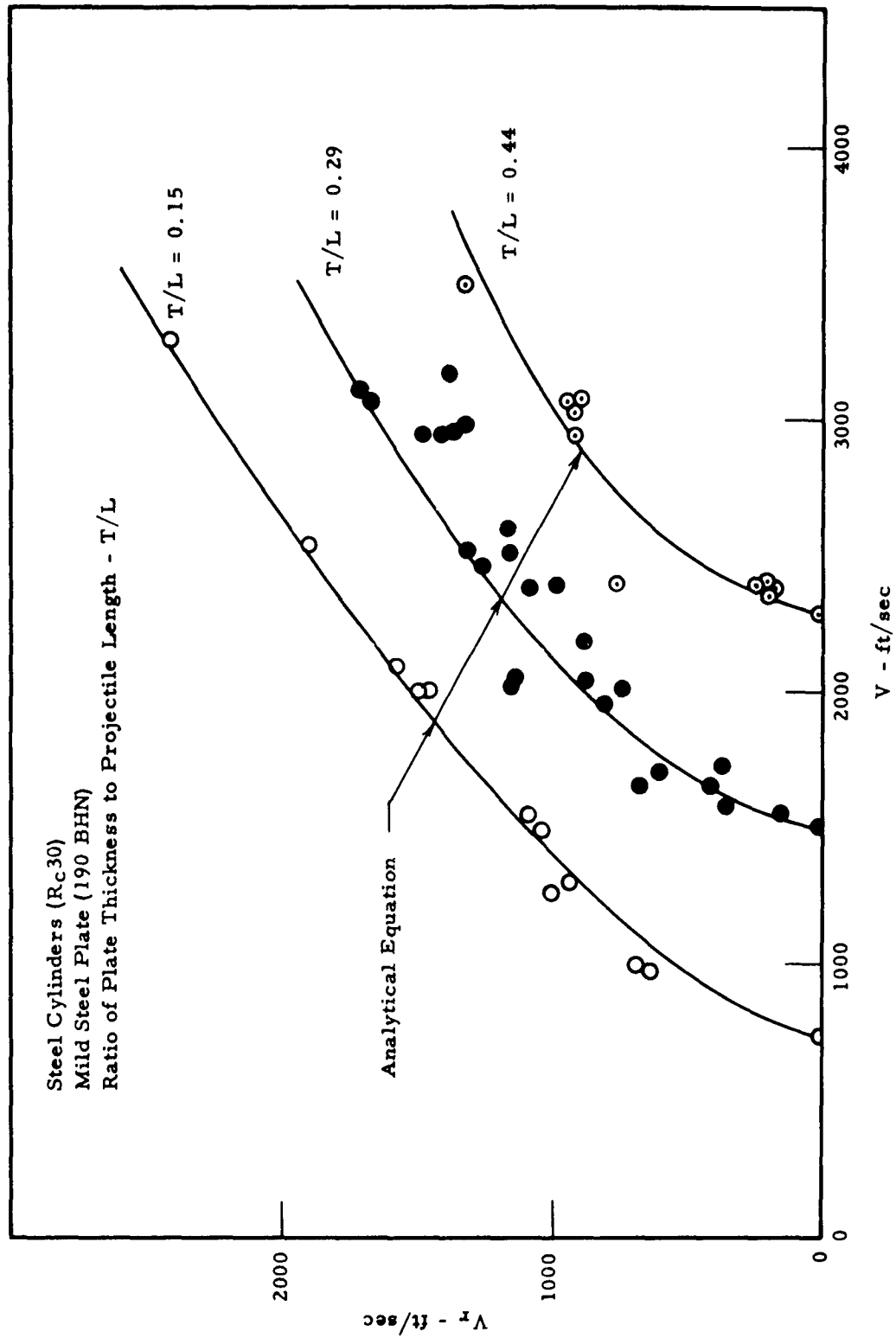


Figure 34. Post-Perforation Velocity of Cylindrical Fragments. Oblique Impact with Relatively Thin Plates

Where Ω is the ratio of plate and projectile material densities.

Justification for this substitution rests upon the assumption that the initial impact step, accompanied by penetration, involves the total displaced mass of the plate, and not just the ejected mass. The use of D^2/d^2 is based upon the observation that fragment deformation takes place early in the perforation; hole diameter is observed to be essentially constant when inspecting test plates.

Thick aluminum plates ($T/L = 1.45$) were used to experimentally verify equation (22) at normal obliquity. Ejected plugs had measured lengths varying downward from 0.50 to 0.44 of initial plate thickness, as impact velocity increased. The curve of Figure 35, page 68, represents equation (22) where, in each case, the values used for M_{snr} , the ejected plug mass, were obtained by weighing the ejected plugs. As can be seen, equation (22) represents the experimental data rather well. To render this equation useful, a relationship will have to be developed which will permit theoretical prediction of ejected plug mass.

The formula for residual velocity concerning oblique perforation of thick plates is obtained by modifying equation (22) in the same manner that equation (13) was modified to obtain equation (15). This results in the following general residual velocity equation for perforation of a plate by a cylindrical fragment:

$$V_r = \cos \beta \sqrt{\frac{V^2 - V_x^2}{\left[1 + \frac{M_{snr}}{M_p \cos \theta}\right] \left[1 + \Omega \frac{D^2}{d^2} \frac{T}{L \cos \theta}\right]}} \quad (23)$$

Plates Perforated by Penetrating Projectiles. The perforation process as outlined for blunt fragments is not characteristic of the perforation of a plate by a penetrating projectile such as an armor-piercing core. The penetrating projectile does not undergo the severe impact with the mass of the plate that represents the important portion of the first perforation step for the blunt fragment. It does not produce a shear plug. Instead, the projectile perforates relatively thin plate in the same manner that it penetrates a quasi-infinite thickness, by displacing and compressing material laterally. The energy balance for this case can be written as follows, using W to represent the work done:

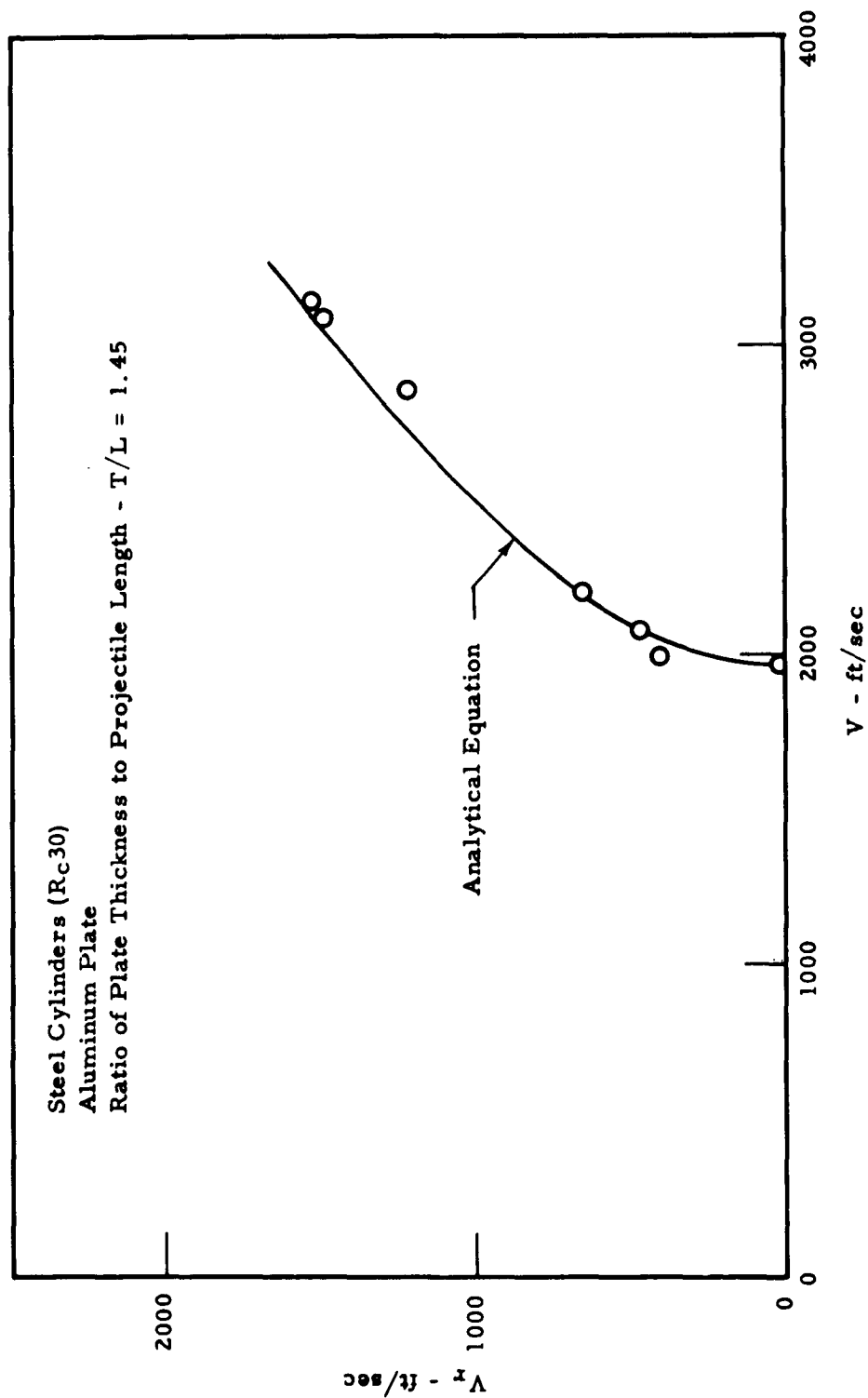


Figure 35. Post-Perforation Velocity of Cylindrical Fragments. Normal Impact with Thick Plates

$$\frac{1}{2} M_p V^2 = \frac{1}{2} M_p V_r^2 + W \quad (24)$$

If $V_r = 0$, $V = V_x$, and,

$$W = \frac{1}{2} M_p V_x^2 \quad (25)$$

The work required to displace the material is related to the dynamic shear strength and, thus, should not be highly velocity dependent. Again, the assumption is made that this work is essentially constant, which results in the following equation for the post-perforation velocity of penetrating projectiles at any impact obliquity:

$$V_r = \sqrt{V^2 - V_x^2} \quad (26)$$

This equation can be written in a form such that all data will plot on the same curve by dividing both sides by V_x . Thus,

$$\frac{V_r}{V_x} = \sqrt{\frac{V^2}{V_x^2} - 1} \quad (27)$$

Figure 36, page 70, shows the degree of correlation obtained from a limited test series involving armor-piercing projectiles.

The Angular Change in Direction, Penetrating Projectiles.

A series of sectioned photographs of armor plate penetrations and perforations is presented in a Watertown Arsenal Laboratory report.⁶ These photographs concern the lowest complete and highest partial penetrations - by AP projectiles for obliquity angles from 0 to 60 degrees. Plate thickness to projectile diameter ratios, T/d , range from 0.5 to 2.0. These photographs can be used to measure the emergent angles of projectiles which succeed in passing through the target plates. Since these measurements concern only the lowest complete penetration (perforation) velocity, the angular change in direction corresponds to β_x , the angle associated with the minimum perforation velocity. This angular change in direction, β_x , is not sensitive to the T/d ratio. Apparently the effects of increased plate thickness are offset almost

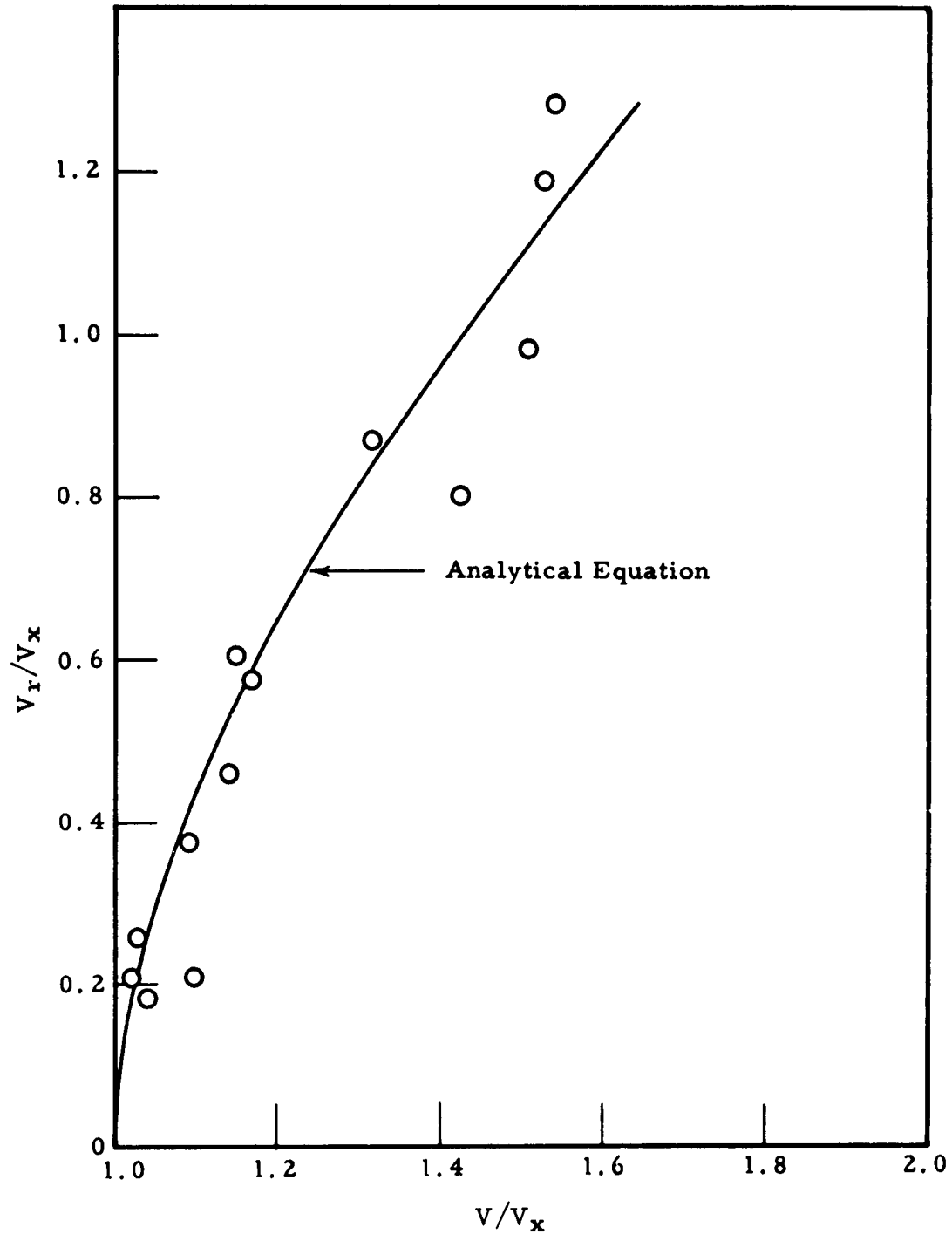


Figure 36. Post-Perforation Velocity of Sharp-Nosed Penetrating Projectiles - Normal Impact

exactly by the associated higher minimum perforation velocity. The derivation of equation (20) should apply to AP projectiles as well as to blunt cylinders; the assumptions made for the cylindrical fragments are consistent with the AP geometry or at least lead to the same results. Substitution of the values obtained for β_x from the WAL report into equation (20) results in the set of curves displayed on Figure A-23, page 35, in Part A of the Appendix. (All curves useful to grille analysis have been placed in Part A of the Appendix for convenience.)

Projectile Break-up. Armor-piercing projectiles break up during perforation in the manner discussed previously with regard to ricochet. The core material is very hard and very little plastic deformation occurs; fractures are brittle or unstable shear failures. The nose portion is likely to shatter into a considerable quantity of fragments while the butt fragments are likely to be large. The mild steel 0.50 caliber Ball core deforms and breaks up when fired against steel targets, but acts very nearly like an AP when penetrating aluminum. The soft 0.30 caliber Ball projectile deforms and breaks up readily during any sort of perforation. While a ring of metal is often sheared from the mushroomed FSP when perforating steel plate, the reduction of mass is usually comparatively small.

It will be important to determine whether or not an AP breaks up on impact. If it does not break up, it may continue on as an AP; if it does break up, subsequent impacts will be fragment impacts and will require different treatment during analyses. A grille design might incorporate built-in obliquity angles which would guarantee AP break-up, thereby reducing the potency of the AP.

The unpublished results of the National Science Foundation sponsored stress analyses which considered the stresses set up in ricocheting AP projectiles, were compared with experimental results. The comparison showed that when the tensile stress in the outer fiber exceeded the static tensile strength of the core material the projectile would break. This would be expected, since the dynamic tensile strength is very nearly equal to the static tensile strength in brittle materials such as the hard

(63 R_C) AP cores; increased strength due to the delay time associated with fracture is not pertinent since delay times are much shorter than the times associated with the impulse.⁷ The primary source of tensile stresses is the bending due to a resultant force component acting perpendicular to the axis of the projectile. This component produces a moment equal to the product of the lateral force and the perpendicular distance between its action line and the center of gravity of the core. Compressive axial loading decreases the tensile stress due to the bending torque to some extent; however, bending stresses increase so rapidly with impact obliquity that it is reasonable to ignore the stress contribution due to axial loading in compression.

The NSF analyses showed that at all obliquities the maximum stress occurred at a section very near the center of gravity. The bending force required to break up an AP at the section corresponding to the center of gravity can be computed as follows. Stress in the outer fiber due to bending is given by the flexure formula,

$$\sigma = \frac{M_r}{\bar{I}} = \frac{F_b \bar{x} r}{\bar{I}} = \frac{4 F_b \bar{x}}{\pi r^3} \quad (28)$$

Where,

σ is the maximum bending fiber stress - psi
(360,000 psi for R_C 63 cores)

M is the moment or torque acting about the C.G. -lb-in

r is the radius of the projectile -in.
(0.214 inches, 0.50 caliber core; 0.123 inches,
0.30 caliber core)

\bar{I} is the moment of inertia of a circular area about a
diameter - in⁴ $\left(\frac{\pi r^4}{4}\right)$

F_b is the applied resultant force component perpendicular
to the axis required to break the projectile -lb.

\bar{x} is the perpendicular distance between the C.G. and the
action line of F_b (≥ 0.7 inches, 0.50 caliber core;
 ≥ 0.4 inches, 0.30 caliber core) - in.

The lateral break-up force, F_b , as calculated for the two projectiles is 4000 lb. for the 0.50 caliber AP core and 1300 lb. for the 0.30 caliber core.

Now if the lateral force, F_t , acting upon the core can be determined, the ratio F_t/F_b will provide the required break-up information. If the ratio exceeds unity, the projectile will break; if it does not, the projectile will not break. The assumption that the lateral force is constant during the impact is conservative, since the maximum force will be somewhat higher than the average; thus, if the ratio exceeds unity, break-up is almost a certainty. The momentum triangle of Figure 30 (a), page 57, is appropriate to the analysis, if the plug mass, M_s , is set equal to zero. The lateral change in momentum will occur as the result of the application of the lateral force component, F_t , through the time of force application. This lateral change in momentum is,

$$\Delta (MV)_t = M_p V_r \sin \beta \quad (M_s = 0) \quad (29)$$

The maximum time of force application is a function of the maximum length through which the force could possibly be applied. This length is the sum of the length of the core and the thickness of the plate in the direction of perforation, or approximately $L_0 + T$. Average velocity in the direction of perforation is given by $\frac{1}{2} (V \cos \beta + V_r)$. Thus, the maximum time of the impulse is,

$$t = \frac{2 (L_0 + T)}{V \cos \beta + V_r} \quad (30)$$

And the minimum value of the lateral force is given by,

$$F_t = \frac{\Delta (MV)_t}{\Delta t} = \frac{M_p V_r \sin \beta (V \cos \beta + V_r)}{2 (L_0 + T)} \quad (31)$$

Using equation (28), the dimensionless ratio, F_t/F_b , becomes,

$$F_t/F_b = \frac{2 M_p V_r \sin \beta (V \cos \beta + V_r) \bar{x}}{\pi (L_0 + T) r^3 \sigma} \quad (32)$$

Equation (32) reduces to the following for the AP projectiles being considered:

$$F_t/F_b (0.50 \text{ cal.}) = 2.7 \times 10^{-6} \frac{(V_r \sin \beta)(V \cos \beta + V_r)}{T + 1.43} \quad (33)$$

$$F_t/F_b (0.30 \text{ cal.}) = 1.7 \times 10^{-6} \frac{(V_r \sin \beta)(V \cos \beta + V_r)}{T + 0.89} \quad (34)$$

Where,

V is impact velocity in ft/sec

V_r is residual velocity in ft/sec

M_p is core mass in slugs (1.8×10^{-3} and 3.7×10^{-4} ; 0.50 and 0.30 caliber AP)

L_o is core length in inches (length of equivalent cylinder) (1.43 and 0.89; 0.50 and 0.30 caliber AP)

Again, when these ratios exceed unity, break-up is virtually guaranteed. Ignoring the reduction in tensile fiber stress due to axial compressive stress is more than compensated by the two assumptions, (1) that lateral force is constant, and (2) that the force acts through the time required for the entire projectile to pass through the plate. These equations will be even more applicable to partial or edge impacts, since no reversal of torque is encountered during edge impacts.

3. Ballistic Perforation Dynamics; Partial or Edge Impact

The ability to assess dynamic conditions during an edge impact or partial strike is of utmost importance during grille evaluations, due to their frequent occurrence. Consider the simplest case, where a blunt cylindrical projectile strikes the edge of a plate of uniform thickness in a direction normal to the surface. If the projectile were to pass through the edge without deforming or deviating from its original direction, the plug sheared out would have the mass, bM_{sn} , where b is the ratio of the intercepted circular segment to the cross sectional area of the cylindrical projectile. Figure A-24, page 36, Part A. of the Appendix, shows the relationship between b and R , the distance between the projectile

centerline and the edge of the plate (R is positive when the centerline is off the plate, negative when the centerline is on the plate). The intercepted circumferential shear area is related to the full strike shear area by the ratio $\phi/360$, where ϕ is the angle in degrees subtended by the chord represented by the edge of the plate. (Figure A-26, page 38, in Part A of the Appendix displays this relationship graphically as a function of R . It will be noted that b and $\phi/360$ are equal when R is zero, or when R is maximum in either the positive or negative direction.

Residual Velocity Equation for Edge Impacts. It will be shown in Section 4 that the minimum perforation velocity or ballistic limit velocities can be determined quite satisfactorily for edge impacts of the simple type discussed above. This can be done even though the assumptions of unidirectional perforation and an irrotational projectile do not apply to real impacts.

In the real case of normal impact with an edge, as defined above, the projectile will change its direction. Thus, in order to use a minimum perforation velocity obtained from the unidirectional model, it is necessary, and very convenient, to define an equivalent edge whose surface is oriented in the direction normal to the post-impact direction. This procedure is especially useful when considering the myriad of possible edge impacts which can occur during a ballistic attack upon a grille. If all such edges can be reduced to equivalent edges of the simplified type, the dynamic analysis of an edge impact can be standardized and greatly simplified.

Assume that it is possible to define an equivalent edge as described in the previous paragraph. Only the component of the initial momentum of the projectile parallel to the post-impact direction (normal to the equivalent edge) will be involved in the edge perforation; the lateral component will be transferred to the plate. Thus, the perforation can be considered as a normal unidirectional perforation of the equivalent edge by a projectile having an initial velocity of $V \cos \beta$. Equation (13) for normal impact will apply if the indicated modifications are made. Substituting $V \cos \beta$ for V , V_{xne} for V_{xn} , and bM_{sne} for M_{sn} , results in the following equation for residual velocity of a cylindrical projectile,

$$V_r = \sqrt{\frac{V^2 \cos^2 \beta - V_{xne}^2}{1 + bM_{sne}/M_p}} \quad (35)$$

This equation can be modified for cylindrical fragments to,

$$V_r = \sqrt{\frac{V^2 \cos^2 \beta - V_{xne}^2}{1 + \Omega b \frac{T}{L}}} \quad (36)$$

Where Ω is the ratio of plate material and projectile material densities.

The ratio, $\frac{D^2}{d^2}$, is considered to be unity since it cannot be accurately accounted for; it is doubtful that it even applies to edge impacts.

Similar modifications can be made to equation (26) for edge impacts involving penetrating projectiles. As the angular change in direction increases, the penetrating projectile will be subjected to stresses which will cause break-up. Only when β is small will the projectile remain intact. When the projectile does not break up equation (26) takes the form,

$$V_r = \sqrt{V^2 \cos^2 \beta - V_{xne}^2} \quad (37)$$

for the same reasons given in the development of equation (35). In the event of break-up, the form of the equation should be the same; however, the value of V_{xne} will be higher. Use of the lower value of V_{xne} will be conservative in grille analyses since the prediction of residual velocity will be slightly high.

Equations (35) through (37) depend upon assumptions that need experimental confirmation. For this reason a short experimental program was performed. Figures 37 through 41, pages 77 through 81, display the resulting edge impacts. Caliber 0.50 FSP and APM 2 projectiles were fired normal to the surface of 1/2-inch steel armor plate in such a manner as to strike the edge. The armor plate was held in a pendulum capable of measuring the impulse transferred during impact. Velocity screens were

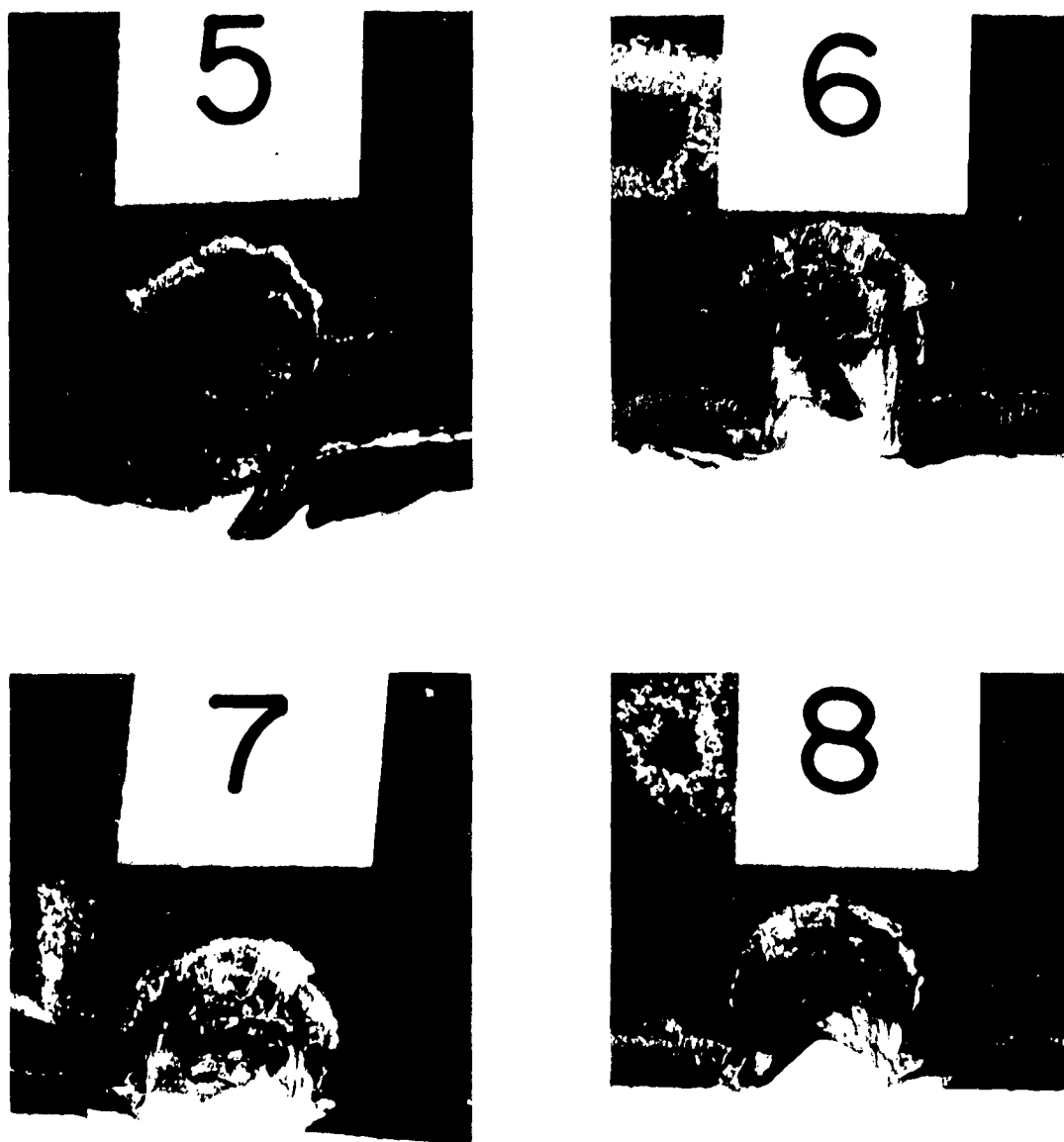


Figure 37. Edge Perforation. 0.50 Cal., 207-Grain WAL FSP
Fired Normal to Surface of 1/2-inch Homogeneous
Steel Plate MIL 12560. Tests 5, 6, 7, 8

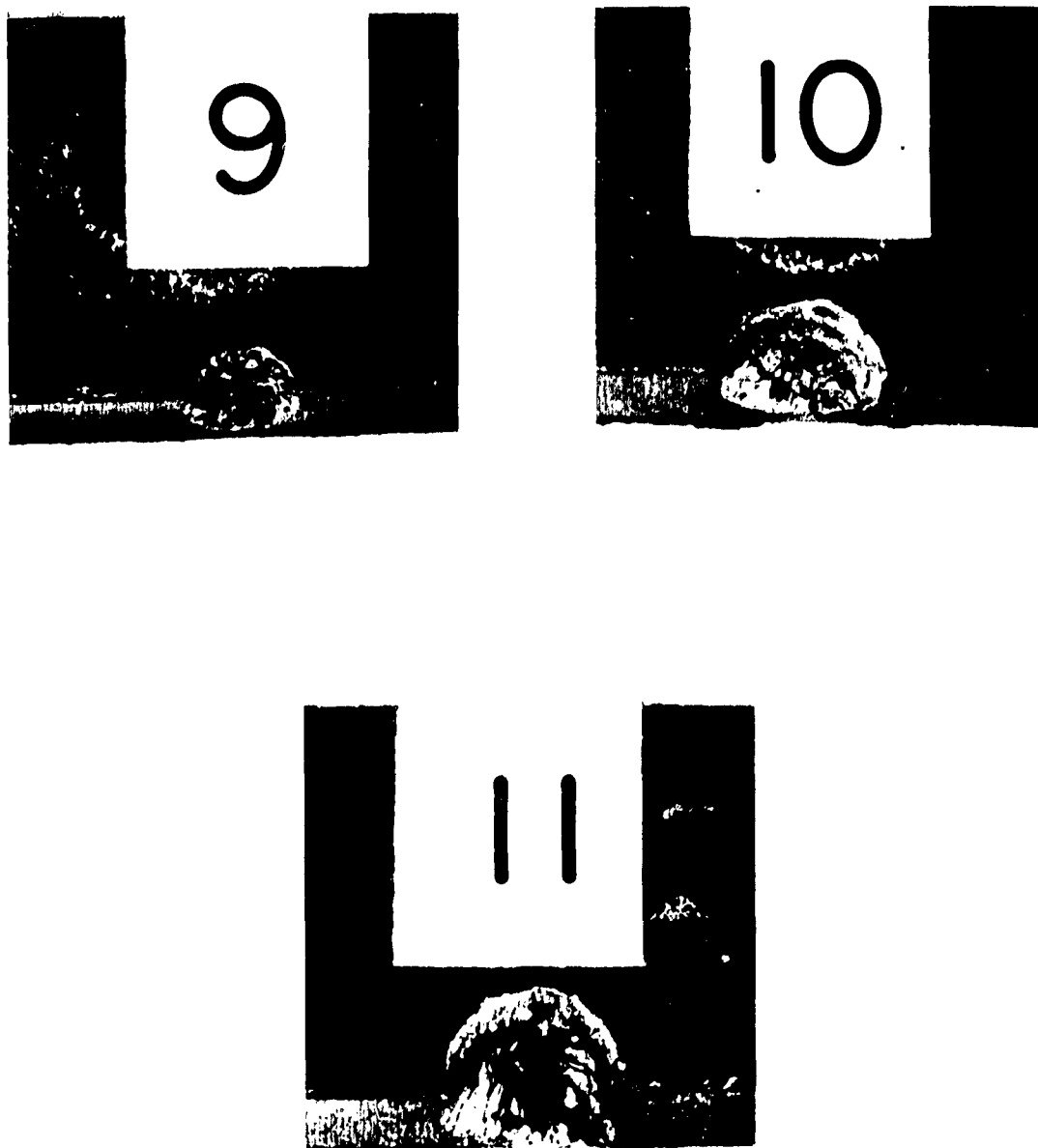


Figure 38. Edge Perforation. 0.50 Cal., 207-Grain WAL FSP
Fired Normal to Surface of 1/2-inch Homogeneous
Steel Plate MIL 12560. Tests 9, 10, 11

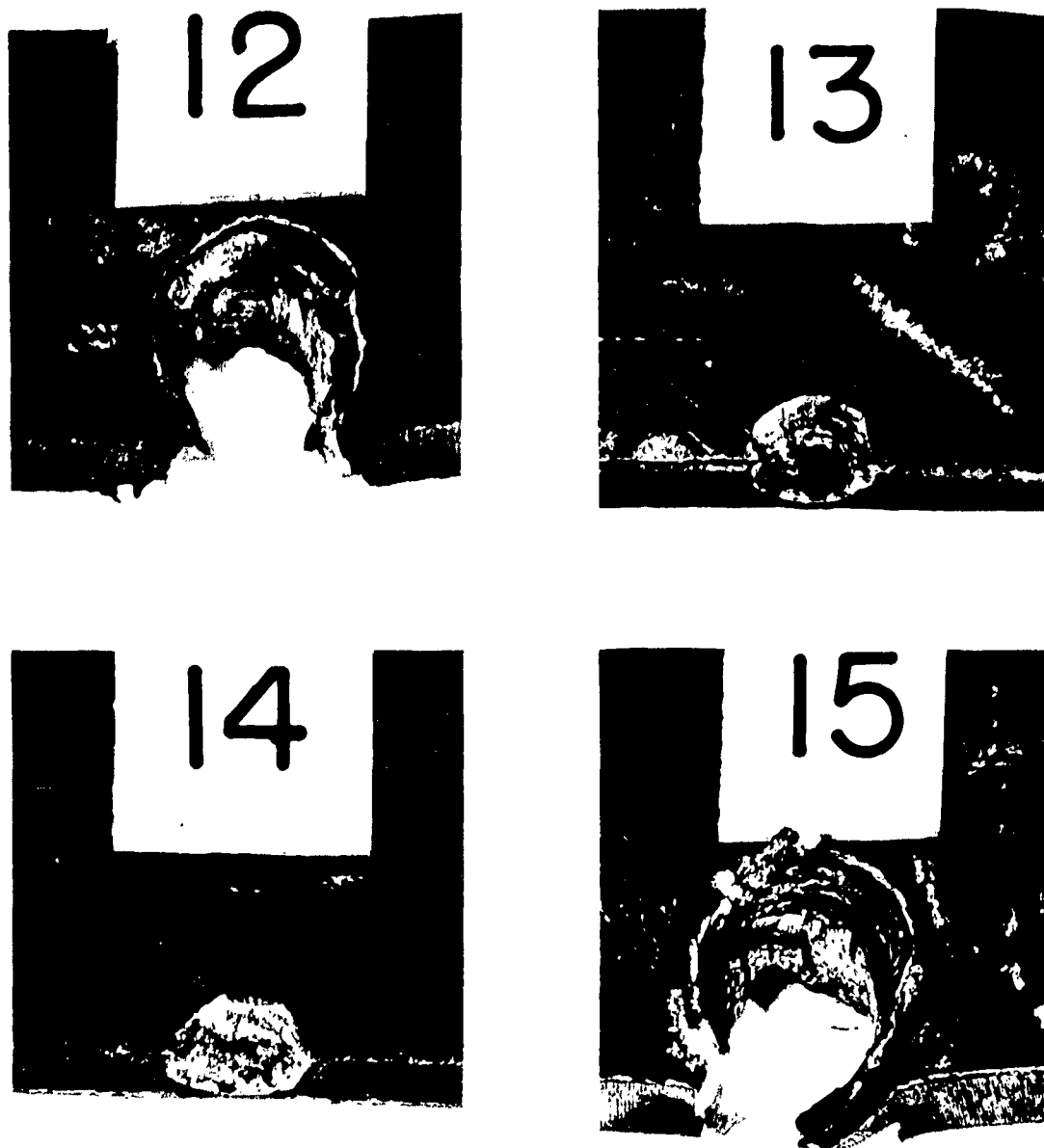


Figure 39. Edge Perforation. 0.50 Cal., 207-Grain WAL FSP
Fired Normal to Surface of 1/2-inch Homogeneous
Steel Plate MIL 12560. Tests 12, 13, 14, 15

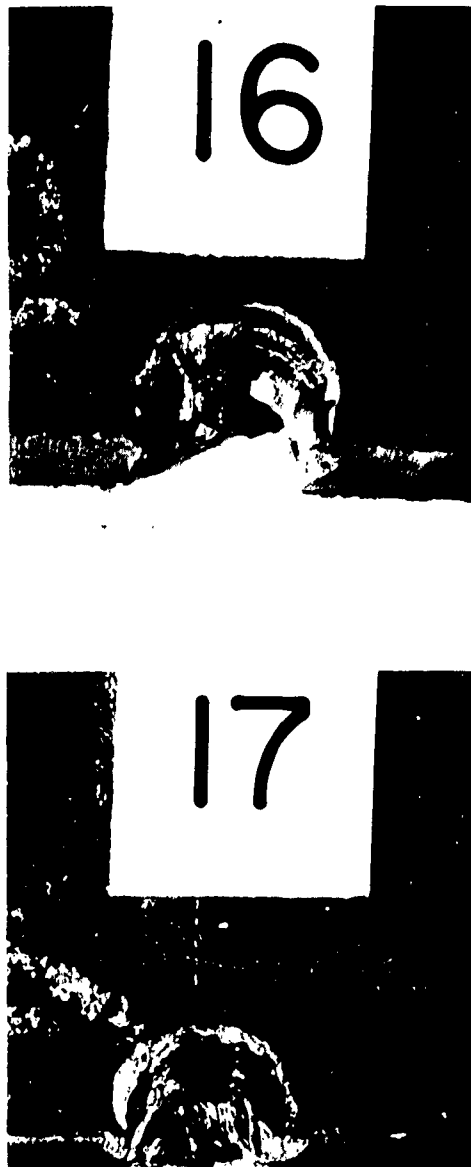


Figure 40. Edge Perforation. 0.50 Cal., 207-Grain WAL FSP
Fired Normal to Surface of 1/2-inch Homogeneous
Steel Plate MIL 12560. Tests 16, 17

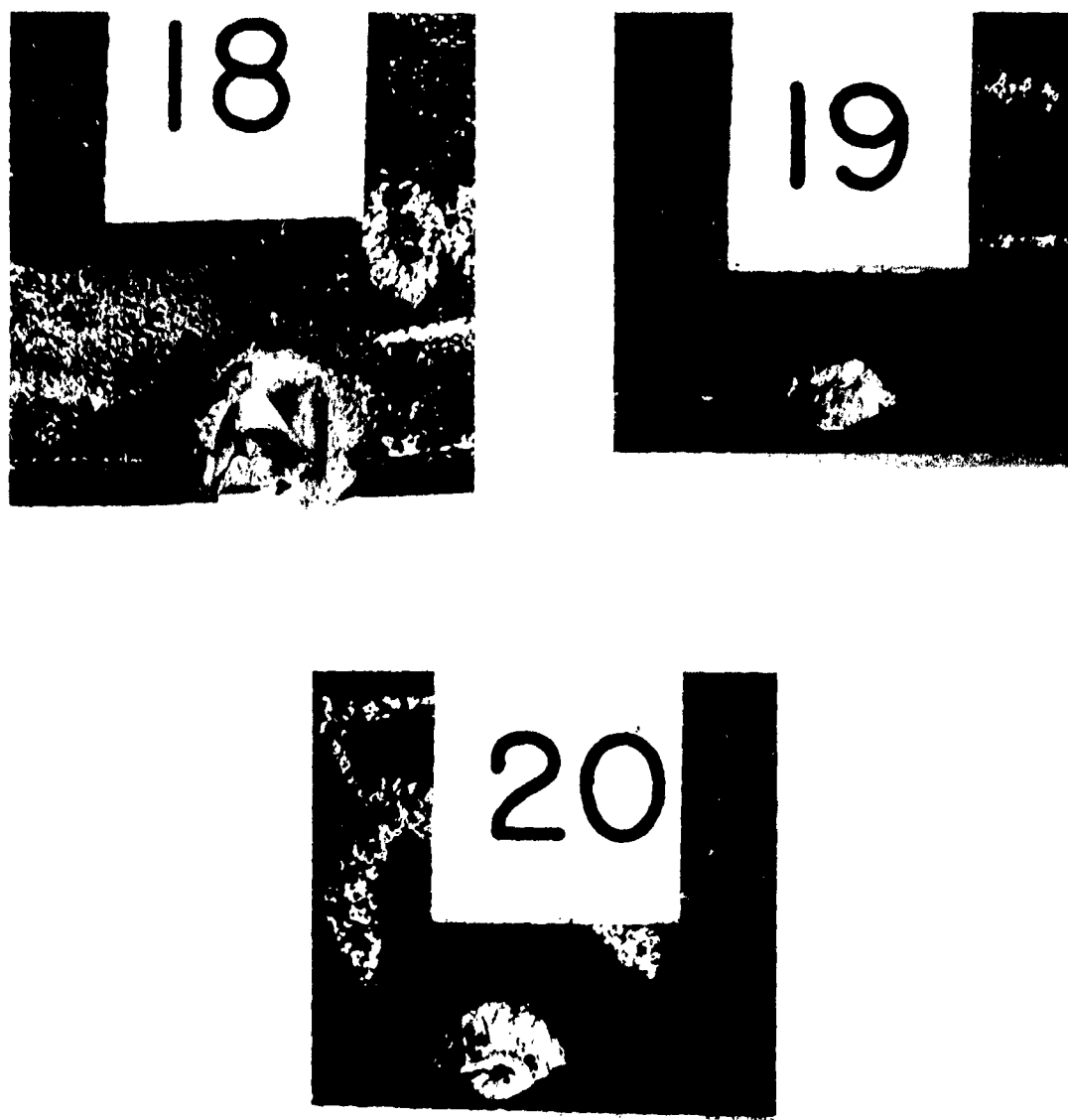


Figure 41. Edge Perforation. 0.50 Cal. APM 2 Projectile Fired Normal to Surface of 1/2-inch Homogeneous Steel Plate MIL 12560. Tests 18, 19, 20

used to measure the initial velocity of the projectile. Knowing the initial momentum, $M_p V$, and the impulse, I , transferred to the armor plate, momentum triangles may be constructed similar to that shown on Figure 30, page 57. The remaining momentum, $(M_p + M_s) V_r$, must be equal to that vector which closes the triangle. Assuming that the projectile and plate fragment have the same residual velocity and direction, the residual velocity may be obtained by dividing the remaining momentum by the sum of the masses of the projectile and fragment. The change in direction, β , is determined by the direction of the remaining momentum vector. In the table of test data, Table A-VIII, page 8, the values of the remaining momentum which were found for each test are shown on line 5 (in the Appendix).

In order to verify the residual velocity equations, expressions for the minimum perforation velocity had to be derived. These derivations will be presented in the following section. For FSP the derived equation is,

$$V_{xne} = \psi V_{xn\phi} \quad (38)$$

$$\text{Where, } \psi = \sqrt{\frac{L + bT}{L + \frac{\phi T}{360}}}$$

$V_{xn\phi}$ is the minimum perforation velocity for a full impact with a plate having a thickness equal to $\frac{\phi}{360} T$ (ft/sec).

For AP the derived equation is,

$$V_{xne} = \sqrt{b} V_{xn} \quad (39)$$

It is probable that equation (39) can be applied with confidence only when the centerline of the projectile intercepts the edge (R is negative). A conservative value may be obtained for positive values of R (centerline off the edge), by substituting $\phi/360$ for b in the equation.

The procedure for defining the equivalent edge will be presented in Section B, page 91. Equivalent thickness, T , for this case is taken to be the distance between (1) the intersection

of the pre-impact and the post-impact projectile path outlines (point m in Figure 42) and (2) the intersection of the post-impact projectile path outline and the exit surface (point n in Figure 42).

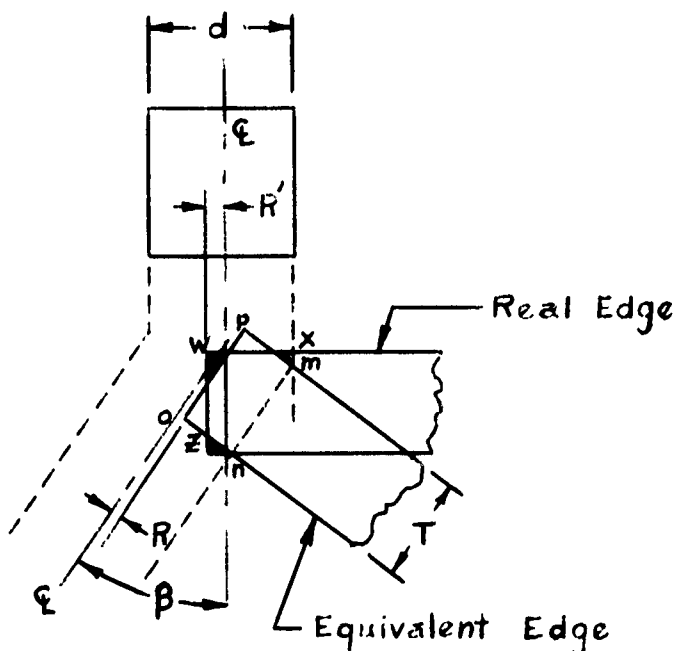


Figure 42
Equivalent Edge Construction for Edge Impact Tests

R' is the distance between the centerline of the pre-impact projectile path and the real edge. R is the distance between the centerline of the post-impact path and the equivalent edge. The position of the line $o-p$ on Figure 42, is determined by requiring the intercepted rectangle, $mnpz$, on the equivalent edge to have the same area as the intercepted area, $wxmz$, on the real edge.

Since β was determined experimentally, the impacts were diagrammed readily to obtain values of R . ψ , b and ϕ are functions of R and may be determined by referring to the appropriate graphs in Part A of the Appendix (Figures A-24 through A-30, pages 36 through 42). The pendulums measure

momentum. Equations (35) and (37) can be rearranged so that both sides will equal the remaining momentum, as follows:

$$(MV)_r = (M_p + bM_{sn\epsilon}) V_r = M_p \sqrt{V^2 \cos^2 \beta - V_{xn\epsilon}^2} \quad (35)(40)$$

(cylindrical projectiles)

$$(MV)_r = M_p V_r = M_p \sqrt{V^2 \cos^2 \beta - V_{xn\epsilon}^2} \quad (37)(41)$$

(AP projectiles)

These expressions can be further modified by substituting equations (38) and (39) for $V_{xn\epsilon}$.

$$(MV)_r = M_p \sqrt{V^2 \cos^2 \beta - \psi^2 V_{xn\phi}^2} \quad (35)(42)$$

(cylindrical projectiles)

$$(MV)_r = M_p \sqrt{V^2 \cos^2 \beta - bV_{xn}^2} \quad (37)(43)$$

(AP projectiles)

Equation (42) was used to compute values of remaining momentum for the tests performed with FSP. Equation (43) was used to compute values for the tests performed with AP. Table A-VIII in Part A of the Appendix, page 8, displays the results and provides a comparison of the observed and calculated remaining momentum values.

The average deviation, which includes experimental errors as well as errors imposed by the equations, was less than 3 percent for the tests involving FSP. The test apparatus cannot measure separately the momentum of the AP core and AP jacket; thus, the assumption that the jacket retains the same velocity as the core leads to high calculated values for remaining momentum. Note that the highest deviation (Test E-18, Table A-VIII) concerns an impact which approaches a full impact; in such a case, the jacket is always stripped from the core and has a much lower remaining velocity. Assuming the jacket to be stopped completely leads to a computed value of 3.34 lb-sec for remaining momentum; the observed experimental value lies in between the computed values as expected. The other AP impacts involved a much smaller segment of the edge and the deviations are much smaller.

The Angular Change in Direction, Partial Impact. The above test series also provides a limited amount of data concerning the angular change in direction, β , of the projectile as the result of the impact. This data is plotted on Figure A-31, page 43, Part A of the Appendix.

Projectile Break-up, Edge Impact. As stated in the previous section, equations (32) through (34) apply even more precisely to break-up during partial or edge impacts than they do to full impacts. The resultant lateral force always acts in the same direction on the projectile; this is not true, in general, of the full impact perforation due to the reversal of torque which may occur. The assumptions made for the analysis are, for this reason, more closely representative of the actual conditions. Equations (32) through (34) are conservative in the sense that break-up is almost guaranteed when the numerical value of the ratio, F_t/F_b , exceeds unity.

4. Minimum Perforation Velocity and Ballistic Limit Velocity

The minimum perforation velocity (V_x , V_{xn} , V_{xne}) used in the residual velocity equations is that impact velocity which will cause the projectile to perforate and pass completely through the plate or edge, emerging with no residual velocity. It is the maximum impact velocity which results in a zero residual velocity. In many instances, the minimum perforation velocity is nearly the same as a specific ballistic limit velocity. In the case of FSP, all of the usual ballistic limit velocities are not much lower than the minimum perforation velocity. Ballistic limit velocities concerning AP projectiles may be significantly lower than the minimum perforation velocity.

Perforation is an important term as used here. In the case of a large number of types of edge impact, the projectile will retain a residual velocity, no matter how low the impact velocity. However, unless there is a partial perforation of the edge, this is simply a ricochet; the residual velocity is not the result of the failure of the edge. No such problem of definition exists during full impact, since a ricochet is recognized instantly; the projectile never appears behind the plate unless the plate

fails. If the impact velocity exceeds the minimum perforation velocity of the edge, a partial perforation will occur; if it does not, a ricochet will occur. The residual velocity equations concerning perforation will apply only when the radical appearing in the equations is numerically real; i. e., equations (13) and (21).

Full Impact. The term, Army Ballistic Limit, usually refers to a ballistic limit velocity (impact velocity) based upon an armor perforation which will permit the passage of light. AP projectiles commonly succeed in perforating, on this basis, by penetrating armor plate to the extent of producing a small pinhole at the rear surface. Obviously, higher velocities are required to cause the projectile to pass through the plate. The Navy Ballistic Limit is based upon the passage through the plate of at least half of the projectile; for this reason the Navy Ballistic Limit velocity nearly coincides with the definition of the minimum perforation velocity. The Protection Ballistic Limit, now becoming an Army Ordnance standard, is based upon damage to a 0.020-inch Dural sheet placed at a specified distance behind the plate. Perforation of the Dural sheet by any fragment whatsoever is considered to be a complete penetration. For armor-piercing projectiles of plates, back-spalling does not occur and the Protection Limit velocity is very nearly equivalent to the minimum perforation velocity (the core must pass completely through the plate to perforate the Dural sheet). Blunt fragments may cause back-spall which will perforate the Dural sheet. Thus, for armor materials which spall readily, the Protection Limit may be lower than the minimum perforation velocity.

Either the Protection Ballistic Limit velocity or Navy Ballistic Limit velocity may be substituted for minimum perforation velocity in residual velocity equations. The expressions for residual velocity are insensitive to small variations in the value used for minimum perforation velocity except at impact velocities very near the minimum perforation velocity. Hence, either of the ballistic limit velocities will quite adequately represent the minimum perforation velocity. Experimentally determined values for the various ballistic limit velocities may be obtained from Figures A-32 through A-52, pages 44 through 64, in Part A of the Appendix.

These curves were plotted from curves and data originally obtained from Ordnance Tank Automotive Command and the referenced documents.^{8,9}

During ballistic analyses concerning blunt fragments, plug mass picked up during a full impact can effectively increase the projectile mass for a subsequent impact. Figures A-53 through A-55, pages 65 through 67, can be used to obtain the normal Army Ballistic Limit for WAL FSP having non-standard lengths. The normal Army Ballistic Limit is approximately equivalent to the minimum perforation velocity, V_{xn} for FSP. A good approximation of the minimum perforation velocity for oblique impact, V_x , can be obtained using equation (44).

Experimentally determined values of ballistic limit velocities automatically include the effects of projectile break-up at a given obliquity. At impact velocities exceeding ballistic limit velocities, break-up will occur at even lower obliquities. As impact velocities increase, the residual perforation velocity equations rapidly become insensitive to the value used for minimum perforation velocity (or ballistic limit velocity). Thus, it will not be important to change the value used for minimum perforation velocity in these equations.

In the case of fragment simulators perforating steel, the minimum perforation velocity or ballistic limit velocity at any obliquity can be estimated with the accuracy required for residual velocity calculations, by the following relation,

$$V_x = V_{xn} / \cos \theta \quad (44)$$

Table A-IX in Part A of the Appendix, page 9, provides verification for this observation. Hence, it is not necessary to consult ballistic limit data concerning other than normal impact. This same equation can also be used for FSP perforation of aluminum armor plate. Furthermore, the equation is almost exact for the case of AP projectile perforation of aluminum plate. As stated above, this relationship is especially useful when considering multiple impacts involving FSP, where the effective length of the projectile changes.

Minimum Perforation Velocity for Edge Impacts. In Section 3, equations (38) and (39) page 82, were presented, representing the minimum perforation velocities for FSP and AP respectively. In that section, the accuracy of the expression concerning FSP was adequately demonstrated by the results of an experimental test program. While the few tests performed with AP do not conclusively validate equation (39), the data does not argue with the calculated values, if the different residual velocities of the core and jacket are taken into account.

Equation (38) is derived as follows. Consider the simplest partial or edge perforation. A cylindrical projectile strikes the edge in a direction normal to the surface; the axis of the cylinder is parallel to the direction of motion. Assume that the projectile passes through the edge without tumbling, deforming, or changing direction, shearing out the segment of the edge intercepted by the projectile. The ejected plug mass is bM_{sn} (see Figure A-24, Part A of the Appendix, page 36).

Assume that the velocity of the projectile is the minimum perforation velocity, V_{xne} , for the edge. Temporarily, consider the plug mass to be unattached to the plate. For an inelastic collision between the projectile and the free plug, the equation for the free impact energy consumed is derived in exactly the same manner as equation (4), and is,

$$E_{fe} = \left[1 - \frac{M_p}{M_p + bM_{sn}} \right] \frac{1}{2} M_p V_{xne}^2 \quad (45)$$

which can be written in terms of the projectile dimensions as follows:

$$E_{fe} = \left[1 - \frac{L}{L + \Omega b T} \right] \frac{1}{2} M_p V_{xne}^2 \quad (46)$$

The dynamic shear strength is relatively insensitive to strain rate at high strain rates. Thus, the contribution of the circumferential shear area to the energy required for perforation will be essentially the same as that same contribution in the case of a full impact with the same total shear area.

This assertion rests upon the observation that the primary contribution to the energy consumed is made by the shear area during the first perforation step. This primary contribution is a force component which increases the deceleration force and pressure, and thereby increases the deformation of the projectile and plate. As noted in a previous section, the actual shear work associated with plug ejection (second perforation step) is negligible, except during perforation of very thin plates.

The equivalence of the energies consumed due to the presence of the circumferential shear areas in the edge and full impacts, defined above, provides the means for computing the value of this energy for edge impact. For the full impact with a plate of thickness $(\phi/360)T$, the energy consumed due to the presence of the shear area is the difference between the total perforation energy (at the minimum perforation velocity) and the free impact energy.

$$E_{s\phi} = \frac{1}{2} M_p V_{xn\phi}^2 - E_{b\phi} \quad (47)$$

Where the ϕ in the subscript refers to the full impact with a plate of thickness, $(\phi/360)T$, and T is the thickness of the edge.

Note again that equation (47) also defines the energy consumed due to the presence of the shear area during the edge impact. Substituting $(\Omega\phi/360)M_{sn}$ for M_{sn} , and V_{xn} for V , in equation (4) results in the expression for the free impact energy associated with the full impact.

$$E_{b\phi} = \left[1 - \frac{M_p}{M_p + \frac{\Omega\phi}{360} M_{sn}} \right] \frac{1}{2} M_p V_{xn\phi}^2 \quad (48)$$

which, in terms of the dimensions of the edge impact becomes,

$$E_{b\phi} = \left[1 - \frac{L}{L + \frac{\Omega\phi}{360} T} \right] \frac{1}{2} M_p V_{xn\phi}^2 \quad (49)$$

The total energy consumed during perforation at the minimum perforation velocity of the edge, $V_{xn\phi}$ is the sum of equations (46) and (47). Substituting equation (49) into equation (47), the equation for the total energy is,

$$\begin{aligned} \frac{1}{2} M_p V_{xn\epsilon}^2 = & \left[1 - \frac{L}{L + \Omega b T} \right] \frac{1}{2} M_p V_{xn\epsilon}^2 + \frac{1}{2} M_p V_{xn\phi}^2 \\ & - \left[1 - \frac{L}{L + \frac{\Omega \phi}{360} T} \right] \frac{1}{2} M_p V_{nx\phi}^2 \end{aligned} \quad (50)$$

Solving for the minimum perforation velocity of the edge results in the following equation:

$$V_{xn\epsilon} = \psi V_{xn\phi} = V_{xn\phi} \sqrt{\frac{L + \Omega b T}{L + \frac{\Omega \phi}{360} T}} \quad (51)$$

Where ψ represents the radical.

For the AP projectile, the edge impact is diagrammed using the procedure outlined on page 76, concerning the development of equations (35) and (37). An equivalent rectangular edge is defined whose surface is normal to the post-impact direction of the projectile. The impact is then treated as a unidirectional impact in the post-impact direction involving only the component of initial velocity in that direction, $V \cos \beta$. In this way the AP projectile encounters a mass, bM_{sne} , where M_{sne} is the mass of a full plug having the thickness of the equivalent edge. The AP projectile does not shear a plug, but pushes the material aside. If the plate mass is pushed aside during the unidirectional partial impact in the same manner as the same mass is pushed aside in a full impact, the energy required will be approximately proportional to the ratio of masses. This would be strictly true only if the partial impact involved sectors (pie-shaped) rather than segments; however, the assumption is still approximately correct. The equation which results from this assumption is written as follows:

$$\frac{1}{2} M_p V_{xn\epsilon}^2 = b \frac{1}{2} M_p V_{xn}^2 \quad (52)$$

Solving for $V_{xn\epsilon}$

$$V_{xn\epsilon} = \sqrt{b} V_{xn} \quad (53)$$

As long as the centerline of the projectile intercepts the edge (R is negative) this equation will represent the facts. See Figure A-25, page 37 in the Appendix. It should be reasonably accurate even when the centerline is off the edge (R is positive).

During grille analyses it may be advisable to substitute $\phi/360$ for b , when R is positive, to be conservative. In the usual case, the AP will break up during the first or second impact when the residual velocity is relatively insensitive to the value of the minimum perforation velocity. Thus, in the usual case, use of equation (53) will not affect the analysis significantly.

B. Procedure for the Ballistic Evaluation of Armored Grille Designs

Grilles are ballistically evaluated on paper in a manner similar to the way in which they are evaluated at a Proving Ground. A projectile is "fired" at the grille at a given velocity and orientation. It is usually easy to identify the two or three positions and attack angles which will most likely permit a projectile to defeat the grille; thus, only a few "rounds" need be fired to establish the minimum perforation velocity of a grille. The initial impact is analyzed to determine the residual velocity and new direction taken by the projectile. In the case of an AP projectile, a determination is also made concerning whether the projectile breaks up or not; if it does, subsequent impacts are considered from the standpoint of fragment attack rather than AP attack.

If the projectile is a fragment (Fragment Simulating Projectile), the plug it removes during a full impact perforation may add to the fragment mass; thus, in the instance of full impact it is conservative practice to add this mass to the projectile when considering the subsequent impact. When performing a ballistic analysis, the mass picked up during a given full impact perforation is added to the mass of the projectile (in terms of length) when subsequent impact is being considered. When an edge impact or ricochet occurs, plug masses will usually separate from the projectile; thus, the initial mass (in terms of length, L_0) of the projectile is used when considering the subsequent impact.

Occasionally, several normal full impact perforations will occur in sequence. In this case, the plug masses will remain with the projectile; the mass of the projectile (in terms of length) will be equal to the initial mass plus the masses accumulated in this fashion prior to the impact under consideration. Refer to the definition of projectile length, L , in Table I, page 93. (It is important to mention that ballistic impacts are highly inelastic so that this assumption is not overly conservative).

The analysis of impacts proceeds down through the grille until the projectile is defeated or defeats the grille. If the final residual velocity is low compared to the minimum perforation velocity (ballistic limit velocity) of the last impact, the minimum perforation velocity, V_{xg} , for the grille can be determined by setting the final residual velocity equal to zero, assuming the same path, and working backwards up through the grille to determine a new initial velocity. If the residual velocity is high, it is necessary to start over again with a slower projectile, determine the new path, and then work backwards using the new path, providing the new final residual velocity is low. In some cases (depending on the final impact or impacts) residual velocities up to 500 feet per second can be considered low. Working backwards along a previously determined path rarely requires more than five minutes if a computation form has been used; all constants have already been evaluated. (See Form 198-5, Figures 43, 44, and 45, pages 94, 95, and 96, which is used to analyze impacts.)

There are three distinct types of impact to be considered:

1. Full Impact Perforation
2. Partial (Edge) Impact Perforation
3. Ricochet

The first two involve the solution of pertinent equations (as derived in Section A, page 13) and referral to charts and graphs. Ricochet is handled empirically.

In the case of Partial Impact Perforation, the geometry of the edge is modified so as to create an equivalent rectangular edge impact. This equivalent edge is always oriented so that its upper and lower surfaces are perpendicular to the post-impact

TABLE I

GRILLE BALLISTIC ANALYSIS. DETERMINATION OF RESIDUAL VELOCITY AND CHANGE IN DIRECTION. FULL IMPACT PERFORMANCE.

$$\text{GENERAL EQUATION* } V_r = \frac{\cos \beta}{1 + \Omega D^2/d^2} \frac{T}{L \cos \theta} \sqrt{V^2 - V_x^2}$$

Equation No. (21) - FSP

Equation No. (26) - AP ($D^2/d^2 = 0$)

Guide to evaluation of equation parameters

PROJECTILE AND GRILLE MATERIAL

Parameter	WAL FSP			APM 2			0.50 Cal. Ball M 2		
	Steel MIL 12560	Alum. MIL 46027	Titanium 6Al-4V	Steel MIL 12560	Alum. MIL 46027	Titanium 6Al-4V	Steel MIL 12560	Alum. MIL 46027	Titanium 6Al-4V
β	Fig. No. A-22	Fig. No. A-22	Fig. No. A-22	Fig. No. A-23	Fig. No. A-23	Fig. No. A-23	Fig. No. A-22	Fig. No. A-23	Fig. No. A-22
Equation (20)	1.00	0.34	0.57	-- not required --			1.00	not req'd.	0.57
D^2/d^2	Assume to be unity. This predicts a slightly high residual velocity and is conservative. Assume to be zero when T/L exceeds unity; plug will be much shorter than T .			0	0	0	Assume zero. Plug will be small compared to projectile.		
L	Initial projectile length plus plug from previous full impact perforation. (If several normal full impacts occur immediately before impact being considered, all such plugs should be added to the projectile mass in terms of length. If previous impact is an edge impact or ricochet use only initial projectile length, L_0 .) $L_0 + (D^2/d^2 \frac{\Omega T}{\cos \theta})^{n-1}$			-- not required in equation for AP --			-- not required in equation for Ball --		
T and θ	See Fig. Nos. 46 & 47 (A-56 & A-57)			See Fig. Nos. 46 & 47 (A-56 & A-57) Required only for calculation of V_x and β			See Fig. Nos. 46 & 47 (A-56 & A-57) Required only for calculation of V_x and β		
V_x See Equation(44)	V_{xa} , V_{xp} , V_{xc} or $V_{xn}/\cos \theta$ If $L > L_0$ value for V_x must be obtained to correspond with L (not L_0). Use $V_{xn}/\cos \theta$ If $L > L_0$			V_{xp} or V_{xc}	V_{xp} , V_{xc} or $V_{xn}/\cos \theta$	V_{xp} or V_{xc}	V_{xp} or V_{xc}	Same as APM 2	V_{xp} or V_{xc}
V_{xn}	Fig. No. A-53 Use L (Not L_0)	Fig. No. A-54 Use L (Not L_0)	Fig. No. A-55 Use L (Not L_0)	Fig. Nos. A-32, A-33 A-38, A-39	Fig. Nos. A-34, A-35	Fig. Nos. A-36, A-37	No Data	Same as APM 2	No Data
V_{xp} (Protection)	No Data	No Data	Fig. Nos. A-50, 51, 52	Fig. Nos. A-32, A-33	Fig. Nos. A-34, A-35	Fig. Nos. A-36, A-37	No Data	Fig. Nos. A-34, A-35	No Data
V_{xc} (Navy)	No Data	No Data	No Data	Fig. Nos. A-38, A-39	No Data	No Data	No Data	Same as APM 2	No Data
V_{xa} (Army)	Fig. Nos. A-44, A-45 A-46	Fig. Nos. A-47, A-48 A-49	No Data	Do not use Fig. Nos. A-40 A-41	Do not use Fig. Nos. A-42, A-43	No Data	No Data	Same as APM 2	No Data

* Equation (21) is not completely general since it assumes that projectile mass remains constant and plug mass has a constant length, T . See equations (22) and (23). Equation (21) is used because it is easily evaluated and it is completely adequate for grille analyses.

COMPUTATION SHEET
V_r EQUATIONS

1/3

FULL IMPACT				PARTIAL IMPACT			
TYPE OF IMPACT				TYPE OF IMPACT			
IMPACT NO. - 11				IMPACT NO. - 11			
①	T			T			①
②	$L = L_0 + \frac{24(n-1)}{T/L}$			$L = L_0 + \frac{24(n-1)}{T/L}$	FSP		②
③	$T/L = \frac{1}{2}$			$T/L = \frac{1}{2}$	FSP		③
④	Θ			β (FROM SHEET 1/3)			④
⑤	$\cos \Theta = \cos ④$			R			⑤
⑥	V_{xn}			b			⑥
⑦	$V_x = \frac{⑥}{⑤}$			$Vb = \sqrt{⑥}$	AP/BALL FSP		⑦
⑧	$V_x - AP \& BALL$			$V_{xn} @ T = ①$			⑧
⑨	V			$V_{xns} = ⑦ \times ⑧$			⑨
⑩	$V/V_x = ⑨/V_x$			$⑨/360$			⑩
⑪	β			$① \times ⑩ = \frac{⑧ T}{360}$			⑪
⑫	Θ_r			$V_{xns} = V_{xn} @ T = ⑪$			⑫
⑬	$V^2 = ⑨^2$			ψ			⑬
⑭	V_x^2			$V_{xns} = ⑫ \times ⑬$			⑭
⑮	$V^2 - V_x^2 = ⑬ - ⑭$			V			⑮
⑯	$W^2 - V_x^2 = \sqrt{⑮}$			$\cos \beta = \cos ④$			⑯
⑰	$\cos \beta = \cos ⑪$			$V \cos \beta = ⑮ \times ⑬$			⑰
⑱	$⑮ \times ⑰ = V_r (AP, BALL)$			$V^2 \cos^2 \beta = ⑰^2$			⑱
⑲				V_{xns}^2			⑲
⑳	$\frac{\Omega}{D^2/d^2}$			$⑱ - ⑲$			㉑
㉑	$\Omega \frac{D^2}{d^2} = ⑲ \times ⑲$			$V_{20} = V_r (AP, BALL)$			㉑
㉒	$\Omega \frac{D^2}{d^2} \times T = ⑲ \times ⑲$			Ω			㉒
㉓	$\frac{⑲}{\cos \Theta} = \frac{⑲}{③}$			$kTb\Omega = ⑲ \times ⑲$	FSP ONLY		㉓
㉔	$\frac{⑲}{L} = \frac{⑲}{②}$			ZERO FOR PARTIAL IMP			㉔
㉕	$⑲ + 1.0$			$\frac{⑲}{L} = \frac{⑲}{②}$			㉕
㉖	$1/⑲$			$⑲ + 1.0$			㉖
㉗	$V_{r(FSP)} = ⑱ \times ⑲$			$1/⑲$			㉗
㉘	$V_r (RICOCHET) *$			$V_{r(FSP)} = ⑲ \times ⑲$			㉘

FORM 198-5 (*USE FOR RICOCHET) DENVER RESEARCH INST.

PROJECTILE - _____

GRILLE - _____

Figure 43. Grille Ballistic Analysis Computation Form. Form 198-5. Sheet 1/3

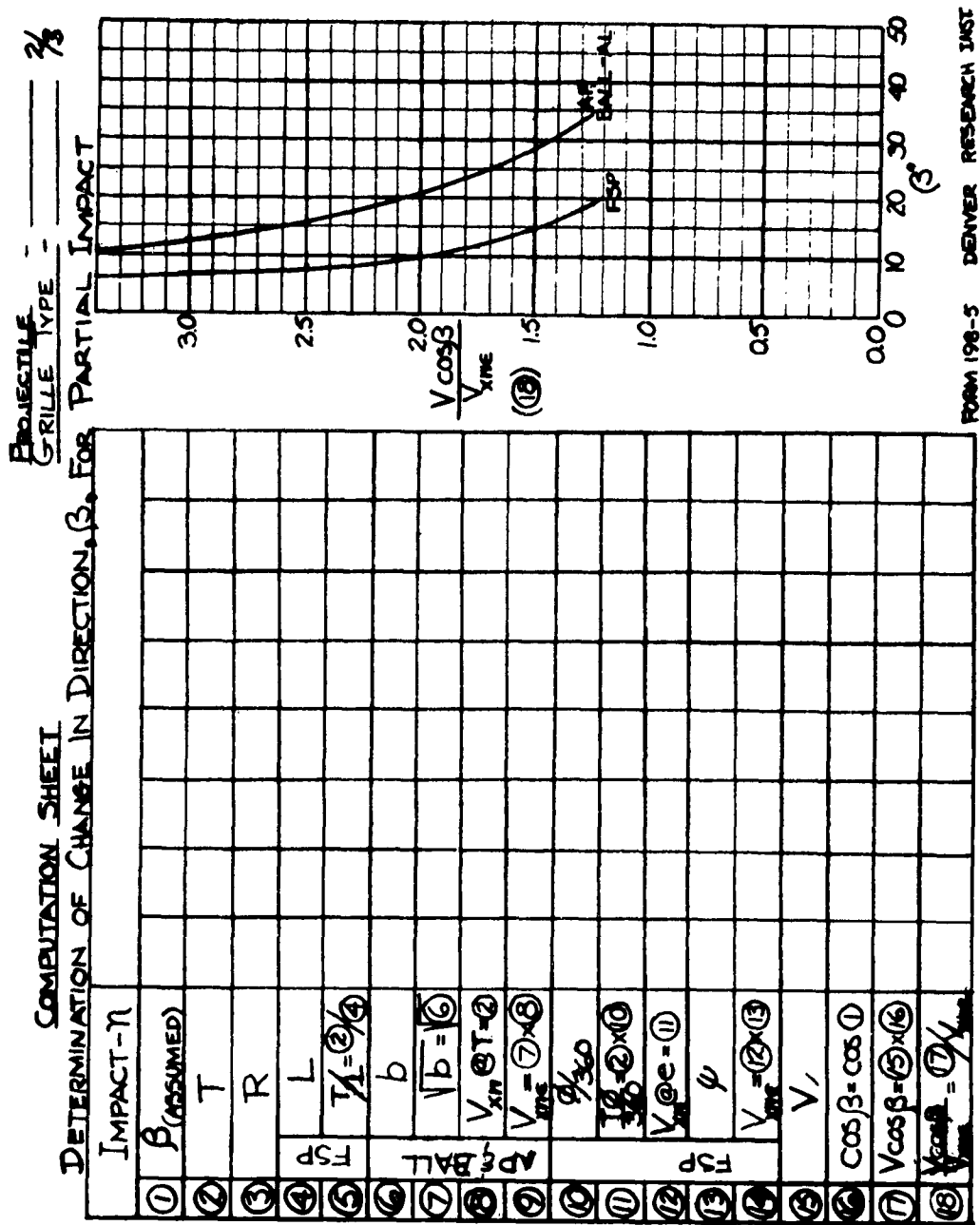


Figure 44. Grille Ballistic Analysis Computation Form. Form 198-5. Sheet 2/3

COMPUTATION SHEET

DETERMINATION OF AP PROJECTILE BREAK-UP

(IF $F_c/F_b > 1.0$ PROJECTILE
WILL BREAK)

* FULL IMPACT					* PARTIAL IMPACT				
IMPACT NO. - n					IMPACT NO. - n				
32	$V \cos \beta = 9 \times 17$					$V \cos \beta = 17$			32
31	$V_r = 18$					$V_r = 21$			31
32	$V \cos \beta + V_r = 30 + 31$					$V \cos \beta + V_r = 32 + 31$			32
33	$\sin \beta = \sin 11$					$\sin \beta = \sin 4$			33
34	$V_r \sin \beta = 31 \times 33$					$V_r \sin \beta = 21 \times 33$			34
35	32×34					32×34			35
36	$C, **$					$C, **$			36
37	35×36					35×36			37
38	$L, **$					$L, **$			38
39	$T = 1$					$T = 1$			39
40	$L_p + T = 38 + 39$					$L_p + T = 38 + 39$			40
41	$F_c/F_b = 37/40$					$F_c/F_b = 37/40$			41

FORM 198-5

DENVER RESEARCH INST.

* NUMBERS LESS THAN 30 REFER TO SHEET 1/3

** 0.30 CAL. AP; $C_1 = 1.7 \times 10^{-6}$, $L_0 = 0.89$ INCHES0.50 CAL. AP; $C_1 = 2.6 \times 10^{-6}$, $L_0 = 1.43$ INCHES

PROJECTILE - _____

GRILLE - _____

Figure 45. Grille Ballistic Analysis Computation Form. Form 198-5. Sheet 3/3

direction of the projectile or fragment. Since the post-impact direction is not known beforehand, a trial and error procedure has been developed by which it can be determined. Several post-impact directions are assumed and the ratio of the normal component of the impact velocity ($V \cos \beta$) to the minimum perforation velocity (V_{xn}) of the equivalent edge in the assumed direction is computed for each direction. The results are superimposed upon a plot of this ratio as a function of β which was determined by a firing program, Figure No. A-31, page 43, in Part A of the Appendix. A smooth curve is plotted through the points; the intersection of the curve, which is characteristic of the edge, and the plotted experimental curve reveals the value of β , the angular change in direction. If the ratio, V/V_{xn} in the initial direction ($\theta = 0$) is greater than 4.0, β can be assumed to be zero without computation.

With the general procedure in mind it will now be well to consider each type of impact in detail.

1. Perforation - Full Impact.

Equation (21) page 60 permits computation of the residual post-impact velocity, V_r . The values to be assigned to each parameter in the equation depend upon the projectile type and size, the armor material, and the initial dynamic conditions. They are obtained by referring to a variety of graphs, and in some instances, additional computations are involved. Table I, page 93, completely defines the means by which each parameter is evaluated and provides a guide to the proper charts and graphs to be used for a particular type of impact. Form 198-5, Figures 43, 44 and 45, pages 94, 95 and 96, is merely a means by which the equation can be solved in an orderly fashion; it also provides a standard record of each ballistic analysis. In some instances, often in the case of AP, the computation is so simple that the form need not be used; the computation can be shown directly on the Firing Sheet (a drawing of the grille assembly cross section), upon which the shot is diagrammed directly over the grille outline. However, it is convenient to record the impact on the form, since equation (26), which concerns the AP projectile against steel and aluminum and the 0.50 caliber Ball projectile against aluminum, is the same as equation (21) with D^2/d^2 set equal to zero; thus, Form 198-5 can be used to compute the radical portion of equation (21) and to record the impact.

The values of the equivalent thickness, T , and obliquity, θ , depend upon the manner in which the projectile impacts the target. Figures 46 and 47, pages 99 and 100, illustrate the procedures used in diagramming impacts. These procedures are based upon detailed studies of all possible types of impact; to guarantee uniformity in the ballistic analyses, the diagramming rules should always be observed when possible. Each of the diagrams considers a free impact with an isolated edge. Confinement of the projectile by other edges will obviously require modification of diagramming procedures. Often edges will consist of two materials, i. e., steel and aluminum. Usually, it is apparent as to what modifications are required; practice leads to confidence in making these modifications and it is impractical to try to consider, in detail, every possible exception to the rules.

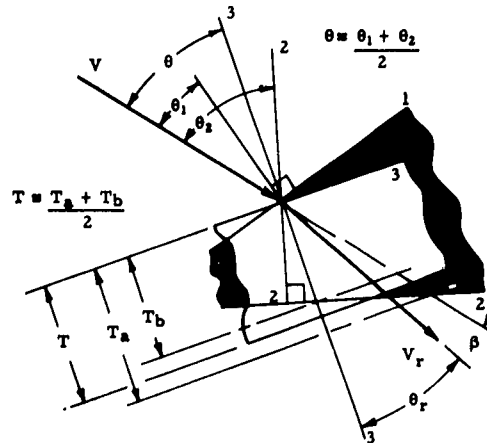
When considering a full impact it is not always possible to diagram the impact as shown, Figure 46 (a), page 99. It is often advisable to consider the full impact to be a partial impact treated as illustrated in Figure 47 (b), page 100. The rules which apply in this case are exactly the same as those which apply to partial impacts. Since partial impact will be considered subsequently, no further discussion is required here.

Where it is possible to diagram the full impact in the standard manner, Figure 46 (a) applies. If the impact and rear surfaces are irregular, straight lines are drawn to represent the surfaces (best fits for the irregular lines within the path outlines). Since the point of emergence is not exactly known, the straight line representing the rear surface must be based on an estimate of the position of path outlines; usually this estimate will be quite adequate. If an equivalent plate can be defined which accurately represents the edge, the equations for residual velocity and angular change in direction, based on uniform plates, can be used to obtain accurate values of V_r and β .

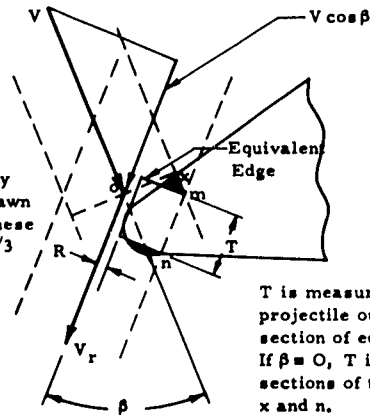
Except for the fact that the rear surface is not parallel to the impact surface, the perforation is the same as that illustrated in Figure 29 (b), page 49. As demonstrated in the discussion of perforation, Section A. 2, page 48, primary deceleration of the projectile and acceleration of the plug occur very early in the

(a) FULL IMPACT

(See also, Figure 47(b)
Impact treated as a
partial)

(b) PARTIAL IMPACT

Turning point o is determined by drawing a perpendicular to the projectile centerline through x (the first intercept of edge and projectile outline). The value of β must be determined by trial. Several diagrams are drawn using assumed values for β . These diagrams are used with sheet 2/3 of the Ballistic Analyses. Form 198-5, to find the actual value of β graphically.



Dark area on grille bar equals area of equivalent edge which is off bar

T is measured from (1) the intersection of projectile outlines at m and (2) the intersection of edge and projectile outline at n. If $\beta = 0$, T is the distance between intersections of the projectile outline and edge, x and n.

R is (+) when \mathcal{Q} is off edge

R is (-) when \mathcal{Q} is on edge

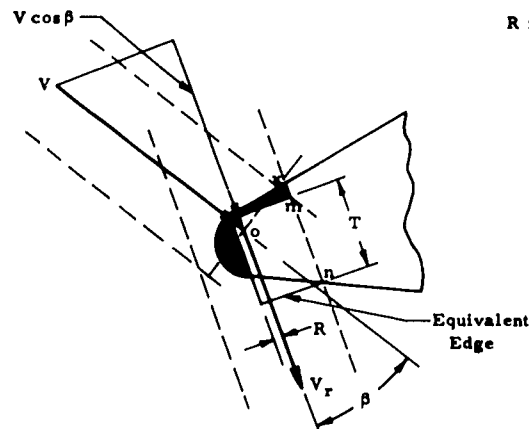
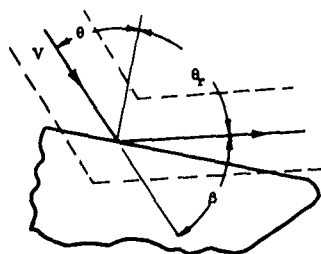
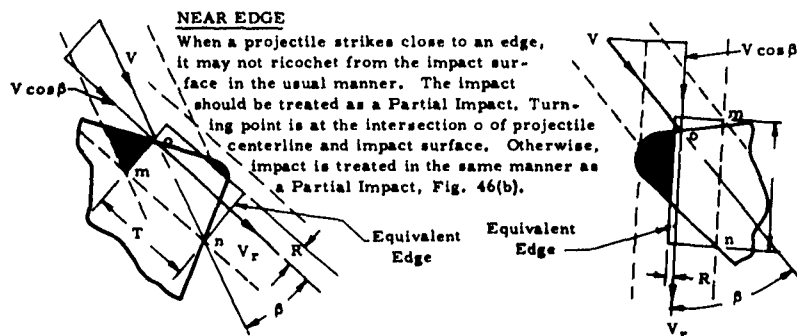
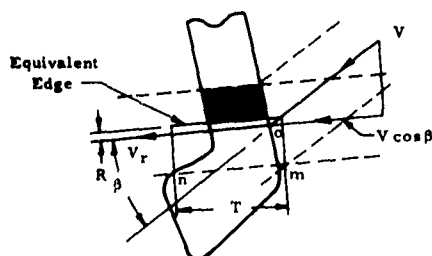


Figure 46. Grilled Ballistic Analysis. Procedures for Diagramming Impacts. Full and Partial (Edge) Impacts

(a) RICOCHET(b) FULL IMPACT TREATED AS A PARTIALIRREGULAR SHAPE

Often it is difficult to diagram the Full Impact as shown in Fig. 46(a). It is then convenient to diagram the impact as a partial. Turning point o is at intersection of projectile centerline and impact surface. β is determined in the manner shown for Partial Impacts, Fig. 46(b).

Figure 47. Grille Ballistic Analysis. Procedures for Diagramming Impacts. Ricochet and Full Impacts which are Treated as Partial Impacts

perforation. The second perforation step, during which the plug is sheared from the plate, occurs after the projectile and plug have attained nearly identical velocities. Thus, the turning point associated with the change in direction is near the impact surface as shown on Figure 29 (b) and Figure 46 (a), page 99. When a projectile strikes a uniform plate, the obliquity of strike is the same for both impact and rear surfaces. If the impact and rear surfaces are not parallel this is no longer the case. The obliquity angles θ_1 and θ_2 represent the two obliquities associated with the impact and rear surfaces on Figure 46 (a). The rear surface will influence the shear angle of the second perforation step just as much as the impact surface will, i. e., the direction of shear is a function of (1) the shear area encountered in any given direction and (2) the shearing stress in that direction. Thus, the equivalent plate should be oriented at the average value of θ given by $\frac{\theta_1 + \theta_2}{2}$.

This holds even when the perpendiculars to the surfaces, drawn through the impact point, lie on either side of the velocity vector; θ_1 and θ_2 would have opposite signs in such a case. Evaluation of sign need be of no concern in diagramming, since it is only necessary to geometrically bisect these perpendiculars to obtain the perpendicular associated with the equivalent plate. This procedure is consistent with a uniform plate impact since the average value of the impact and rear surface obliquities is the impact obliquity, θ .

The projectile will emerge somewhere between the perpendicular to the equivalent plate and the original trajectory line. If it proceeds straight through, it will encounter a plate thickness, T_a ; if it proceeds in the direction normal to the equivalent plate, it will encounter a plate thickness, T_b . The average value, $\frac{T_a + T_b}{2}$, will be very close to the plate thickness actually en-

countered since T_a and T_b will rarely differ greatly from this average. Use of the average is usually conservative during grille analyses since β is almost always smaller than θ_r ; the plate thickness encountered will be slightly greater than the average value for the type of impact shown in Figure 46 (a).

To construct the equivalent impact, draw perpendiculars 1 and 2 through the impact point as shown on Figure 46 (a). Bisect these perpendiculars with perpendicular 3 and draw the impact surface 3 of the equivalent edge. (Or, more simply, orient the impact surface 3 to intersect the impact point at an angle equal to one-half the angle between the actual impact and rear surfaces.) Draw two parallels to impact surface 3 which pass through the points of intersection of the original trajectory, and perpendicular 3, with the actual rear surface. Draw the equivalent rear surface parallel to and midway between these two parallel lines. Residual velocity, V_r , and change in direction, β , can now be found as indicated in Table I which concerns full impact with uniform plates.

2. Perforation - Partial Impact

Equation (36) page 76, applies to partial (edge) impacts as derived from the general expression for full impact perforation. Values for the parameters are found in the manner indicated on Table II, page 103. It is important to understand that the equation as written, applies to an equivalent impact defined by an equivalent rectangular edge which the projectile strikes normally and passes through unidirectionally in the post-impact direction. For this equivalent impact, the component of impact velocity, $V \cos \beta$, which is parallel to the post-impact direction is taken as the impact velocity for the equivalent edge. The minimum perforation velocity, V_{xne} , for the edge in the post-impact direction is obtained as indicated on Table II.

The accuracy of this procedure for determining the residual velocity, V_r , for FSP and AP was experimentally confirmed. Results of this test program are discussed in Section A. 3, page 76, and presented on Table A-VIII, page 8 in Part A of the Appendix.

As shown on the diagrams of partial impact Figure 46 (b), page 99, the projectile turning point is determined by the intercept at x , of the projectile outline and the edge (which is carried over to the projectile centerline at o). β is not known and it must be determined by a graphical solution. Several values of β are assumed, and T and R are determined for each case. The equivalent impact plate thickness, T , is measured on the bar as the distance between m ,

TABLE II

GRILLE BALLISTIC ANALYSIS. DETERMINATION OF RESIDUAL VELOCITY AND CHANGE IN DIRECTION.
PARTIAL OR EDGE IMPACT PERFORMANCE

$$\text{GENERAL EQUATION*} \quad V_r = \frac{1}{1 + k \frac{\Omega}{b} \frac{T}{L}} \sqrt{V^2 \cos^2 \beta - V_{xn}^2}$$

Equation No. (36) FSP
Equation No. (37) AP ($k = 0$)

Parameter	Guide to evaluation of equation parameters									
	PROJECTILE					AND GRILLE MATERIAL				
	WAL FSP		APM 2			0.50 Cal. Ball M 2				
	Steel MIL 12560	Alum. MIL 46027	Titanium 6Al-4V	Steel MIL 12560	Alum. MIL 46027	Titanium 6Al-4V	Steel MIL 12560	Alum. MIL 46027	Titanium 6Al-4V	
k	1	1	1	0	0	0	1	0	1	
Ω	1.00	0.34	0.57	--	Not required --	--	1.00	Not req'd.	0.57	
b	Figure No. A-24						Figure No. A-25			
T and θ	See Fig. Nos. 46 & 47 (A-56 & A-57)			See Fig. Nos. 46 & 47 (A-56 & A-57)			See Fig. Nos. 46 & 47 (A-56 & A-57)			
L	$L_0 + (D^2/d^2) \frac{\Omega T}{\cos \theta}$	$\frac{n-1}{\cos \theta}$		Not required in equation for AP			Not required in equation for Ball			
β	Same as L in Table I									
	Use computation sheet 2/3 (Form 198-5, Figure 44). Estimate values of β and compute corresponding values for $V \cos \beta$, line 18. Plot values on the graph on sheet 2/3. Draw a curve through the plotted values. The intersection of the plotted curve and the appropriate (AP or FSP) curve reveals the value to be used for β .									
V_{xn}	See Figure No. A-31. Multiply $V_{xn}\phi$ by ψ See Equation (51)			$\sqrt{b} V_{xn}$ See Equation (53) To be conservative it may be advisable to substitute $\phi/360$ for b when R is positive (+)			$\psi V_{xn}\phi$ Same as FSP	$\sqrt{b} V_{xn}$ See Equation (53)	$\psi V_{xn}\phi$ Same as FSP	
$V_{xn}\phi$	V_{xn} for plate thickness = $\frac{\phi}{360} T$ See Equation (47) Fig No. A-53	Fig. No. A-54	Fig. No. A-55				Same as 0.50 cal. FSP. Use $L = 1.0$ Fig. No. A-53	Not applicable	Same as 0.50 cal. FSP. Use $L = 1.0$ Fig. No. A-55	
V_{xn}	Same as indicated in Table I. If $L > L_0$ use L to obtain V_{xn}									
ψ	Fig. Nos. A-28, 29, 30			Not applicable			Fig. No. A-29	Not applicable	Fig. No. A-29	
$\phi/360$	Figure No. A-26			Figure No. A-27			Fig. No. A-27	Not applicable	Fig. No. A-27	

* The equation depends upon the construction of an equivalent edge and involves a unidirectional perforation of the equivalent rectangular edge in the post-impact direction, at an initial velocity, $V \cos \beta$; see page 59. k merely permits the general form to be equivalent to the two equations.

the intersection of the initial and post-impact projectile outlines, and, n, the intersection of the post-impact outline and the bottom surface of the edge. R is the distance between the equivalent edge and the projectile centerline. The equivalent edge is constructed by establishing T, the thickness of the equivalent rectangular edge; the top and bottom surfaces are drawn perpendicular to the post-impact path centerline. The rectangle is closed by a line parallel to the "T" line at a location, R, such that the area intercepted on the equivalent edge is equal to that intercepted on the real edge. Sheet 2/3 of Form 198-5, Figure 44, page 95, is used to compute $\frac{V \cos \beta}{V_{xne}}$ for each assumed value of β ; these

points are plotted on the graph found on this sheet (this graph is a reproduction of Figure A-31, page 43, in Part A of the Appendix). A smooth curve is drawn through the points. Actual β is the value determined by the intercept of this curve and appropriate (AP or FSP) curve shown on the form. These two curves were determined experimentally for the type of impact characterized by the equivalent impact geometry (the tests were mentioned in the previous paragraph). If the striking velocity, V, is at least 4 times greater than the minimum perforation velocity of the edge, V_{xne} , (in the initial impact direction) β can be assumed to be zero.

When treating a full impact as a partial, the impact is diagrammed as shown on Figure 47 (b) and all of the rules governing partial impacts apply except for the determination of the turning point, o.

3. Ricochet

Once it has been determined that a projectile will not perforate, the impact must be treated as a Ricochet. The intersection of the projectile centerline and the impacted surface is used as a turning point for ricochet; scoop depth and projectile flattening during ballistic testing justify this assumption for characteristic ricochet. See Figure 47 (a), page 100. Ricochet velocity, V_r , and Post-Impact Obliquity, θ_r , are determined by referring to the graphs listed in Table III, page 105.

TABLE III

GRILLE BALLISTIC ANALYSIS. DETERMINATION OF RICOCHET DYNAMICS.

If V and θ are known, V_r and θ_r can be determined from the indicated figures.

Parameter	Guide to evaluation of dynamic parameters											
	PROJECTILE AND GRILLE MATERIAL											
	WAL FSP				APM 2				Ball M 2			
	Steel MIL 12560	Alum. MIL 46027	Titanium 6Al-4V	Steel MIL 12560	Alum. MIL 46027	Titanium 6Al-4V	Steel MIL 12560	Alum. MIL 46027	Titanium 6Al-4V	Steel MIL 12560	Alum. MIL 46027	Titanium 6Al-4V
V_r	Fig. Nos. A-1 A-2 A-3	Fig. Nos. A-8 A-9 A-10	Fig. Nos. A-15 A-16 A-17	Fig. Nos. A-4 A-5	Fig. Nos. A-11 A-12	Fig. Nos. A-18 A-19	Fig. Nos. A-6 A-7	Fig. Nos. A-13 A-14	Fig. Nos. A-6 A-7	Fig. Nos. A-13 A-14	Fig. Nos. A-20 A-21	Fig. Nos. A-20 A-21
θ_r	Fig. Nos. A-1 A-2 A-3	Fig. Nos. A-8 A-9 A-10	Fig. Nos. A-15 A-16 A-17	Fig. Nos. A-4 A-5	Fig. Nos. A-11 A-12	Fig. Nos. A-18 A-19	Fig. Nos. A-6 A-7	Fig. Nos. A-13 A-14	Fig. Nos. A-6 A-7	Fig. Nos. A-13 A-14	Fig. Nos. A-20 A-21	Fig. Nos. A-20 A-21

4. Grille Minimum Perforation Velocity

After a particular shot has been fired against a grille, the Grille Minimum Perforation Velocity, V_{xg} , can often be found simply by setting the final residual velocity equal to zero and working backwards up through the grille along the same path. If the minimum perforation velocity of the final impact is high (at least twice as great) compared to the final residual velocity, the residual velocity can almost always be reduced to zero without greatly affecting the path. If the minimum perforation velocity of the final impact is much lower than the residual velocity, it may be necessary to fire again at a lower initial velocity to establish a new path. Then the Grille Minimum Perforation Velocity may be found by setting the new final residual velocity equal to zero and working backwards to find the initial velocity (which is the Grille Minimum Perforation Velocity by definition). This is very conveniently done on sheet 1/3 of Form 198-5, Figure 43, page 94, by writing in the new values above those determined previously in the direction of the projectile.

5. Form 198-5 (Figures 43, 44 and 45)

Equations (21), (26), (36) and (37) can be used directly to compute values of V_r ; Tables I and II, and Figures 46 and 47 explain the manner by which parameters are evaluated. Form 198-5 merely provides a means for solving these equations in a tabulated manner, thereby producing a standard record of the progress of a given projectile through the grille being evaluated. As mentioned in the previous paragraph, use of the form greatly simplifies the determination of the Grille Minimum Perforation Velocity, V_{xg} . The form is used in conjunction with the Firing Sheet (a grille assembly cross section drawing) upon which the progress of the projectile is charted directly over the outline; values of θ , T , and R are measured on the Firing Sheet. When using the form for the first time it will be helpful to identify each step with the pertinent formula and with the procedures for determining the values of parameters.

Sheet 1/3. Figure 43, page 94. This page was set up primarily to solve the perforation residual velocity equations.

However, the form provides for completely defining and recording all types of impact. Only the four parameters on the left hand side marked with an asterisk are involved in a ricochet; thus, a ricochet can be completely recorded by filling in these four values. The equation for Full Impact is solved by performing the operations indicated on the left side; it is wise to cross out all boxes which do not apply for a given impact prior to the computation. The equation for Partial Impact is solved by performing the operations indicated on the right side. Note that many of the computations required for fragments are not required for penetrating projectiles.

The sheet has been set up to automatically add the mass of the plug from a full impact to the mass of the projectile for the subsequent impact. If, as sometimes occurs, several normal full perforations occur sequentially, the plug mass from each impact should be added to the projectile for the consideration of subsequent impacts, until after a partial or oblique impact intervenes. The sheet does not automatically perform this summation but does supply all required information.

Sheet 2/3. Figure 44, page 95. This page is used to compute the value for β , the change in direction of a projectile, as the result of a Partial (Edge) Impact only. β has been experimentally found to be a function of the ratio of the impact velocity and edge minimum perforation velocity as shown in the graph at the right side of the page. (See also Figure A-31, page 43, Part A of the Appendix.) The procedure for finding β consists of assuming several values (three will usually suffice) and solving for the minimum perforation velocity in each of the assumed directions. The ratios, $\frac{V \cos \beta}{V_{xne}}$, are then computed. (Note

that the computation scheme is essentially the same as that for Partial Impact on Sheet 1/3.) These calculated values are then plotted on the graph on the right hand side of the sheet. The intersection of the plotted curve and the appropriate experimental curve (FSP or AP) determines the real value of β .

Sheet 3/3. Figure 45, page 96. This sheet provides for computation of AP projectile breakup. Equation (38), page 82, permits computation of the ratio between the applied force, F_t ,

and the breakup force F_b . When this ratio exceeds unity, the AP will break up. Equations (33) and (34) are equation (32) written in terms of the constants which apply to 0.50 and 0.30 caliber AP. The form is set up to solve equations. Values of equation constants for 0.30 and 0.50 caliber AP are given at the bottom of the sheet. Computation of the equation is tabulated for Full and Partial Impact (left and right respectively).

6. Limitations of the Procedure

Projectile size and shape, path confinement, composite bars and edges, and the mode of projectile breakup are not completely accounted for within the procedures, nor can they be. Therefore, it is important that these limitations of the procedure be kept firmly in mind during analyses. For instance, the analytical procedures are based upon the sequential consideration of individual impacts. Projectiles may be confined by several surfaces at once. The analyst must consider the influence of such confinement upon the path of the projectile. Composite edges can often be handled as two independent impacts, but not always.

It is apparent that a qualitative examination of a grille design should be made before the Procedure is used to perform a quantitative ballistic analysis. While the first purpose of this preliminary examination is to determine whether the design merits further consideration, a second, and perhaps more important, purpose is to identify grille weaknesses quickly. The ballistic analysis will usually confirm the conclusions of the qualitative examination and will supply numerical values for Grille Minimum Perforation Velocities. However, in some cases the ballistic analysis may fail to accurately define a weakness. For instance, a small arms projectile may break up in a confined space; most of the fragments may be caught in a trap. If the space is open to the rear side of the grille impacts between fragments piling up in the trap may cause some fragments to ricochet through the opening. The procedure only considers impact with the grille itself and would not predict this type of defeat.

A general agreement between the preliminary qualitative examination and the quantitative ballistic analysis will provide evidence to show that the limitations of the ballistic analysis procedures have not led to erroneous conclusions.

7. Form 198-3C (Figure 48, page 110)

Form No. 198-3C, Grille Performance Evaluation, is a convenient means of summarizing the performance of a grille. The grille is ballistically compared to the armor it replaces. The Grille Minimum Perforation Velocities, V_{xg} , at the weakest attack obliquities are compared with the Minimum Perforation Velocity, V_{xp} , of the armor at the same obliquities. The form also provides for weight and air flow evaluation.

C. Grille Design

The general specifications for grille designs are determined by their location and available area on a vehicle. The principal design considerations are those of air flow, ballistic performance, weight and Infrared detection. This report deals with bar or louvered grilles for which the I-R consideration usually is limited to observance of line-of-sight rules which specify that the grilles be completely opaque in any direction to the direct transmittal of light or heat radiation from the interior.

The ideal grille would provide the same protection as the armor it replaces without any increase in weight and would offer no restriction to the flow of air. Obviously these three design considerations are antagonistic. Air passages which represent little resistance to air flow also tend to offer little resistance to the passage of projectiles and fragments. Weight may be added to the grille to increase ballistic protection without a drastic reduction in air flow efficiency. A compromise between good air flow, light weight and adequate ballistic protection is required. Optimum designs will approach the perfect grille as closely as possible; it will be up to the designer as to which parameter will be compromised the most. Often air flow and ballistic protection are favored with added weight as the compromise; sometimes ballistic protection is sacrificed. Air flow requirements are based on engine heating and are less easily compromised.

It is doubtful that a design procedure can be formulated which will automatically yield the optimum grille for a given application. Instead, a valid means of evaluating ballistic

GRILLE PERFORMANCE SUMMARY

GRILLE - _____

PROJECTILE →		30 CAL. AP	50 CAL. AP	300 CAL. FSP	50 CAL. FSP	20 MM FSP	30 CAL. BALL	50 CAL. BALL
BALLISTICS								
DECK ARMOR	TYPE							
THICKNESS	T INCHES							
ATTACK ORUGITY	1 2 3							
	Θ_g							
DEFEAT VELOCITY	1 2 3							
GRILLE	V_{xg}							
ARMOR	1 2 3							
	V_{xp}							
WEIGHT								
GRILLE	W_g							
ARMOR	W_a							
AIR FLOW								
GRILLE								
FLOW	Q_g							
HEAD LOSS	h_g							
STANDARD								
FLOW	Q_a							
HEAD LOSS	h_a							
HEAD LOSS	h_{a1}							
RATIO	$\frac{Q_g}{Q_a}$							
	$\frac{h_g}{h_a}$							
	$\frac{h_{a1}}{h_a}$							
FORM 198-3C		DENVER RESEARCH INST.						

Figure 48. Grille Evaluation. Performance Summary. Form 198-3c

performance of any design will be available to the designer. The designer can create a number of designs which he can proof test ballistically on paper rather than through actual ballistic proofing of prototypes. This will provide the means for identifying the best designs and the weak points of each design. Design modification can be made to optimize the best designs, which can be verified by performing subsequent ballistic analyses. Final proof testing of prototypes will be required only for one or two optimized designs. His considerations of air flow can be verified through air flow testing of wood models. The ballistic performance evaluation procedures presented in Section B, page 91, and demonstrated in this Section provide a fast and convenient means for checking the ballistic design of a grille against fragments (FSP) and small arms projectiles (AP and Ball).

1. Prototype Designs

Figures A-58 through A-64, in Part A of the Appendices display several prototype designs which were submitted to Ordnance Tank Automotive Command for their consideration. In each case projectiles pass in the direction, top to bottom. Figures A-65 through A-71 are Evaluation Sheets upon which the ballistic and air flow performances and weight of these grilles are tabulated. Figures A-58 through A-60 are light weight designs and are not capable of stopping AP projectiles. Figures A-61 and A-62 are also light weight designs which are nominally designed to be equivalent to 1 1/2-inch aluminum armor. Figures A-63 and A-64 are medium weight designs which are nominally designed to be equivalent to 3/4-inch rolled homogeneous steel armor.

Figure A-58. This chevron style incorporates an included angle which prevents ricochet toward the bottom openings. Thus, all fragments are forced to perforate the bottom leg or the knee area. Air flow losses are slightly greater than those observed for the standard T-41 grille.

Figure A-59. This design causes the plug ejected from the relatively thin section and fragment to be trapped. Air flow losses are considerably greater than standard T-41 grille losses.

Figure A-60. The modified form of this design permits passage of a fragment, fired into the grille, through a relatively thin section as did the previous design. In this case the heavy knee causes the plug and fragment to ricochet into the trap. Air flow efficiency is very good; better than the standard T-41 grille.

Figure A-61. The steel upper bar intercepts and breaks up AP projectiles fired across the bars. The aluminum absorbs remaining fragment energies. In one direction into the bars the AP projectile can escape break up, but must pass through two thicknesses of aluminum before striking the heavier knee section. Air flow efficiency is very good.

Figure A-62. This design is similar to the previous one; however, the vertical aluminum section provides some advantages in intercepting and guiding projectiles toward the horizontal direction. The caliber 0.50 AP does not have free access to the aluminum section. Fragments reaching the hook will have been greatly slowed down. Air flow for this design is excellent.

Figure A-63. The upper steel bar will tend to break up AP projectiles. Fragments which enter the lower trap will ricochet upward and to the right, behind the knee. Perforation of the lower trap is more difficult than if the pieces were welded together, since bending will absorb some energy. Air flow efficiency is poor.

Figure A-64. The heavy aluminum sections are capable of breaking AP projectiles or absorbing kinetic energy so that the hook can contain the remaining energy. Impact angles during firing into the grille break up AP projectiles. Air flow efficiency should be excellent.

2. Ballistic Analyses

Presentation of all of the ballistic analyses concerning the prototype grilles would take too much space. As a means for illustrating the ballistic procedures, the analysis of the 198-051 grille, Figure A-64 is presented in the Appendix.

3. Prototype Evaluation

Results of prototype evaluations are presented on Form 198-3C, Figures A-65 through A-71, in the Appendix. Comparisons of ballistic performance, weight, and air flow performance can be made using these sheets.

VI. BIBLIOGRAPHY

1. Merchant, M. E., "Mechanics of the Metal Cutting Process", I and II, Journal of Applied Physics, Vol. 16, May 1945, pp. 267-275, June 1945, pp. 318-324.
2. Siekmann, H. J., "The Use of an Ultra High Speed 150 Horsepower Lathe for Machinability Studies", Paper No. 82, Vol. 58, A. S. T. E., May 1958.
3. Recht, R. F., "The Feasibility of Ultra-High Speed Machining", Master's Thesis, University of Denver, May 1960.
4. Jameson, R. L., and J. S. Williams, "Velocity Losses of Cylindrical Steel Projectile Perforating Mild Steel Plates", Report No. 1019, Ballistic Research Laboratories, July, 1957.
5. Project Thor, "A Study of Residual Velocity Data for Steel Fragments Impacting on Four Materials; Empirical Relationships (U)", Technical Report No. 36, Contract No. DA-36-034-ORD-1678, Institute for Cooperative Research, The Johns-Hopkins University, April 1958, Confidential.
6. Mascianica, F. S., and P. V. Riffin, "Performance of Rolled Homogeneous Armor Against Scale-Model Monobloc and Capped Armor-Piercing Projectiles at 0° to 70° Obliquity (U)", Principles of Armor Protection, 5th Partial Report, WAL 710/607-4, Watertown Arsenal Lab., May 1956, Confidential.
7. Cottrell, A. H., "Deformation of Solids at High Rates of Strain", The Chartered Mechanical Engineer, pp. 448-460, November 1957.
8. Whitlock, F. W., "Investigation of Variables Affecting the Performance of Light Weight Armor (U)", Final Report, Contract No. DA-23-072-ORD-815, WAL File No. 710/1049, Midwest Research Institute, June 1955, Confidential.

9. Project Thor, "A Suggested Technique for Predicting the Performance of Armor-Piercing Projectiles Acting on Rolled Homogeneous Armor (U)", Technical Report No. 14, Contract No. DA-36-034-ORD-1678, Institute for Cooperative Research, The Johns-Hopkins University, September 1954, Confidential.

DISTRIBUTION LIST

<u>Addressee</u>	<u>Number of Copies</u>	<u>Copy Numbers</u>
1. Chief of Ordnance Department of the Army Washington 25, D. C. ATTN: ORDTB-BALLISTIC SECTION	1	1
2. Chief of Ordnance Department of the Army Washington 25, D. C. ATTN: ORDTU	1	2
3. Chief of Ordnance Department of the Army Washington 25, D. C. ATTN: ORDTW	1	3
Canadian Army Staff (through ORDTW)	2	4-5
4. Defense Research Attache British Embassy Washington 25, D. C. (through ORDTW)	4	6-9 Incl.
5. Office, Chief of Engineers Department of the Army Washington 25, D. C. ATTN: ENGE Structure Dev. Branch	1	12
6. Commanding Officer Engineer Res. and Dev. Laboratories Ft. Belvoir, Virginia ATTN: Tech. Intell. Branch	1	13
7. Chief, Bureau of Weapons Department of the Navy Washington 25, D. C. ATTN: RRE-5, Mr. William August	1	14
8. Chief, Bureau of Weapons Department of the Navy Washington 25, D. C. ATTN: RMMO	2	15-16 Incl.

DISTRIBUTION LIST (Cont.)

<u>Addressee</u>	<u>Number of Copies</u>	<u>Copy Numbers</u>
9. Director Naval Research Laboratory Washington 25, D. C. ATTN: Tech. Information Div.	1	17
10. ASTIA Reference Center Library of Congress Washington 25, D. C.	2	20-21
11. Armed Services Technical Information Agency Arlington Hall Station Arlington, Virginia	5	22-26 Incl.
12. Commanding General Aberdeen Proving Ground, Maryland ATTN: Ballistic Res. Laboratories	1	27
13. Commanding General Aberdeen Proving Ground, Maryland ATTN: Development and Proof Services Technical Information Branch	1	29
14. Commanding General Ordnance Tank-Automotive Command Detroit Arsenal Center Line, Michigan ATTN: ORDMC-REM. 1	3	30-32
15. Commanding Officer Detroit Arsenal Center Line, Michigan ATTN: ORDMX-AL	1	33
16. Commanding Officer Office of Ordnance Research Box CM, Duke Station Durham, North Carolina	1	36

DISTRIBUTION LIST (Cont.)

<u>Addressee</u>	<u>Number of Copies</u>	<u>Copy Numbers</u>
17. Commanding Officer Picatinny Arsenal Dover, New Jersey ATTN: Technical Division	1	37
18. Commanding Officer Frankford Arsenal Philadelphia 37, Pennsylvania	1	38
19. Commanding Officer Watertown Arsenal Watertown 72, Massachusetts ATTN: Mr. P. V. Riffin	1	39
20. Commander U.S. Naval Ordnance Test Station Inyokern China Lake, California ATTN: Technical Library	2	43-44
21. Commander Naval Ordnance Laboratory White Oak Silver Spring 19, Maryland	2	45-46
22. Commander U.S. Naval Air Development Center Johnsville, Pennsylvania ATTN: Aviation Armament Laboratory	1	47
23. Commander U.S. Naval Proving Ground Dahlgren, Virginia	1	48
24. U.S. Army Ordnance District, St. Louis 4300 Goodfellow Boulevard St. Louis 20, Missouri	1	49

DISTRIBUTION LIST (Cont.)

<u>Addressee</u>	<u>Number of Copies</u>	<u>Copy Numbers</u>
25. Director, Applied Physics Laboratory Silver Spring, Maryland ATTN: Mr. H. S. Morton THRU: Naval Inspector of Ordnance Applied Physics Laboratory 8621 Georgia Avenue Silver Spring, Maryland	1	10
26. Stanford Research Institute Palo Alto, California ATTN: Dr. T. D. Poulter THRU: Commanding Officer San Francisco Ordnance District 1515 Clay St., P.O. Box 1829 Oakland 12, California	1	11
27. Arthur D. Little, Inc. 30 Memorial Drive Cambridge 42, Massachusetts THRU: Commanding Officer Boston Ordnance District Boston Army Base Boston 10, Massachusetts	1	18
28. Cornell Aeronautical Laboratory Buffalo, New York VIA: Commanding Officer New York Ordnance Laboratory 770 Broadway New York 3, New York	1	19
29. Carnegie Institute of Technology Schenley Park Pittsburgh 13, Pennsylvania VIA: Commanding Officer Philadelphia Ordnance District 128 N. Broad Street Philadelphia 2, Pennsylvania	1	28

DISTRIBUTION LIST (Cont.)

<u>Addressee</u>	<u>Number of Copies</u>	<u>Copy Numbers</u>
30. Aerojet General Corporation Azusa, California ATTN: K. N. Krezenhogen Ann R. Chase, Libr. at Downey, California VIA: Bureau of Naval Weapons Rep.	1	34
31. Aircraft Armaments, Inc. Cockeysville, Maryland VIA: Philadelphia Ordnance District 128 North Broad Street Philadelphia 2, Pennsylvania	1	35
32. Cleveland Ordnance Plant Cadillac Motor Car Division 6200 Riverside Drive Cleveland 35, Ohio ATTN: Mr. R. Hayes VIA: Cleveland Ordnance District 1367 E. Sixth Street Cleveland 14, Ohio	1	40
33. Johns Hopkins University 3506 Greenway Baltimore, Maryland VJ · Philadelphia Ordnance District 128 North Broad Street Philadelphia 2, Pennsylvania	1	41
34. University of Denver Colorado Seminary University Park Denver 10, Colorado VIA: St. Louis Ordnance District 4300 Goodfellow Boulevard St. Louis 20, Missouri	1	42

ABSTRACT

The terminal ballistic dynamics of small arms projectiles and fragment simulating projectiles are presented. These dynamics include the post-impact residual velocity and direction of projectiles, projectile break-up and dispersion of projectile fragments, and the mechanics of plate perforation. Ricochet dynamics concerning steel, aluminum, and titanium armor materials have been determined experimentally for impact obliquities up to 60 degrees. Analytical equations which accurately predict the dynamics of ballistic perforation were derived and confirmed by experimental data. These equations consider the effects of obliquity, plate thickness, edge impact and projectile shape.

A ballistic evaluation procedure, based upon the defined terminal ballistic dynamics, was developed. While the procedure was developed specifically for the evaluation of grilles, it can be used equally well for evaluating any armoring concept or the performance of projectiles.

Several prototype grilles were designed and evaluated. Some of these will be fabricated and ballistically proof-tested.

Cross-references: Terminal Ballistics, Armor, Projectiles, Material Properties, Vehicles. Report is UNCLASSIFIED. Separate Appendix is classified CONFIDENTIAL. Abstract Cards are UNCLASSIFIED.

ABSTRACT

The terminal ballistic dynamics of small arms projectiles and fragment simulating projectiles are presented. These dynamics include the post-impact residual velocity and direction of projectiles, projectile break-up and dispersion of projectile fragments, and the mechanics of plate perforation. Ricochet dynamics concerning steel, aluminum, and titanium armor materials have been determined experimentally for impact obliquities up to 60 degrees. Analytical equations which accurately predict the dynamics of ballistic perforation were derived and confirmed by experimental data. These equations consider the effects of obliquity, plate thickness, edge impact and projectile shape.

A ballistic evaluation procedure, based upon the defined terminal ballistic dynamics, was developed. While the procedure was developed specifically for the evaluation of grilles, it can be used equally well for evaluating any armoring concept or the performance of projectiles.

Several prototype grilles were designed and evaluated. Some of these will be fabricated and ballistically proof-tested.

Cross-references: Terminal Ballistics, Armor, Projectiles, Material Properties, Vehicles. Report is UNCLASSIFIED. Separate Appendix is classified CONFIDENTIAL. Abstract Cards are UNCLASSIFIED.

ABSTRACT

The terminal ballistic dynamics of small arms projectiles and fragment simulating projectiles are presented. These dynamics include the post-impact residual velocity and direction of projectiles, projectile break-up and dispersion of projectile fragments, and the mechanics of plate perforation. Ricochet dynamics concerning steel, aluminum, and titanium armor materials have been determined experimentally for impact obliquities up to 60 degrees. Analytical equations which accurately predict the dynamics of ballistic perforation were derived and confirmed by experimental data. These equations consider the effects of obliquity, plate thickness, edge impact and projectile shape.

A ballistic evaluation procedure, based upon the defined terminal ballistic dynamics, was developed. While the procedure was developed specifically for the evaluation of grilles, it can be used equally well for evaluating any armoring concept or the performance of projectiles.

Several prototype grilles were designed and evaluated. Some of these will be fabricated and ballistically proof-tested.

Cross-references: Terminal Ballistics, Armor, Projectiles, Material Properties, Vehicles. Report is UNCLASSIFIED. Separate Appendix is classified CONFIDENTIAL. Abstract Cards are UNCLASSIFIED.

ABSTRACT

The terminal ballistic dynamics of small arms projectiles and fragment simulating projectiles are presented. These dynamics include the post-impact residual velocity and direction of projectiles, projectile break-up and dispersion of projectile fragments, and the mechanics of plate perforation. Ricochet dynamics concerning steel, aluminum, and titanium armor materials have been determined experimentally for impact obliquities up to 60 degrees. Analytical equations which accurately predict the dynamics of ballistic perforation were derived and confirmed by experimental data. These equations consider the effects of obliquity, plate thickness, edge impact and projectile shape.

A ballistic evaluation procedure, based upon the defined terminal ballistic dynamics, was developed. While the procedure was developed specifically for the evaluation of grilles, it can be used equally well for evaluating any armoring concept or the performance of projectiles.

Several prototype grilles were designed and evaluated. Some of these will be fabricated and ballistically proof-tested.

Cross-references: Terminal Ballistics, Armor, Projectiles, Material Properties, Vehicles. Report is UNCLASSIFIED. Separate Appendix is classified CONFIDENTIAL. Abstract Cards are UNCLASSIFIED.

AD _____ ACCESSION _____

University of Denver (Colorado Seminary), The Denver Research Institute, Denver 10, Colorado. Report No. DRI 2025 Final Report. "The Dynamics of Terminal Ballistics" (Ballistic Evaluation Procedures for Armor Grille Designs) (U), Rodney F. Recht and Thomas W. Ipson. Unclassified Report contains 116 pages, including 3 tables and 48 illustrations. Separate Classified Appendices contain 12 tables and 72 graphs of ballistics data and a pertinent annotated bibliography of the literature. Contract No. DA-23-072-ORD-1302 Dept. of the Army Project No. 548-03-001, Research and Engineering Directorate, Ordnance Tank Automotive Command, Detroit Arsenal. 1 February 1962.

(over)

AD _____ ACCESSION _____

University of Denver (Colorado Seminary), The Denver Research Institute, Denver 10, Colorado. Report No. DRI 2025 Final Report. "The Dynamics of Terminal Ballistics" (Ballistic Evaluation Procedures for Armor Grille Designs) (U), Rodney F. Recht and Thomas W. Ipson. Unclassified Report contains 116 pages, including 3 tables and 48 illustrations. Separate Classified Appendices contain 12 tables and 72 graphs of ballistics data and a pertinent annotated bibliography of the literature. Contract No. DA-23-072-ORD-1302 Dept. of the Army Project No. 548-03-001, Research and Engineering Directorate, Ordnance Tank Automotive Command, Detroit Arsenal. 1 February 1962.

(over)

AD _____ ACCESSION _____

University of Denver (Colorado Seminary), The Denver Research Institute, Denver 10, Colorado. Report No. DRI 2025 Final Report. "The Dynamics of Terminal Ballistics" (Ballistic Evaluation Procedures for Armor Grille Designs) (U), Rodney F. Recht and Thomas W. Ipson. Unclassified Report contains 116 pages, including 3 tables and 48 illustrations. Separate Classified Appendices contain 12 tables and 72 graphs of ballistics data and a pertinent annotated bibliography of the literature. Contract No. DA-23-072-ORD-1302 Dept. of the Army Project No. 548-03-001, Research and Engineering Directorate, Ordnance Tank Automotive Command, Detroit Arsenal. 1 February 1962.

(over)

AD _____ ACCESSION _____

University of Denver (Colorado Seminary), The Denver Research Institute, Denver 10, Colorado. Report No. DRI 2025 Final Report. "The Dynamics of Terminal Ballistics" (Ballistic Evaluation Procedures for Armor Grille Designs) (U), Rodney F. Recht and Thomas W. Ipson. Unclassified Report contains 116 pages, including 3 tables and 48 illustrations. Separate Classified Appendices contain 12 tables and 72 graphs of ballistics data and a pertinent annotated bibliography of the literature. Contract No. DA-23-072-ORD-1302 Dept. of the Army Project No. 548-03-001, Research and Engineering Directorate, Ordnance Tank Automotive Command, Detroit Arsenal. 1 February 1962.

(over)